Chemosensing Strategies
Utilizing the Novel Sulfonamidohydroxyquinoline Amino Acid Sox

by

Melissa Dawn Shults

B.S. Chemistry (2000)
University of California, San Diego

Submitted to the Department of Chemistry
in Partial Fulfillment of the Requirements for the Degree of
Doctor of Philosophy in Organic Chemistry

at the

Massachusetts Institute of Technology

June 2005

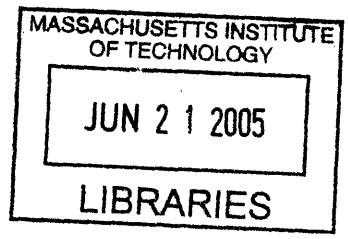

Signature of Author: _____
Department of Chemistry
May 5, 2005

Certified by: _____
Barbara Imperiali
Class of 1922 Professor of Chemistry and Professor of Biology
Thesis Supervisor

Accepted By: _____
Robert W. Field
Chairman, Departmental Committee on Graduate Students

This doctoral thesis has been examined by a committee of the Department of Chemistry as follows:

Timothy M. Swager
Professor of Chemistry
Chair

Barbara Imperiali
Class of 1922 Professor of Chemistry and Professor of Biology
Thesis Supervisor

Douglas A. Lauffenburger
Whitaker Professor of Biological Engineering, Professor of Chemical Engineering and Biology

Stephen J. Lippard
Arthur Amos Noyes Professor of Chemistry

Chemosensing Strategies
Utilizing the Novel Sulfonamidohydroxyquinoline Amino Acid Sox

by
Melissa Dawn Shults

Submitted to the Department of Chemistry
on May 5, 2005 in partial fulfillment of the
requirements for the Degree of Doctor of Philosophy
in Organic Chemistry

ABSTRACT

Modular peptide-based fluorescent chemosensors utilizing the chelation-sensitive fluorophore 8-hydroxy-5-(*N,N*-dimethylsulfonamido)-2-methylquinoline are powerful tools for sensing Zn^{2+} and for sensing protein kinase activity. This signaling component is prepared as the protected amino acid derivative Fmoc-Sox-OH, and integrated into peptide sequences.

Selective and tunable chemosensors for Zn^{2+} can afford qualitative and quantitative information about the presence, distribution and concentration of this biologically-important metal ion. Nineteen synthetic peptides incorporating Sox exhibit a range of affinities for Zn^{2+} through variation of the type and number of Zn^{2+} ligands, ligand arrangement and the β-turn sequence that acts as a preorganization element between the ligands. The binding stoichiometry and fluorescence response to pH changes and various relevant competing metal ions was carefully characterized. Eleven of these sequences form only 1:1 complexes with Zn^{2+} and their affinities range from 10 nM to nearly 1 μM. When used in concert, the relative intensities of different chemosensor readouts can provide Zn^{2+} concentration information in a valuable range. This modular scaffold is useful for ratiometric sensing when an additional fluorophore is incorporated in the peptide sequence.

New methods to quantify protein kinase activities are critical for understanding biological regulatory pathways. Fluorescent chemosensors of protein kinase activity utilizing Sox and physiological Mg^{2+} concentrations report phosphorylation with dramatic fluorescence changes in a continuous, high-throughput sensing format. The chemosensor comprises a small sensing module, containing Sox and a β-turn sequence, appended to an optimized peptide substrate for the target kinase. The Mg^{2+}-binding affinity of the product phosphopeptide is much greater than the substrate peptide, which results in a large fluorescence increase upon phosphorylation. Notably, the reactivity of substrates is not affected by introduction of the sensing module on either side of the serine, threonine or tyrosine to be phosphorylated. Further, a homogeneous kinase assay utilizing these probes was developed that was reproducible, linear and highly preferential for monitoring changes in cellular activity of the target kinase in unfractionated cell lysates. These kinase chemosensors are powerful tools for studying the activity of recombinant kinases *in vitro* and endogenous kinases *ex vivo*.

Thesis Supervisor: Barbara Imperiali
Title: Class of 1922 Professor of Chemistry and Professor of Biology

Acknowledgements

First and foremost, I would like to thank my advisor, Professor Barbara Imperiali, for her support, both professional and personal, as well as encouragement over the last five years. Under her guidance, I have received an excellent graduate education. Barbara, your creativity, enthusiasm for science, and teaching ability have been truly inspiring. I am grateful for your ideas and broad vision that improved my research. I sincerely appreciate your trust and the wealth of opportunities to learn, even when I did not fully realize it. The breadth of your knowledge and interests has generated a lab environment with quite diverse projects, from which I have learned a great deal. I am especially grateful for your selection of talented, helpful and diverse scientists. Also, thank you for entrusting me with your old iBook to get me through this thesis.

I would like to thank the members of my thesis committee for their support during my time at MIT: Professor Doug Lauffenburger, Professor Tim Swager and Professor Steve Lippard. Doug has been an incredible champion of my work and a real pleasure with which to collaborate. I admire his positive attitude, creativity and scientific curiosity. I truly admire Tim's ideas and appreciate his willingness to attend my thesis defense from England via iChat, and will always remember our "virtual handshake". Tim, thank you for your contacts that enabled my interview for my new position at Illumina, Inc. Steve, thank you for your thoughtful comments and careful reading of this thesis.

My co-workers in the Imperiali lab have provided a wonderful work environment and on many occasions have offered much-appreciated scientific advice and instruction. They made the lab a friendly, supportive and fun place to spend a significant portion of my life. In addition, I am grateful to all of them for sharing their time and feedback on many practice talks. I owe a special thank you to Dora Carrico, Elvedin Lukovic, and Bianca Sculimbrene for each proofreading portions of this thesis.

Most importantly, Debbie Rothman and Beth Vogel have been truly wonderful friends. Debbie, I have really enjoyed many good talks with you about anything and everything, at lunch, in the thesis-writing "cave", and outside the lab. I am so grateful to have shared many experiences, conferences, and opinions with you (and even a hood!)! Your support and listening ear when I was stressed and freaking out have meant so much to me. I continue to be inspired by

your organization and sense of humor, both of which were helpful for me as I was plowing through this thesis. You are a fantastic friend and I will miss you a lot. Beth, the balance that you have attained and your positive attitude are an inspiration to me and I thank you for helping me to see many things from a different perspective. Thank you for showing me all the best things about New England, and especially fruit picking! Thank you also for motivating me to go to the gym and for being a fantastic workout partner. I have really enjoyed our talks and will really miss you.

I am incredibly grateful to my first co-worker in the lab, Dr. Dierdre Pearce, for teaching me so much and helping me to adjust to graduate school. Dierdre, I really appreciated your scientific inspiration and moral support for the Zn^{2+}-sensing project. I thank Kathy Franz and Kevin McDonnell for a lot of very helpful research advice early in my PhD. I am also grateful to Dr. K. Jebrell Glover for spending a significant portion of his own time and energy to provide advice, to answer my questions, and to help me with biochemistry and computers. Jebrell, I admire your philosophy about research and have enjoyed speaking about research, music and politics with you. I owe many thanks to Elizabeth Fong for taking care of tons of little things for me and explaining many administrative things throughout my graduate career. Elizabeth, I have enjoyed our many chats, and thank you for sharing you love of plants and some clippings with me! To my co-workers on the kinase sensing project – Elvedin Lukovic and Dora Carrico – I cannot think of two better people to carry on the project and I look forward to many exciting results in the future. Elvedin, thank you for always listening to my research frustrations and for many fun dancing memories. Dora, thank you for checking up on me during the thesis writing, for your openness and for good talks – I will miss a chance to get to know you better. Mayssam Ali, thank you for your friendship, advice, and especially encouragement during the job search. I will also be forever indebted for the suggestion to use phosphoserine in a Zn^{2+}-sensing peptide! Maria Ufret, I am thankful for your continued friendship, for sharing mass spec duties, and for great lunches out in the sunshine! I thank Carlos Bosques for his support, for joking around with me, and for lots of loud salsa music and singing. Bianca Sculimbrene, thank you for helping to keep me sane through the job search and thesis writing, I really appreciate the moral support and that you shared your experiences with me. Langdon Martin, thank you for always keeping me laughing. I really admire your creativity and attitude. The Sox kinase assay will always be

"CHAMP" to me. I continue to be inspired by the dedication to science of my classmates Eranthie Weerapana and Seungjib Choi; I wish both of you many future successes. Christina Carrigan, your enthusiasm and efficiency was incredibly inspiring and I very much enjoyed my first bike ride out to Walden Pond with you. I thank Eugenio Vazquez for his smile and for help both with research and with computers. I have enjoyed many great lunchtime conversations with Debby Pheasant and appreciated her cheerfulness in the instrument room when experiments were going awry. Mary O'Reilly, thank you for listening to my random outbursts at my desk – I enjoyed many talks with you and wish you the best in your post-doc. I thank Jennifer Ottesen for her enthusiasm in giving me a crash course in managing the lab Mac computers. Galen Loving, I wish you much luck with the mass spec – you are already doing a fantastic job with the e-mails. I thank Guofeng Zhang for entertaining Costco trips and thought-provoking debates. I thank Mark Nitz for sharing his knowledge with me and for research advice. I thank Christian Hackenburger for lots of chocolate from Germany and for the humorous pictures of the Governator. I thank Soonsil Hyun for being a good hoodmate and for teaching me some things about her project. I also thank Rob Dempski and Harm Brummerhop for answering many questions when I arrived. I have enjoyed the company of the undergraduates in the lab: Ryu Yoshida, Mike Torrice, Rebecca Maglathlin and Jose Class. I wish the best to several people who recently joined and whom I have not been able to get to know: Mark Chen, Andrew Dutton, Matthieu Sainlos and Nelson Olivier.

My collaboration with Kevin Janes benefited greatly from his work ethic, experimental consistency and wealth of knowledge. Kevin, thank you for being organized, prompt and enthusiastic and for your careful editing of our manuscript. I feel lucky to have been a part of such a rewarding and successful collaboration.

To the "hotbed of [Red] Sox fandom that is the Imperiali lab" (quote courtesy of Jenny Yang) – Beth, Debbie, Bianca and Langdon – I have enjoyed sharing my obsession with the World Champion Boston Red Sox with you all. I will always remember the games, our signs, the player of the week board and the many fun conversations. I would also like to thank the players, especially Gabe Kapler, Curt Schilling and Manny Ramirez, for inspiration.

I thank the building 18 renovations for providing an opportunity for character-building and, in retrospect, some good laughs.

My previous mentors and chemistry teachers who have inspired me and sparked my interest in chemistry deserve special mention: my high school chemistry teacher, Dawn Gamberale, and my undergraduate research advisor at UCSD, Professor Jay S. Siegel.

Many wonderful friends have supported me through busy and often stressful times. I owe special thanks to my awesome roommates, Laurel Ng and Ping Xu. You have both shared my love of good food and I have enjoyed many dinners, good conversations and fun parties with you. Ping, I am also grateful for the Perl script to reformat my fluorescence plate reader data that saved me a great deal of time. To my dear friends Julie Garg and Rachana Sidhu, I treasure your friendship.

To Jey – your support, love, and friendship means so much to me. Thank you for moving to Boston to see me through the end of my PhD, for always making me laugh, for helping me see things in a different light and for helping me to kick back every once in awhile. I love you.

Most importantly, to Mom, Dad and Amanda – words cannot describe how much your support, encouragement, unconditional love, and friendship throughout my life and especially now has meant to me. Mom and Dad, you have encouraged me to do what I love and have never pressured me – I am so grateful. Mom, thank you for your wisdom and for always being there when I need to talk. Dad, thank you for your incredible sense of humor and for much computer assistance. Amanda, thank you for sharing so much of your exciting life with me and yet always finding time to hear about mine. I am so lucky to have such a wonderful sister and best friend. You are the best family a girl could wish for and I am looking forward to being back home again soon. Mom, Dad and Amanda, I love you all very much and I dedicate this thesis to you.

Table of Contents

List of Figures

Chapter 4

Chapter 5

List of Schemes

List of Tables

List of Abbreviations

Standard 3-letter and 1-letter codes are used for the 20 natural amino acids
D preceding the amino acid code indicates D-chirality

Abl	Abelson tyrosine kinase
Ac	acetyl
ADP	adenosine-5′-diphosphate
AFP	*Aequoria victoria* fluorescent protein
ATP	adenosine-5′-triphosphate
BSA	bovine serum albumin
Bzl	benzyl
cAMP	adenosine cyclic 3′-5′-phosphate
CHEF	chelation-enhanced fluorescence
Ches	2-(cyclohexylamino)ethanesulfonic acid
cpAFP	circularly-permuted AFP
DCM	dichloromethane
DIPEA	*N,N*-diisopropylethylamine
DMF	*N,N*-dimethylformamide
DMSO	dimethylsulfoxide
DTT	dithiothreitol
ε	extinction coefficient or molar absorptivity
EDT	ethanedithiol
EDTA	ethylenediaminetetracetic acid
EGTA	ethylene glycol-bis-(2-aminoethylether)-*N,N,N′,N′*-tetraacetic acid
ELISA	enzyme-linked immunosorbent assay
ESI-MS	electrospray ionization mass spectrometry
Φ	quantum yield
FDAA	Marfey's reagent or 1-fluoro-2,4-dinitrophenyl-5-L-alanineamide
Fmoc	fluoren-9-ylmethyloxycarbonyl
FP	fluorescence polarization
FRET	fluorescence resonance energy transfer
HATU	*O*-(7-azabenzotriazol-1-yl)-1,1,3,3-tetramethyluronium hexafluorophosphate
HBTU	2-(1*H*-benzotriazole-1-yl)-1,1,3,3-tetramethyluronium hexafluorophosphate
Hepes	*N*-(2-hydroxyethyl)piperazine-*N′*-ethanesulfonic acid
HOBt	*N*-hydroxybenzotriazole
HPLC	high-performance liquid chromatography
HRMS	high-resolution mass spectrometry
IC_{50}	concentration that gives 50% inhibition
Ipa	3-(imidazol-4-yl)propionic acid
K_D	dissociation constant
K_M	Michaelis constant
λ_{em}	emission wavelength

λ_{ex}	excitation wavelength
MeCN	acetonitrile
Mes	2-morpholinoethanesulfonic acid
MK2	mitogen-activated protein kinase-activated protein kinase-2
NBD	7-nitrobenz-2-oxa-1,3-diazole
NBS	*N*-bromosuccinimide
NMP	*N*-methylpyrrolidinone
NMR	nuclear magnetic resonance
Oxn	8-hydroxyquinoline or oxine
PBS	phosphate-buffered saline
Pen	penacillamine or β-dimethylcysteine
PET	photoinduced electron transfer
PKA	cAMP-dependent protein kinase
PKC	protein kinase C
pSer	phosphoserine
pThr	phosphothreonine
pTyr	phosphotyrosine
PyBOP	benzotriazole-1-yl-oxy-tris-pyrrolidino-phosphonium hexafluorophosphate
QAA	quantitative amino acid analysis
RP-HPLC	reverse-phase HPLC
s.e.m.	standard error
SPPS	solid-phase peptide synthesis
std. dev.	standard deviation
TBS	tributylsilyl
TBDMS	*tert*-butyldimethylsilyl
TBDPS	*tert*-butyldiphenylsilyl
tBu	*tert*-butyl
TFA	trifluoroacetic acid
TIS	triisopropylsilane
TMS	tetramethylsilane
t_R	retention time
TLC	thin layer chromatography
Tris	tris(hydroxymethyl)aminomethane
UV-Vis	ultraviolet-visible
Xaa	used to denote any amino acid
V_{max}	maximum velocity
vol%	volume percent

Chapter 1
Introduction

Introduction to Biological Signaling

Signaling processes in biological systems are extremely complex. Within an individual cell, signaling events are carefully orchestrated in location and time by diverse cellular species, including metal ions, small molecules, enzymes, and multi-protein complexes. Individual signaling events within signaling cascades are vital for cellular function; for example, they mediate the cell cycle. Signaling cascades also transduce extracellular signals, such as growth factor presence, into a myriad of cellular responses. These signaling pathways afford signal amplification and implement a variety of control mechanisms to tightly regulate changes in cellular function. Due to their complexity, understanding the spatial and temporal roles of each signaling species remains a significant challenge in biology.

Many biological, biochemical and physical approaches have provided a wealth of information regarding the high specificity of cellular signaling. Genes can be knocked out to determine their function, and certain species may be studied by immunoblot analysis or reconstitution *in vitro*. Further, metal ions can be detected by methods such as atomic absorption spectroscopy. However, these methods all lack the critical element of real-time analysis. Genetic methods require several days or weeks to perform,[1] and other methods either provide total concentration measurements that are often not relevant to signaling or alternatively remove the components from their native environment.[2]

To study species in their native cellular environment on a significant signaling time-scale, chemically-driven strategies that allow for spatial and temporal resolution are finding widespread use.[1,3,4] These chemical strategies provide a means to perturb cellular signaling to observe downstream effects. Certain small molecules can modulate of cellular function[1,5] and caged bioactive species allow controlled release of function.[6,7] In addition, chemosensors report the location and activity of signaling species, such metal ions,[8] small molecules,[4] or enzymes.[9]

Specifically, chemosensors are an attractive approach for studying signaling because they generate an electrically or spectroscopically measurable signal upon binding or modification. Chemosensors may be of biotic or abiotic origin. Biotic chemosensors can be produced exclusively via genetic methods and are expressed and used within cells; for example, sensors based on the *Aequoria victoria* fluorescent proteins (AFPs). These endogenous probes have the advantage that introduction into the cell is not disruptive and that chemosensor size is not

prohibitive. Abiotic probes are prepared *ex vivo* and may be introduced into living cells *via* microinjection, transfection, or through utilization of protein transduction domains. These exogenous chemosensors include both small molecules and peptides; they provide unique and versatile sensing approaches because nonnatural elements may be incorporated. At the current time, abiotic and biotic probes complement each other; while the endogenous probes are large and limited in their composition, exogenous probes can be difficult to introduce to cells. An exciting combination of the power of both biotic and abiotic approaches has been achieved by site-specifically directing an exogenous label to an endogenous species.[10-12]

The chemosensing strategies described in this dissertation are designed to monitor two very different signaling species in biological systems: divalent zinc cations and protein kinase enzymes. The individual chapters will provide detailed descriptions of work in these fields while this introductory chapter will provide a general background to chemosensing and the general strategy utilized herein.

Properties of an Ideal Chemosensor

The ultimate goal is to study physiological processes in their native environment in a noninvasive manner. Fluorescence detection is ideal since it is noninvasive and exhibits a low background signal. The properties of an ideal fluorescent chemosensor have been discussed in depth elsewhere (refs. 2,3,13,14), and are summarized in Figure 1-1. Notably, chemosensors should rapidly bind the species that is relevant for signaling with good selectivity and signal sensitivity (Figure 1-1a-d). Additionally, the affinity for the target analyte should approximate the expected concentration; this condition prevents disruption of normal cellular signaling processes and allows detection of increases and decreases of the analyte (Figure 1-1e). The chemosensor should be stable to all aspects of the sensing environment (Figure 1-1f) and have appropriate fluorescence properties (Figure 1-1g). Ideally, a readout independent of chemosensor concentration is desirable; chemosensor concentration can be difficult to determine within a cell (Figure 1-1h). Finally, the chemosensor should be easily introduced and distributed uniformly within a cell (Figure 1-1i).

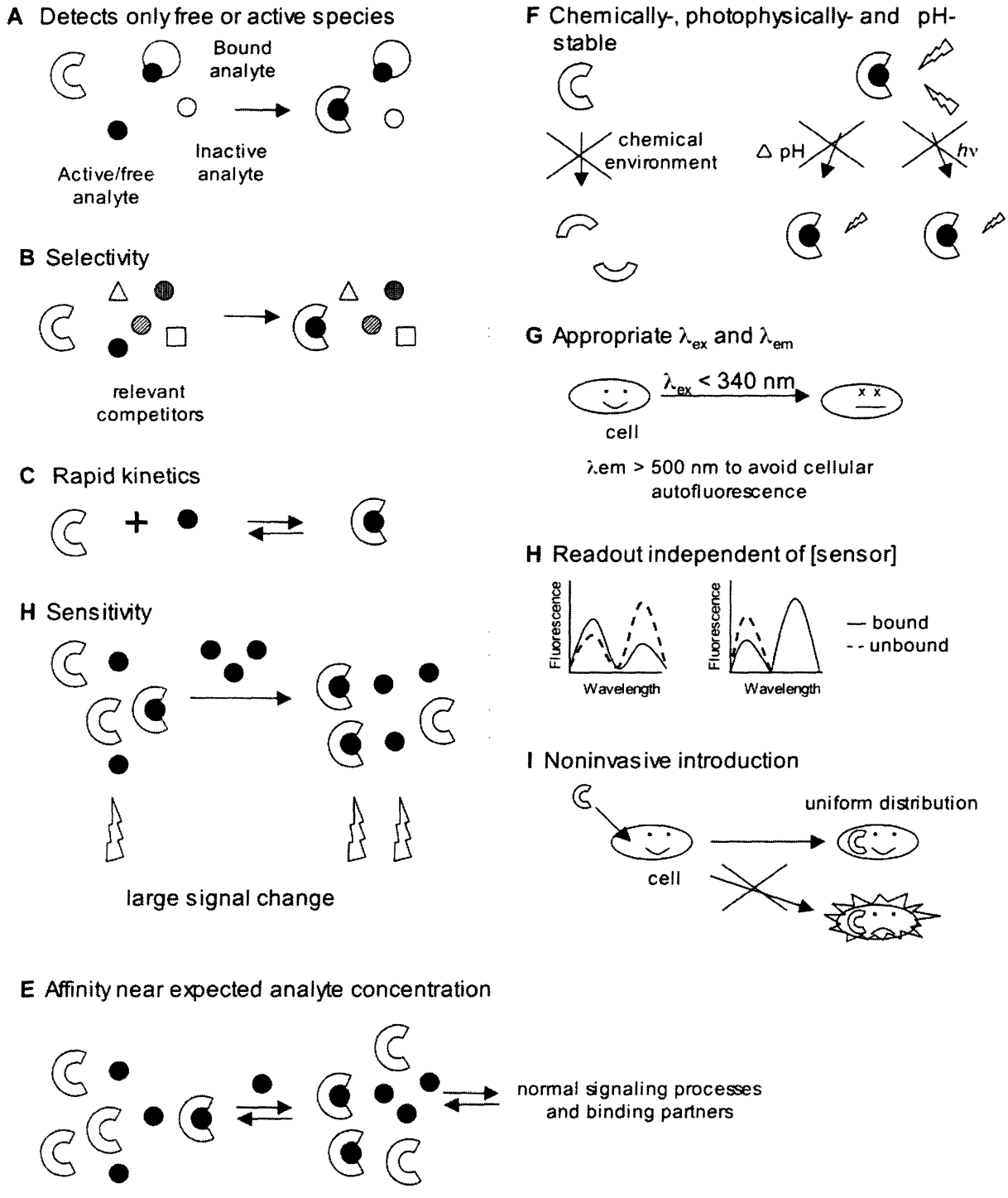

Figure 1-1. Properties of an ideal chemical sensor.

Advantages of Peptide-Based Chemosensors

A chemosensor built from a modular peptide scaffold offers many advantages. The modular architecture allows incorporation of both natural and nonnatural amino acids via combinatorial or rational design approaches, made facile via solid-phase peptide synthesis. Optimization and tuning can be easily achieved by altering the peptide sequence. A number of fluorescence-based sensing mechanisms have been implemented with peptide-based chemosensors in the Imperiali laboratory: chelation-enhanced fluorescence,[15-18] environment-sensitive fluorescence,[19-22] fluorescence quenching,[23,24] fluorescence resonance energy transfer (FRET),[25] and in some cases, metal-based fluorescence.[26,27] Incorporation of other functionalities is also feasible via amide bond formation, e.g. an additional fluorophore for an internal standard or a cellular internalization sequence[28-31] to transport the chemosensors into cells. In addition, the chemosensors could be attached to a solid support for diagnostic applications.

Metal-Chelating Peptides

Both sensing strategies described in this dissertation were inspired by previous work in this laboratory on the design of metal-binding peptides, many of which contained novel nonnatural chelating amino acids. In all cases, the β-turn motif (Figure 1-2), which causes a directionality change in a peptide sequence, has been used as a template for metal coordination between sets of natural or nonnatural amino acid ligands. β-turn motifs are classified into many different types, defined by the ϕ and ψ dihedral angles of the i+1 and i+2 residues. Many of these conformations promote hydrogen-bond formation between the carbonyl of the i residue and the amide proton of the i+3 residue. In particular, optimized type II and II' β-turns contain a heterochiral sequence in the two core residues (one D-amino acid and one L-amino acid) and are defined by the dihedral angles listed in Table 1-1.[32]

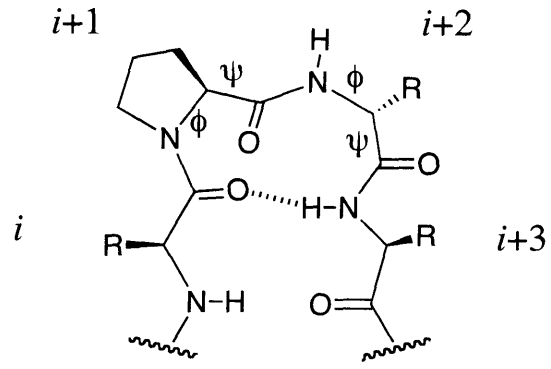

Figure 1-2. Structure of a β-turn

Table 1-1. φ and ψ dihedral angles and examples of Type II and II′ β-turns

Turn	ϕ_{i+1}	ψ_{i+1}	ϕ_{i+2}	ψ_{i+2}	Literature examples
II	-60	120	80	0	Pro-DSer, Pro-Gly
II'	60	-120	-80	0	DPro-Ser, Ser-DPro

Previous researchers in the Imperiali laboratory have defined reverse-turn motifs in short peptides sequences in aqueous solution and applied this knowledge to preorganize a metal-binding site. When a peptide sequence with significant type II β-turn propensity, Ac-Val-Pro-DSer-Phe-NH_2,[33] was flanked by metal-binding histidine or carboxylate ligands, chelation of Zn^{2+} and Co^{2+} was effectively promoted. The turn sequence was essential for metal-binding, as no metal-binding was observed when both *i*+1 and *i*+2 were glycine residues.[34] Further work involved replacing natural histidine and aspartate residues with nonnatural phenanthroline metal-chelating residues to alter the affinity of the peptide for Zn^{2+} and Co^{2+}. In addition, the use of sequences with a weaker propensity for type II β-turn structure, such as Thr-Pro-DAla-Val, could be incorporated to weaken the affinity for the metal ion. Thus, the affinity could be tuned over 5 orders of magnitude through modulation of both the turn sequence and the ligating residues.[35] Since these seminal investigations, the β-turn has been used as an important structural element in the *de novo* design of independently-folded proteins[36,37] and in metal-coordinating peptides[15,16]. In this dissertation, the β-turn sequence has been optimized for metal binding.

Dissertation Objective

Herein two types of modular peptide-based fluorescent chemosensors will be reported: tunable Zn^{2+} chemosensors and versatile probes of protein kinase activity. Both of these sensing strategies exploit a chelation-enhanced fluorescence (CHEF) sensing mechanism with an optimized two-residue β-turn sequence and the novel sulfonamidohydroxyquinoline amino acid Sox (Figure 1-3). This amino acid contains a derivative of the bidentate chelate fluorophore 8-hydroxyquinoline (Oxn) as the side chain and is named for the fluorophore unit sulfonamido-oxine. Oxn derivatives undergo an increase in fluorescence quantum yield upon metal binding to enable detection of certain metal ions. Additional background on the choice of fluorophore can be found in Chapter 2. The synthesis of the Sox amino acid will be presented in Chapter 2, and employs an asymmetric alkylation as the key synthetic step. Chapter 2 also provides relevant spectroscopic properties of the fluorophore.

A family of intensity-based Zn^{2+} chemosensors for use in monitoring a range of Zn^{2+} concentrations will be described in Chapter 3. This family of smaller, improved chemosensors for Zn^{2+} was inspired by previous metallopeptide designs. The optimized 2-residue β-turn sequence provided a smaller chemosensor with improved metal-binding properties. The binding stoichiometry, as well as the influence of other metal ions and pH, was carefully characterized for each chemosensor. Chapter 3 highlights the ability to design probes whose affinities have been tuned over two orders of magnitude with a modular peptide scaffold. The use of these chemosensors in concert for monitoring Zn^{2+} concentration will be illustrated. An extension of this peptide-based sensing platform to design ratiometric peptide-based Zn^{2+} chemosensors is also investigated. These chemosensors employ an additional fluorophore to provide internal calibration, and include both excitation and emission ratiometric chemosensors.

The Zn^{2+} chemosensors inspired a novel approach to use the Sox amino acid, a β-turn motif and the biologically available Mg^{2+} ion to sense phosphorylation of protein kinase peptide substrates. This versatile strategy, introduced in Chapter 4, allows detection of serine, threonine and tyrosine phosphorylation. These probes are the most sensitive for assessing kinase activities reported to date. The design involves an optimized peptide substrate for the target kinase, with a small sensing module appended, containing Sox and a β-turn. This module may be placed either N- or C-terminal to the residue to be phosphorylated. The probes are extremely effective due to

the large signal change upon phosphorylation and good reactivity with the target kinase. Notably, the reactivity of substrates is not affected by introduction of the sensing motif. High-throughput applications are introduced and further described in the following chapter. Chapter 5 details one valuable application of these probes in a multiplex high-throughput assay of kinase activity in unfractionated cell lysates. These kinase chemosensors are powerful tools for studying the activity of recombinant kinases *in vitro* and endogenous kinases *ex vivo*.

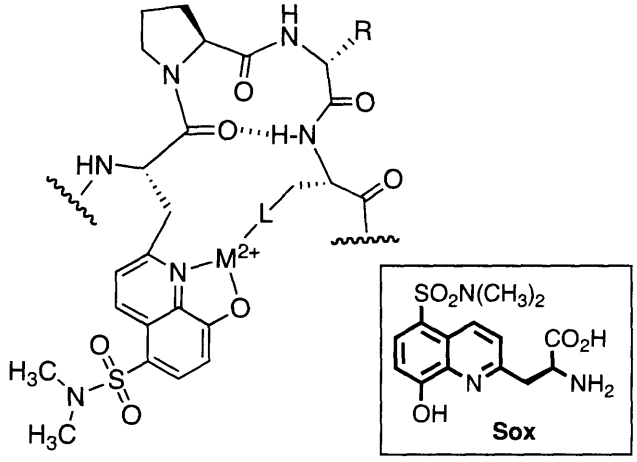

Figure 1-3. The metal-binding framework for fluorescent chemosensors containing the amino acid Sox, a two-residue β-turn motif and an additional ligand for the metal ion. Inset: chemical structure of Sox.

References

(1) Shogren-Knaak, M. A.; Alaimo, P. J.; Shokat, K. M. Recent advances in chemical approaches to the study of biological systems. *Annu. Rev. Cell Dev. Biol.* **2001**, *17*, 405-433.

(2) Tsien, R. Y. Fluorescent and photochemical probes of dynamic biochemical signals inside living cells. In *Fluorescent Chemosensors for Ion and Molecule Recognition*; Czarnik, A. W., Ed.; American Chemical Society: Washington, DC, 1993, p 130-146.

(3) Czarnik, A. W. Desperately seeking sensors. *Chem. Biol.* **1995**, *2*, 423-428.

(4) Zhang, J.; Campbell, R. E.; Ting, A. Y.; Tsien, R. Y. Creating new fluorescent probes for cell biology. *Nat. Rev. Mol. Cell. Biol.* **2002**, *3*, 906-918.

(5) Schreiber, S. L. The small-molecule approach to biology. *Chem. Eng. News* **2003**, *81*, 51-61.

(6) Shigeri, Y., Tatsu, Y., Yumoto, N. Synthesis and application of caged peptides and proteins. *Pharmacol. Ther.* **2001**, *91*, 85-92.

(7) Marriott, G., Roy, P., Jacobson, K. Preparation and light-directed activation of caged proteins. *Methods Enzymol.* **2003**, *360*, 274-288.

(8) Kikuchi, K.; Komatsu, K.; Nagano, T. Zinc sensing for cellular application. *Curr. Opin. Chem. Biol.* **2004**, *8*, 182-191.
(9) Baruch, A.; Jeffery, D. A.; Bogyo, M. Enzyme activity - it's all about image. *Trends Cell Biol.* **2004**, *14*, 29-35.
(10) Chen, I.; Ting, A. Y. Site-specific labeling of proteins with small molecules in live cells. *Curr. Opin. Biotechnol.* **2005**, *16*, 35-40.
(11) Miller, L. W.; Cornish, V. W. Selective chemical labeling of proteins in living cells. *Curr. Opin. Chem. Biol.* **2005**, *9*, 56-61.
(12) Jessani, N.; Cravatt, B. F. The development and application of methods for activity-based protein profiling. *Curr. Opin. Chem. Biol.* **2004**, *8*, 54-59.
(13) Lakowicz, J. R. *Principles of Fluorescence Spectroscopy*; 2nd ed.; Kluwer Academic/Plenum Publishers: New York, 1999.
(14) Czarnick, A. W. Supramolecular chemistry, fluorescence and sensing. In *Fluorescent Chemosensors for Ion and Molecule Recognition*; Czarnick, A. W., Ed.; American Chemical Society: Washington, DC, 1993, p 1-9.
(15) Walkup, G. K.; Imperiali, B. Stereoselective synthesis of fluorescent α-amino acids containing oxine (8-hydroxyquinoline) and their peptide incorporation in chemosensors for divalent zinc. *J. Org. Chem.* **1998**, *63*, 6727-6731.
(16) Jotterand, N.; Pearce, D. A.; Imperiali, B. Asymmetric synthesis of a new 8-hydroxyquinoline-derived α-amino acid and its incorporation in a peptidyl sensor for divalent zinc. *J. Org. Chem.* **2001**, *66*, 3224-3228.
(17) Shults, M. D.; Pearce, D. A.; Imperiali, B. Modular and tunable chemosensing scaffold for divalent zinc. *J. Am. Chem. Soc.* **2003**, *125*, 10591-10597.
(18) Shults, M. D.; Imperiali, B. Versatile fluorescence probes of protein kinase activity. *J. Am. Chem. Soc.* **2003**, *125*, 14248-14249.
(19) Walkup, G. K.; Imperiali, B. Design and evaluation of a peptidyl fluorescent chemosensor for divalent zinc. *J. Am. Chem. Soc.* **1996**, *118*, 3053-3054.
(20) Walkup, G. K.; Imperiali, B. Fluorescent chemosensors for divalent zinc based on zinc finger domains. enhanced oxidative stability, metal binding affinity, and structural and functional characterization. *J. Am. Chem. Soc.* **1997**, *119*, 3443-3450.
(21) Vazquez, M. E.; Nitz, M.; Stehn, J.; Yaffe, M. B.; Imperiali, B. Fluorescent caged phosphoserine peptides as probes to investigate phosphorylation-dependent protein associations. *J. Am. Chem. Soc.* **2003**, *125*, 10150-10151.
(22) Vazquez, M. E.; Blanco, J. B.; Imperiali, B. Photophysics and biological applications of the environment-sensitive fluorophore 6-N,N-dimethylamino-2,3-naphthalimide. *J. Am. Chem. Soc.* **2005**, *127*, 1300-1306.
(23) Torrado, A.; Imperiali, B. New synthetic amino acids for the design and synthesis of peptide-based metal ion sensors. *J. Org. Chem.* **1996**, *61*, 8940-8948.
(24) Torrado, A.; Walkup, G. K.; Imperiali, B. Exploiting polypeptide motifs for the design of selective Cu(II) ion sensors. *J. Am. Chem. Soc.* **1998**, *120*, 609-610.
(25) Pearce, D. A.; Walkup, G. K.; Imperiali, B. Peptidyl chemosensors incorporating a FRET mechanism for detection of Ni(II). *Bioorg. Med. Chem. Lett.* **1998**, *8*, 1963-1968.
(26) Franz, K. J.; Nitz, M.; Imperiali, B. Lanthanide-binding tags as versatile coexpression probes. *ChemBioChem* **2003**, *4*, 265-271.

(27) Nitz, M.; Franz, K. J.; Maglathlin, R. L.; Imperiali, B. A powerful combinatorial screen to identify high-affinity terbium(III)-binding peptides. *ChemBioChem* **2003**, *4*, 272-6.
(28) Wadia, J. S.; Dowdy, S. F. Protein transduction technology. *Curr. Opin. Biotechnol.* **2002**, *13*, 52-56.
(29) Kabouridis, P. S. Biological applications of protein transduction technology. *Trends Biotechnol.* **2003**, *21*, 498-503.
(30) Zorko, M.; Langel, Ü. Cell-penetrating peptides: mechanism and kinetics of cargo delivery. *Adv. Drug Deliv. Rev.* **2005**, *57*, 529-545.
(31) Dunican, D. J.; Doherty, P. Designing cell-permeant phosphopeptides to modulate intracellular signaling pathways. *Biopolymers* **2001**, *60*, 45-60.
(32) Rose, G. D.; Gierasch, L. M.; Smith, J. A. Turns in peptides and proteins. *Adv. Protein Chem.* **1985**, *37*, 1-109.
(33) Imperiali, B.; Fisher, S. L.; Moats, R. A.; Prins, T. J. A conformational study of peptides with the general structure Ac-L-Xaa-Pro-D-Xaa-L-Xaa-NH_2: Spectroscopic evidence for a peptide with significant β-turn character in water and in dimethyl sulfoxide. *J. Am. Chem. Soc.* **1992**, *114*, 3182-3188.
(34) Imperiali, B.; Kapoor, T. M. The reverse turn as a template for metal coordination. *Tetrahedron* **1993**, *49*, 3501-3510.
(35) Cheng, R. P.; Fisher, S. L.; Imperiali, B. Metallopeptide design: tuning the metal cation affinities with unnatural amino acids and peptide secondary structure. *J. Am. Chem. Soc.* **1996**, *118*, 11349-11356.
(36) Struthers, M. D.; Cheng, R. P.; Imperiali, B. Design of a monomeric 23-residue polypeptide with defined tertiary structure. *Science* **1996**, *271*, 342-345.
(37) Struthers, M. D.; Cheng, R. P.; Imperiali, B. Economy in protein design: evolution of a metal-independent ββα motif based on the zinc finger domains. *J. Am. Chem. Soc.* **1996**, *118*, 3073-3081.

Chapter 2:

Synthesis, Characterization and Fluorescence Properties of (*S*)-2-Amino-N^{α}-(9-fluorenylmethyloxycarbonyl)-3-(8-hydroxy-5-(*N*,*N*-dimethylsulfonamido)quinoline-2-yl) Propionic Acid (Fmoc-Sox-OH)

A significant portion of the work described in this chapter has been published in:
Shults, M. D.; Pearce, D. A.; Imperiali, B. Modular and tunable chemosensing scaffold for divalent zinc. *J. Am. Chem. Soc.* **2003**, *125*, 10591-10597.

Introduction

Fluorescence chemosensors utilizing CHEF to signal metal ion binding with a fluorescence signal consist of receptor and fluorophore domains; typically, these domains are separated by a spacer and can be quite large.[1] Analyte binding to the receptor is signaled to the attached fluorophore by a variety of mechanisms, reviewed in reference 2. A few CHEF fluorophores have receptor and fluorophore moieties that coexist; one example of such a fluorophore was introduced in Chapter 1, 8-hydroxyquinoline (Oxn, Figure 2-1). Oxn has been substantially used in analytical chemistry for metal ion detection.[3,4] Its small size and low susceptibility to photobleaching are desirable for sensing applications.

Oxn is weakly fluorescent in aqueous solution, but strongly fluorescent in the presence of certain metal ions. There are two theories regarding the origin of this large fluorescence change. The first is that the lowest electronic excited state of unbound Oxn (n -> π^* transition) is non-fluorescent due to rapid intersystem crossing. Metal chelation modulates the lowest energy excited state to the π -> π^* transition, which does not undergo intersystem crossing and thus is fluorescent.[3] Since intersystem crossing in unbound Oxn has been difficult to verify, an alternate theory is that photo-induced proton transfer from the phenolic hydroxyl to the quinoline nitrogen in the excited state of unbound Oxn results in fluorescence quenching.[5,6] Metal complexation results in deprotonation of the phenolic hydroxyl (due to a significantly lowered pK_a), thereby disrupting the quenching mechanism.[7]

The bidentate chelate moiety of Oxn is capable of binding many metal ions, with varying affinities. For example, the affinity of Oxn for Zn^{2+} is 4 orders of magnitude greater that that for Mg^{2+}.[8] Metal ions with filled valencies exhibit fluorescent complexes with Oxn, including Mg^{2+}, Ca^{2+}, Al^{3+}, Zn^{2+}, and Cd^{2+};[9] the emission wavelengths and quantum yields of these complexes vary moderately depending on the metal ion.[9,10] Complexes of Oxn with paramagnetic ions or "heavy atoms" are nonfluorescent because these ions perturb the electron spins of the ligand to favor intersystem crossing.[3]

A number of substituted derivatives of Oxn have been prepared with a range of fluorescence properties, in this laboratory[11] as well as in the Anzenbacker laboratory[12]. Chemical substitutions on the Oxn core dramatically alter the excitation wavelength, emission wavelength, ε_{max} and quantum yield of the fluorophore. In particular, the Zn^{2+} complex of 8-hydroxy-5-(*N*,*N*-

dimethylsulfonamido)-2-methylquinoline (**1**, Figure 2-1) is 150 times "brighter" than that of the parent fluorophore, 2-methyl-8-hydroxyquinoline (2-Me-Oxn, Figure 2-1), when compared at their respective fluorescence emission maxima.[11] Brightness is a product of the extinction coefficient (ε), which measures the probability of the electronic transition, and the quantum yield (Φ), which measures how efficiently photons absorbed are translated into photons emitted. Individual values for the Zn^{2+} complexes of 2-Me-Oxn and **1** in aqueous solution are ε_{max} = 2290 M^{-1} cm^{-1}, Φ = 0.004 and ε_{max} = 5560 M^{-1} cm^{-1}, Φ = 0.24, respectively.[11] A building block containing the sulfonamidohydroxyquinoline moiety would allow for unlimited placement within any peptide sequence. Indeed, less sensitive derivatives of Oxn have been successfully incorporated into peptide-based Zn^{2+} chemosensors in the Imperiali laboratory.[13,14]

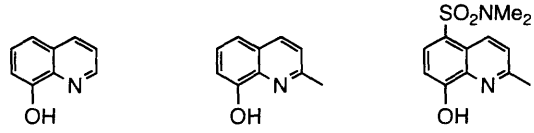

Oxn **2-Me-Oxn** **1**

Figure 2-1. Chemical structures of 8-hydroxyquinoline (Oxn), 2-methyl-8-hydroxyquinoline (2-Me-Oxn) and 8-hydroxy-5-(*N,N*-dimethylsulfonamido)-2-methylquinoline (**1**).

This chapter reports the integration of the enhanced CHEF fluorophore 8-hydroxy-5-(*N,N*-dimethylsulfonamido)-2-methylquinoline into the novel amino acid, Sox. The synthesis of optically pure nonnatural amino acids has been achieved by both asymmetric synthesis[15,16] and enantiomeric resolution.[17,18] Asymmetric synthetic methods typically require fewer synthetic steps and result in a higher yield of the desired enantiomer. In particular, the Corey adaptation[19,20] of the O'Donnell asymmetric alkylation method[15] has been shown to give outstanding yields of target enantiomers, and thus was chosen for the synthesis of Sox.

The general spectroscopic properties of Sox pertinent to the sensing strategies presented in this dissertation will also be investigated. Future chapters will describe the successful application of the Sox fluorophore for Zn^{2+} sensing and for phosphorylation sensing in concert with Mg^{2+}.

Results and Discussion:

Synthesis of Fmoc-Sox-OH

The synthesis of the protected amino acid is outlined in Scheme 2-1. Two modifications to the previously reported[11] synthesis of **1** from 8-hydroxyquinaldine resulted in an improved yield of sulfonamide **1**. First, dilution of the reaction mixture by 4-fold prevented the formation of a side-product with a mass corresponding to a dimer (m/z = 488). Second, restriction of the amount of dimethylamine base to 5 equivalents prevented the formation of a side product (m/z = 294) where the phenolic hydroxyl group was replaced by dimethylamine. This side reaction presumably proceeds through the semiquinone tautomer under highly basic conditions. The phenolic hydroxyl group of **1** was then protected as the *tert*-butyldiphenylsilyl ether. Smaller silyl ether protecting groups such as TBS and TBDMS were found to be significantly more labile on this compound (N. Jotterand, unpublished results).

Installation of a bromide on the 2-methyl group of the quinoline ring was desired to provide an appropriate precursor for the asymmetric alkylation. Conversion to the bromide in one step via a radical bromination was not successful because **2** was not soluble solvents compatible with this reaction (benzene or carbon tetrachloride). To circumvent this difficulty, a three-step procedure was performed without intermediate purification and included oxidation to the aldehyde **3** with selenium dioxide, reduction to the alcohol **4** with sodium borohydride, and bromination with *N*-bromosuccinimide and triphenylphosphine. Intermediate purification was not performed due to the instability of the aldehyde and alcohol on silica gel. Purification of bromide **5** was accomplished via chromatography on florisil. NMR analysis revealed that the purified bromide contains 15% of **1**, brought through from the selenium dioxide oxidation step. This impurity does not affect future reactions and can be washed away during peptide synthesis.

Synthesis of the Sox amino acid from **5** was performed by the Corey adaptation[19,20] of the O'Donnell asymmetric alkylation method,[15] utilizing (*8S,9R*)-*O*-(9)-allyl-*N*-9-anthracenyl methylcinchonidium bromide as the phase-transfer catalyst. Since the benzophenone imine and *tert*-butyldiphenylsilyl ether are relatively acid labile, the adduct from the alkylation reaction was not purified by silica gel chromatography but instead hydrolyzed immediately upon complete formation in refluxing 6 M hydrochloric acid. The product, **Sox**, was isolated as the hydrochloride salt and used without further purification.

A pure sample of this amino acid was derivatized with Marfey's reagent (1-fluoro-2,4-dinitrophenyl-5-L-alanine amide)[21] to determine that the reaction gave 96% e.e. in favor of the L-enantiomer. Preference for L-enantiomer formation with the catalyst *O*-(9)-allyl-*N*-9-anthracenyl methylcinchonidium bromide is well-established over a wide range of electrophiles.[20] Marfey's reagent derivatized the phenolic hydroxyl group in addition to the free amine (Scheme 2-2). Because bis-derivatization began prior to complete consumption of the free amino acid, rigorous e.e. determination required that bis-derivatization to proceed to completion. At this point, it was confirmed that integration of signals from mono-derivatized peaks after 24 hours gave a reasonable estimate of the e.e. for analysis of additional samples.

For subsequent peptide synthesis, the free amine was protected with the 9-fluorenyl-methoxycarbonyl (Fmoc) group by treatment with 9-fluorenylmethyl succinimidyl carbonate (Fmoc-OSu) to give Fmoc-Sox-OH in 70% yield over 3 steps by NMR. For the synthesis of peptides throughout the remainder of this dissertation, Fmoc-Sox-OH is used without further purification in standard Fmoc solid-phase peptide synthesis (SPPS). The small amount of peptide containing D-Sox is separated from the desired peptide during HPLC purification.

Scheme 2-1. Synthesis of Fmoc-Sox-OH

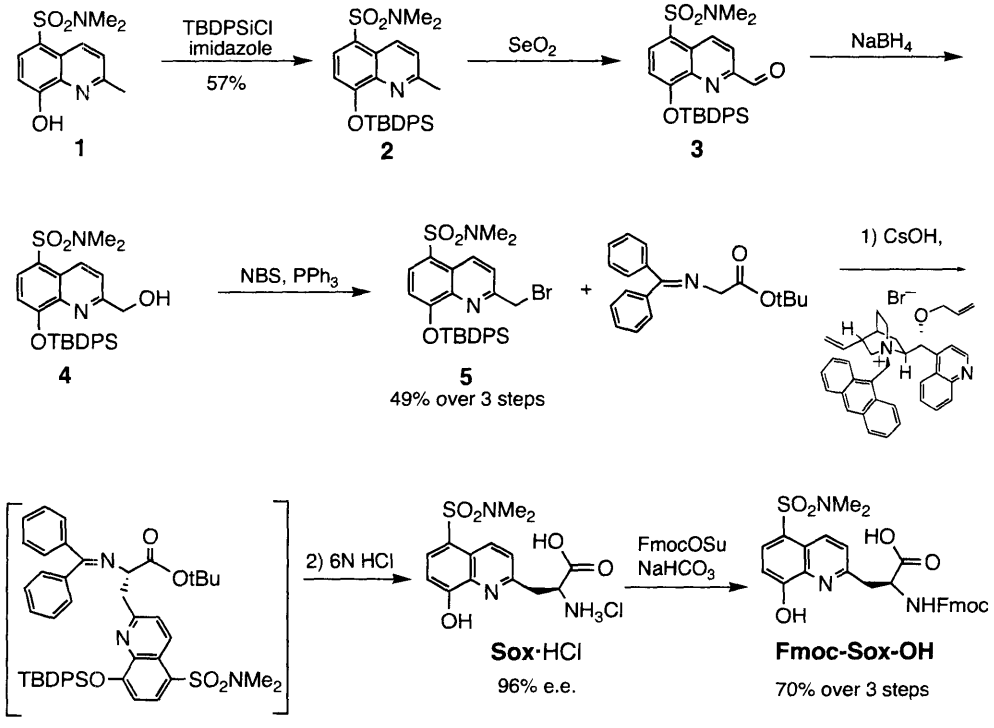

Scheme 2-2. Derivatization of Sox with Marfey's reagent.

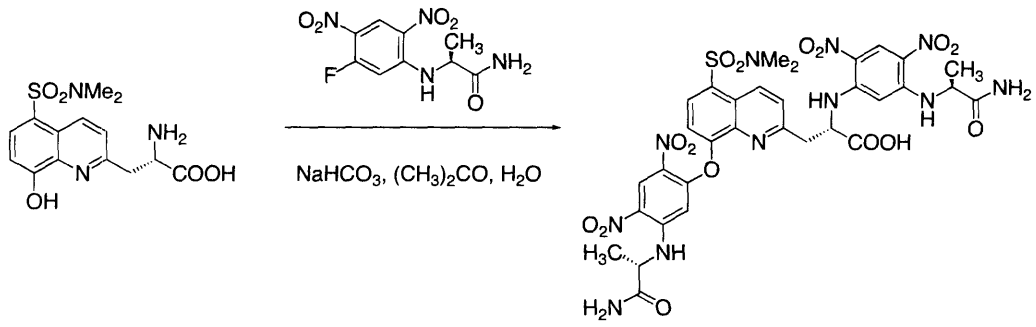

Spectroscopic Properties of Sox

Both UV-Vis and fluorescence spectroscopy were used to characterize Sox. Due to limited solubility of the amino acid, fluorescence properties were assessed with peptides containing Sox. The specific sequences used to obtain spectra are not particularly relevant to the data presented in this chapter but have been noted in the figure legends; their synthesis is also reported in subsequent chapters.

A UV-Vis spectrum of the free Sox ligand shows maximum absorbance bands at 246 nm and 316 nm (Figure 2-2). Upon binding of a variety of metal ions, these bands shift to 260 nm and 360 nm (Figure 2-2). The fact that the same shift is observed with increasing pH indicates that deprotonation of the hydroxyl group results in the observed change in electronic properties upon metal ion binding. The intensity of the 360 nm band does not depend on the type of metal ion but is sensitive to solvent.

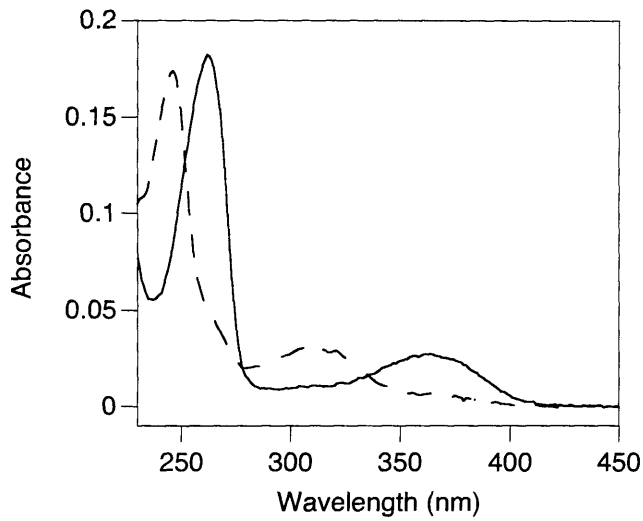

Figure 2-2. UV-Vis absorbance spectra of a peptide containing Sox (Ac-Sox-Val-Pro-DSer-Phe-Glu-Ser-Ser-NH_2, 4 μM) in absence (- -) and presence (—) of Zn^{2+} (80 μM) in 50 mM Hepes (pH 7.0), 150 mM NaCl.

The excitation and emission spectra for the fluorescent complexes of Sox with Zn^{2+}, Cd^{2+}, Mg^{2+}, Ca^{2+} were investigated (Figure 2-3). Saturating concentrations of these metal ions were used to ensure that the 1:1 complex was observed. It is immediately apparent that the fluorescence intensities differ significantly depending on the metal ion. The maximum excitation wavelengths all occur at 360 nm, but there are slight differences in the maximum emission wavelength (Table 2-1). These differences allow some discrimination between metal ions based on the fluorescence emission spectra.

The separation between the excitation and emission wavelengths (the Stokes' shift) for all complexes is quite large. This large Stokes' shift results in low background at the emission wavelength and allows many different excitation and emission wavelengths to be used for sensing applications.

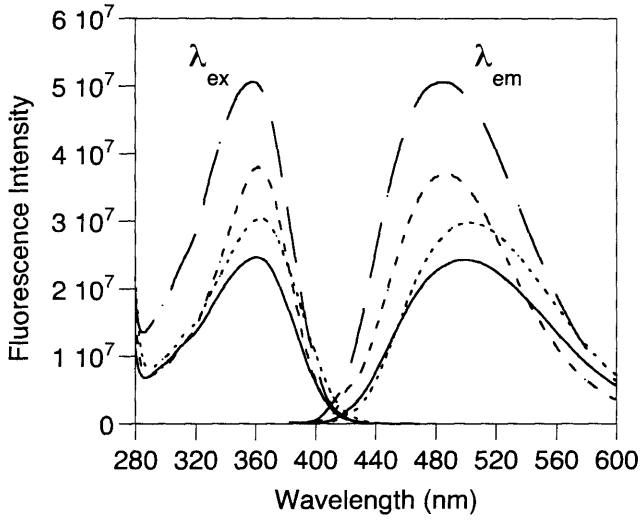

Figure 2-3. Excitation and emission spectra of a peptide containing Sox (Ac-Sox-Pro-DSer-Glu-Ser-Ser-NH_2, 10 μM) in the presence of Zn^{2+} (——, 10 μM), Mg^{2+} (— —, 50 mM), Ca^{2+} (– –, 400 mM), and Cd^{2+} (---, 10 μM) in 50 mM Hepes (pH 7.0), 150 mM NaCl.

Table 2-1. Fluorescence properties of various Sox-metal ion complexes.[a]

Metal Ion	$\lambda_{ex,max}$ (nm)	$\lambda_{em,max}$ (nm)	Relative Intensity
Zn^{2+}	360	500	1
Mg^{2+}	360	485	2
Ca^{2+}	360	483	1.5
Cd^{2+}	360	503	1.2

[a] Data were obtained from spectra in Figure 3.

Conclusion:

The Sox amino acid has been synthesized in good yield and enantiomeric excess for peptide-based sensing applications. This work provides a chemical building block for peptide-based chemosensor construction that can be utilized in laboratories that are not equipped to do chemical manipulations. The spectroscopic properties of peptides containing Sox are influenced by the type of bound metal ion. While absorption and excitation spectra are identical, the fluorescence emission spectra vary in intensity and maximum wavelength. This understanding of the fluorescence properties of Sox will be useful for chemosensing applications.

Acknowledgements

I would like to thank Nathalie Jotterand for early procedures towards the synthesis of Fmoc-Sox-OH and for providing the catalyst used for the asymmetric alkylation. I also thank Dierdre Pearce for many helpful discussion. I am gratefull to Mayssam Ali and Kevin McDonnell for solving the mystery regarding the side-product of formation of **1** (m/z = 294). Research grants were provided by the NSF (CHE-9996335) and an NSF graduate research fellowship. The NMR spectrometers at MIT were provided by a grant from the NSF (DBI-9729592 and CHE-9808061) and NIH (1S10RR13886-01).

Experimental

General Synthetic Procedures and Materials

All starting materials, solvents and reagents except *N*-bromosuccinimide (NBS) from commercial suppliers were used without further purification. The NBS (Aldrich) was recrystallized from 10 times its weight in water to form white flakes.[22] Dry dioxane and *N*,*N*-dimethylformamide (DMF) were purchased from Aldrich. Selenium dioxide (98%+, less than a year old from Aldrich) and was a fine off-white powder (bright white or chunky solid is not effective). *O*-(9)-Allyl-*N*-9-anthracenylmethylcinchonidium bromide was prepared according to the method described by Corey.[19] Dry dichloromethane was distilled from calcium hydride. Dry tetrahydrofuran was distilled from sodium/benzophenone. Glassware for anhydrous reactions was oven-dried overnight, and cooled under nitrogen. Water or air-sensitive reactions were carried out under a positive pressure of nitrogen. Glass-backed thin layer chromatography plates were obtained from EM Science (silica gel 60 F_{254}, 0.25 micron thickness) and visualized by UV or for free amines, 0.2% ninhydrin solution followed by heat. Flash column chromatography was performed on 230-400 mesh silica gel according to the Still procedure.[23] Chemical shifts are reported relative to a value of 0 ppm for TMS or 0 ppm for 3-(trimethylsilyl)-1-propane-sulfonic acid sodium salt for samples in DMSO-d_6 or D_2O.

Instrumentation

NMR Spectrometers: Varian 500 MHz instrument.

High-Performance Liquid Chromatography (HPLC): Waters 400 and 600 systems (solvent A = water, 0.1% v/v TFA; solvent B = MeCN, 0.1% v/v TFA). Columns used: C_{18} analytical, Beckman Ultrasphere ODS, 5 μm, 150 x 4.6 mm; C_{18} preparatory, YMC-Pack Pro, 5 μm, 250 x 20 mm.

*5-(N,N-Dimethyl)sulfonamido-8-hydroxy-2-methylquinoline (**1**):*

A solution of dimethylamine in tetrahydrofuran (2 M, 7 ml, 14 mmol), was added under nitrogen to tetrahydrofuran (300 ml). The 8-hydroxy-2-methylquinoline-5-sulfonyl chloride (665 mg, 2.58 mmol) was added in small portions over 3 hours (about 15 mg per addition every 4 minutes). The solution was stirred an additional 10 minutes, and the solvent was removed by rotary evaporation. Excess dimethylamine was removed by re-dissolving the sticky solid in dichloromethane and removing by rotary evaporation (3 x 50 ml). The slightly pink-orange solid obtained was purified by flash chromatography (silica gel, ethylacetate/hexane, 1:2) to yield a white solid (626 mg, 91%). TLC R_f = 0.38 (silica, 2:1 hexanes/ethyl acetate) ^{1}H NMR, ESI-MS and other data is consistent with that obtained by Pearce *et. al.*[11]

*8-tert-Butyldiphenylsilyloxy-5-(N,N-dimethyl)sulfonamido-2-methylquinoline (**2**):*

8-Hydroxyquinaldine-5-(*N,N*-dimethyl)sulfonamide (515 mg, 1.93 mmol), imidazole (141 mg, 2.07 mmol), dry DMF (3 ml) and *tert*-butyldiphenylsilyl chloride (0.55 ml, 2.11 mmol) were sequentially added to a dry flask under nitrogen and the mixture was stirred for 2 hours. The solution was diluted with ethyl acetate (250 ml), washed with saturated ammonium chloride solution (50 ml), brine (2 x 50 ml) and dried ($MgSO_4$). The solvent was removed by rotary evaporation and the white solid was purified by flash chromatography (silica gel, 9:1 hexanes/ethyl acetate) to yield a white solid (0.55 g, 57%). The silica gel was pretreated by stirring with acetone for 15 min. to decrease product decomposition on the column. m.p. 157.5-158°C. TLC R_f = 0.10 (silica, hexanes/ethyl acetate, 9:1), R_f = 0.32 (silica, hexanes/ethylacetate, 4:1) ^{1}H NMR (500 MHz, $CDCl_3$) δ 8.78 (d, J = 8.5 Hz, 1H), 7.96 (d, J = 8.5 Hz, 1 H), 7.73 (dd, J = 7.5 Hz, 0.5 Hz, 4 H), 7.34 (pseudo-triplet, J = 7.5 Hz, 2 H), 7.28 (t, J

= 7.5 Hz, 4 H), 7.17 (d, J = 8.5 Hz, 1 H), 7.13 (d, J = 8.0 Hz, 1 H), 2.70 (s, 6 H), 2.17 (s, 3 H), 1.15 (s, 9H). ^{13}C NMR (125 MHz, $CHCl_3$) δ 157.6, 156.8, 140.6, 134.8, 134.0, 133.1, 131.1, 129.4, 127.4, 124.5, 123.5, 123.4, 115.0, 37.4, 26.6, 23.7, 20.2. HRMS (+ESI-MS): Calcd for $C_{28}H_{33}N_2O_3SSi$ $[M+H]^+$ 505.1976, Found 505.1973.

*8-tert-Butyldiphenylsilyloxy-5-(N,N-dimethyl)sulfonamido-2-formylquinoline (**3**):*
8-*tert*-Butyldiphenylsilyloxy-2-methyl-5-(*N*,*N*-dimethyl)sulfonamidoquinoline (0.92g, 1.83 mmol) was added to a dry flask under nitrogen, followed by dry dioxane (13.3 ml) and molecular sieves (4 Å, 600 mg). Selenium dioxide (250 mg, 2.25 mmol) was added and the reaction was stirred at 95°C for 17 hours and then cooled to room temperature. The reaction mixture was filtered through celite to remove the black residue and molecular sieves, and the celite was washed with dioxane (~ 30 ml, until no chromophore was detected by UV when spotting on silica gel TLC plates). The dioxane was removed by rotary evaporation and the yellow oil was re-dissolved in ethyl acetate (900 ml), washed with brine (100 ml), water (100 ml), saturated potassium carbonate solution (100ml) and dried ($MgSO_4$). Rotary evaporation of the solvent yielded a sticky yellow oil (932 mg, 95%) which was used in the next step without further purification. TLC R_f = 0.50 (silica, 2:1 hexanes/ethyl acetate). ^1H NMR (500 MHz, $CDCl_3$) δ 9.58 (d, J = 0.5 Hz, 1 H), 9.10 (dd, J = 9 Hz, 1 H), 8.14 (d, J = 8.5 Hz, 1 H), 7.95 (d, J = 9.0 Hz, 1H), 7.70-7.76 (m, 4 H), 7.29-7.46 (m, 6 H), 7.17 (d, J = 8.5 Hz, 1 H), 2.74 (s, 6 H), 1.21 (s, 9 H).

*8-tert-Butyldiphenylsilyloxy-5-(N,N-dimethyl)sulfonamido-2-(hydroxymethyl)quinoline (**4**):*
Sodium borohydride (70 mg, 1.80 mmol) was dissolved in absolute ethanol (15 ml) and cooled to 0°C. To this solution was added dropwise a solution of the crude aldehyde (932 mg, 1.80 mmol) in dry dichloromethane (30 ml). The reaction mixture was stirred for 15 minutes, then diluted with diethyl ether (800ml), washed with saturated ammonium chloride (200 ml), water (2 x 100 ml), brine (100 ml), and dried ($MgSO_4$). The solvent was removed by rotary evaporation to yield a pale yellow sticky solid (804 mg, 86%). This material was used in the subsequent step without purification. TLC R_f = 0.14-0.37 (silica, ethyl acetate). ^1H NMR (300 MHz, $CDCl_3$) δ

8.98 (d, J = 8.7 Hz, 1 H), 7.95 (d, J = 8.1 Hz, 1 H), 7.70-7.77 (m, 4 H), 7.27-7.44 (m, 7 H), 7.05 (d, J = 8.1 Hz, 1 H), 4.67 (s, 2 H), 2.72 (s, 6 H), 1.19 (s, 9 H).

*2-Bromomethyl-8-tert-butyldiphenylsilyloxy-5-(N,N-dimethyl)sulfonamidoquinoline (**5**):*
The alcohol from the previous reaction (804 mg, 1.54 mmol) was dried over P_2O_5 overnight and then was dissolved in dry dichloromethane (8 ml) under nitrogen. The solution was cooled to 0°C and then *N*-bromosuccinimide (275 mg, 1.54 mmol) and triphenylphosphine (445 mg, 1.69 mmol) were added to the reaction. The reaction was stirred at 0°C for 4 hours, after which it was diluted with diethyl ether (1200 ml), washed with water (150 ml), brine (100 ml) and dried ($MgSO_4$). The solvent was removed by rotary evaporation to give a white solid (1.32 g), which was purified by flash chromatography (florisil, 100-200 mesh, 9:1 hexanes/ethyl acetate) to yield a clear oil (538 mg, 49% over 3 steps). This sample contains a 10% impurity, which was not present in its first fractions off the column. These first fractions (also a clear oil) were used for characterization. TLC R_f = 0.10 (silica, hexanes/ethyl acetate, 9:1), R_f = 0.31 (silica, hexanes/ethylacetate, 4:1) ^{1}H NMR (500 MHz, $CDCl_3$) δ 8.93 (d, J = 8.9 Hz, 1 H), 8.02 (d, J = 8.2 Hz, 1 H), 7.73 (dd, J = 7.9, 1.2 Hz, 4 H), 7.51 (d, J = 9.1 Hz, 1 H), 7.37 (tt, J = 7.3, 2.4 Hz, 2 H), 7.30 (t, J = 7.3 Hz, 4 H), 7.16 (d, J = 8.5 Hz, 1 H), 4.12 (s, 2 H), 2.72 (s, 6 H), 1.17 (s, 9 H). ^{13}C NMR (125 MHz, $CDCl_3$) δ 157.4, 155.6, 140.5, 135.1, 134.8, 133.6, 132.6, 129.9, 127.8, 125.6, 124.0, 122.9, 116.0, 37.5, 32.9, 26.8, 20.4. HRMS (+ESI-MS): Calcd for $C_{28}H_{31}BrN_2O_3SSi$ $[M+H]^+$ 583.1083, Found 583.1059.

*(S)-2-Amino-3-(8-hydroxy-5-(N,N-dimethylsulfonamido)quinoline-2-yl)propionic acid hydrochloride salt (**Sox·HCl**):* To a dry flask was added *N*-(diphenylmethylene)glycine *tert*-butyl ester (141 mg, 0.477 mmol), (*8S, 9R*)-*O*-(9)-allyl-*N*-9-anthracenyl methylcinchonidium bromide (29 mg, 0.047 mmol), and cesium hydroxide monohydrate (800 mg, 4.76 mmol). Dry dichloromethane (12 ml) was added and the solution was stirred vigorously. The flask was cooled to –78°C, whereafter a solution of the bromide (300 mg, 0.514 mmol) was added dropwise. The solution was kept at –78°C for 20 hours, and –55°C until the imine was consumed by TLC (31 hours). The suspension was poured into diethyl ether (300 ml), then washed with water (50 ml), brine (40 ml), and dried ($MgSO_4$). The solvent was removed by

rotary evaporation to give a yellow oil (391 mg). This oil was immediately hydrolyzed, due to its instability under column chromatography conditions. 6N HCl (6.8 ml) was added to the flask and the reaction mixture was refluxed for 2 hours. The solution was diluted with 1 M HCl (15 ml) and washed with ethyl acetate (2 x 10 ml). The solvent was removed under reduced pressure to give an orange solid (200 mg). An analytical sample was obtained via preparatory HPLC t_R (5 min. 15% B followed by linear gradient 15-60% B over 25 min.) = 14.9 min. TLC R_f = 0.57 (silica, *n*-butanol/water/acetic acid/ethyl acetate, 1:1:1:1), R_f = 0.34 (silica, *n*-butanol/water/acetic acid, 4:1:1). m.p. 185-186°C (dec.) ^{1}H NMR (500 MHz, $(CD_3)_2SO$) δ 8.97 (d, J = 8.8 Hz, 1 H), 8.08 (d, J = 8.2 Hz, 1 H), 7.72 (d, J = 8.8 Hz, 1 H), 7.28 (d, J = 8.2 Hz, 1 H), 4.75 (bs, 1 H), 3.67 (dd, J = 16.5 Hz, 4.3 Hz, 1 H), 3.52 (dd, J = 16.8 Hz, 7.6 Hz, 1 H), 2.70 (s, 6 H). ^{13}C NMR (125 MHz, $(CD_3)_2SO$) δ 172.6, 159.2, 157.5, 139.0, 135.8, 133.9, 126.0, 125.9, 122.3, 111.6, 52.3, 38.7, 38.6. HPLC (C_{18}; solvent A = water, 0.1% v/v TFA; solvent B = MeCN, 0.1% v/v TFA), t_R (5 min. 25% B followed by linear gradient 25-45% B over 25 min. = 11.42 min. HRMS (+ESI-MS): Calcd for $C_{14}H_{18}ClN_3O_5S$ $[M]^+$ 340.0962, Found 340.0963. $[\alpha]^{20}_D$ = +6.0 (c = 1.0, MeOH/1M HCl, 9:1).

Determination of Enantiomeric Excess

Derivatization of the amino acid with 1-fluoro-2,4-(dinitrophenyl)-5-L-alanineamide (FDAA, Marfey's reagent) was used to determine the enantiomeric excess. To a solution of (*S*)-2-amino-3-(8-hydroxy-5-(*N,N*-dimethyl)sulfonamidoquinoline)propionic acid hydrochloride salt (1.0 mg, 2.66 μmol) in acetonitrile/water (235 μl, 1:1) was added sodium bicarbonate solution (21 μl, 1 M, 21 μmol, 7.9 eq.) and FDAA solution (140 μl, 14 mg/ml, 7.2 μmol). The solution was vortexed and stirred at 40°C. Free amino acid disappeared after 24 hours, but bis-derivatization began after 15 hours and continued up to 7 days, during which additional sodium bicarbonate solution (20 μl) and FDAA solution (50 μl) were added every 24 hours. After completion, the reaction was adjusted to pH 4 with 1 M hydrochloric acid. Following centrifugation, a 10 μl aliquot was diluted to 100 μl with acetonitrile/water (1:1) to be analyzed by HPLC t_R: S derivative = 32.2 min, R derivative = 30.2 min. A 96.5% e.e was calculated by comparison of peak areas at both monitoring wavelengths (228 nm, 340 nm). The identities of both peaks were confirmed by ESI-MS (calcd for $C_{32}H_{33}N_{11}O_{15}S$ $[M+H]^+$ 844.2, Found 844.3).

*(S)-2-Amino-N^{α}-(9-fluorenylmethyloxycarbonyl)-3-(8-hydroxy-5-(N,N-dimethylsulfonamido)quinoline-2-yl) Propionic Acid (**Fmoc-Sox-OH**):* To a suspension of crude amino acid (145.1 mg, 0.386 mmol) and sodium bicarbonate (164.8 mg, 1.96 mmol, 5 eq.) in water (2.2 ml) was added dropwise a solution of (9-fluorenylmethyl)succinimidyl carbonate (144.1 mg, 0.427 mmol, 1.1 eq.) in dioxane (6 ml). The reaction was stirred at room temperature for 18 h, after which the dioxane was removed by rotary evaporation. The aqueous phase was washed with diethyl ether (3 x 7 ml) and then acidified to pH 3 with 1 N hydrochloric acid. The aqueous phase was then extracted with ethyl acetate (4 x 8 ml). The combined ethyl acetate phases were dried ($MgSO_4$) and the solvent was removed by rotary evaporation to yield a yellow solid (160 mg, 74%). An analytical sample was obtained via preparatory HPLC t_R (5 min. 45 % B followed by linear gradient 45-70% B over 25 min.) = 28.6 min. m.p. 114-116°C. TLC R_f = 0.24 (silica, dichloromethane/methanol, 9:1), R_f = 0.17 (silica, dichloromethane/methanol/acetic acid, 94:5:1) ^{1}H NMR (data for major rotamer reported) (400 MHz, $CDCl_3$) δ 9.06 (d, J = 8.8 Hz, 1 H), 8.07 (d, J = 8.4 Hz, 1 H), 7.71 (d, J = 6.8 Hz, 2 H), 7.45-7.53 (m, 3 H), 7.32-7.37 (m, 2 H), 7.19-7.24 (m, 2 H), 7.11 (d, J = 8.4 Hz, 1 H), 5.79 (d, J = 8 Hz, 1 H), 5.05-5.15 (m, 1 H), 4.32-4.44 (m, 2 H), 4.14-4.19 (m, 1 H), 3.69 (d, J = 4Hz, 2 H), 2.73 (s, 6 H). ^{13}C NMR (125 MHz, $CDCl_3$) δ 176.4, 173.1, 156.8, 156.5, 156.0, 143.6, 141.1, 137.0, 135.4, 132.8, 127.7, 127.0, 109.4, 67.2, 51.9, 46.9, 39.0, 37.4. HRMS (+ESMS): Calcd for $C_{29}H_{27}N_3O_7S$ $[M+H]^+$ 562.1642, Found 562.1663. $[\alpha]^{20}_D$ = + 44.3 (c = 1.8, CH_2Cl_2).

Spectroscopic Studies:

Instrumentation: Beckmann DU7500 UV-Vis spectrophotometer, Jobin Yvon FluoroMax-3 fluorimeter (5 nm slits)

Solution preparation: Stock solutions of peptides containing Sox were quantified by UV-Vis based on the extinction coefficient of the fluorophore unit, 5-(*N*,*N*-dimethylsulfonamido)-8-hydroxy-2-methylquinoline (ε_{355} = 8247 M^{-1} cm^{-1} in 0.1M NaOH, 1 mM Na_2EDTA). Metal ion stock solutions were prepared from $ZnCl_2$ (Aldrich, 99.98%), $MgCl_2$ (Alfa Aesar, Puratronic grade), $CaCl_2$ (Alfa Aesar, Puratronic grade), $CdCl_2$ (Mallinckrodt) and were quantified by standardized solution of EDTA (Aldrich) in the presence of an Eriochrome Black T (Aldrich).[24]

References

(1) de Silva, A. P.; Gunaratne, H. Q. N.; Gunnlaugsson, T.; Huxley, A. J. M.; McCoy, C. P.; Rademacher, J. T.; Rice, T. E. Signaling recognition events with fluorescent sensors and switches. *Chem. Rev.* **1997**, *97*, 1515-1566.

(2) Czarnik, A. W. Supramolecular chemistry, fluorescence, and sensing. In *Fluorescent Chemosensors for Ion and Molecule Recognition*; Czarnik, A. W., Ed.; American Chemical Society: Washington, D.C., 1993, p 1-9.

(3) Seitz, W. R. Fluorescence derivatization. In *CRC Critical Reviews in Analytical Chemistry*; CRC Press: Boca Raton, FL, 1980; Vol. 8, p 367-404.

(4) Rao, T. P.; Gladis, J. M. Oxines as preconcentration agents in inorganic trace analysis. *Rev. Anal. Chem.* **2001**, *20*, 145-159.

(5) Goldman, M.; Wehry, E. L. Environmental effects upon fluorescence of 5- and 8-hydroxyquinoline. *Anal. Chem.* **1970**, *42*, 1178-1185.

(6) Bardez, E.; Devol, I.; Larrey, B.; Valeur, B. Excited-state processes in 8-hydroxyquinoline: photoinduced tautomerization and solvation effects. *J. Phys. Chem. B* **1997**, *101*, 7786-7793.

(7) Bronson, R. T.; Montalti, M.; Prodi, L.; Zaccheroni, N.; Lamb, R. D.; Dalley, N. K.; Izatt, R. M.; Bradshaw, J. S.; Savage, P. B. Origins of 'on-off' fluorescent behavior of 8-hydroxyquinoline containing chemosensors. *Tetrahedron* **2004**, *60*, 11139-11144.

(8) Sillen, L. G.; Martell, A. E. *Stability Contants of Metal-Ion Complexes*; The Chemical Society: London, 1964.

(9) Stevens, H. M. The effect of the electronic structure of the cation upon fluorescence in metal-8-hydroxyquinoline complexes. *Anal. Chim. Acta* **1959**, *20*, 389-396.

(10) Lytle, F. E.; Storey, D. R.; Juricich, M. E. Systematic atomic number effects in complexes exhibiting ligand luminescence. *Spectrochimica Acta* **1973**, *29A*, 1357-1369.

(11) Pearce, D. A.; Jotterand, N.; Carrico, I. S.; Imperiali, B. Derivatives of 8-hydroxy-2-methylquinoline are powerful prototypes for zinc sensors in biological systems. *J. Am. Chem. Soc.* **2001**, *123*, 5160-5161.

(12) Pohl, R.; Montes, V. A.; Shinar, J.; Anzenbacker, P. J. Red-green-blue emission from tris(5-aryl-8-quinolinolate)Al(III) complexes. *J. Org. Chem.* **2004**, *69*, 1723-1725.

(13) Walkup, G. K.; Imperiali, B. Stereoselective synthesis of fluorescent α-amino acids containing oxine (8-hydroxyquinoline) and their peptide incorporation in chemosensors for divalent zinc. *J. Org. Chem.* **1998**, *63*, 6727-6731.

(14) Jotterand, N.; Pearce, D. A.; Imperiali, B. Asymmetric synthesis of a new 8-hydroxyquinoline-derived α-amino acid and its incorporation in a peptidyl sensor for divalent zinc. *J. Org. Chem.* **2001**, *66*, 3224-3228.

(15) O'Donnell, M. J. The enantioselective synthesis of α-amino acids by phase-transfer catalysis with achiral schiff base esters. *Acc. Chem. Res.* **2004**, *37*, 506-517.

(16) Calmes, M.; Daunis, J. How to build optically active alpha-amino acids. *Amino Acids* **1999**, *16*, 215-250.

(17) Chen, S.-T.; Wang, K.-T.; Wong, C.-H. Chirally selective hydrolysis of D,L-amino acid esters by alkaline protease. *J. Chem. Soc. Chem. Commun.* **1986**, *20*, 1514-1516.

(18) Chenault, H. K.; Dahmer, J.; Whitesides, G. M. Kinetic resolution of unnatural and rarely occurring amino acids: enantioselective hydrolysis of N-acyl amino acids catalyzed by acylase I. *J. Am. Chem. Soc.* **1989**, *111*, 6354-6364.

(19) Corey, E. J.; Xu, F.; Noe, M. C. A rational approach to catalytic enantioselective enolate alkylation using a structurally rigidified and defined chiral quaternary ammonium salt under phase transfer conditions. *J. Am. Chem. Soc.* **1997**, *119*, 12414-12415.

(20) Corey, E. J.; Noe, M. C.; Xu, F. Highly enantioselective synthesis of cyclic and functionalized α-amino acids by means of a chiral phase transfer catalyst. *Tetrahedron Lett.* **1998**, *39*, 5347-5350.

(21) Fujii, K.; Ikai, Y.; Mayumi, T.; Oka, H.; Suzuki, M.; Harada, K. A nonempirical method using LC/MS for determination of the absolute configuration of constituent amino acids in a peptide: elucidation of limitations of Marfey's method and of its separation mechanism. *Anal. Chem.* **1997**, *69*, 3346-3352.

(22) Dauben, H. J.; McCoy, L. L. N-bromosuccinimide. I. Allylic bromination, a general survey of reaction variables. *J. Am. Chem. Soc.* **1959**, *81*, 4863-4873.

(23) Still, W. C.; Kahn, M.; Mitra, A. Rapid chromatographic technique for preparative separations with moderate resolution. *J. Org. Chem.* **1978**, *43*, 2923-2925.

(24) Basset, J.; Denney, R. C.; Jeffery, G. H.; Mendham, J. *Vogel's Textbook of Quantitative Inorganic Analysis*; William Clowers: London, 1978.

Chapter 3:

Modular and Tunable Chemosensing Scaffold for Divalent Zinc

A significant portion of the work described in this chapter has been published in:
Shults, M. D.; Pearce, D. A.; Imperiali, B. Modular and tunable chemosensing scaffold for divalent zinc. *J. Am. Chem. Soc.* **2003**, *125*, 10591-10597.

Introduction

Selective and tunable chemosensors for selected transition metal ions have the potential to afford qualitative and quantitative information about the presence, distribution and concentration of these metal ions in cells or tissues. Sensing for divalent zinc is particularly desirable because it is a prominent transition metal ion in biological systems.[1-4] Zn^{2+} is involved in cellular signaling pathways,[5,6] signaling at neural synapses,[7-9] and it is co-released with insulin from glucose-stimulated pancreatic islet β-cells.[10-12] Concentrations of Zn^{2+} associated with physiological signaling are in the nM-μM range.[9]

A plethora of examples exist in the literature of zinc fluorophore sensors, for extensive reviews, please see references 13-17. Small-molecule probes as well as peptide- and protein-based chemosensors have been developed for Zn^{2+}. These chemosensors signal the presence of Zn^{2+} by either changes in intensity ("intensity sensors") or a change in the excitation or emission wavelength ("ratiometric sensors"). These two classes will be introduced separately.

Intensity-based Zn^{2+} Chemosensors

Intensity-based Zn^{2+} chemosensors report the present of Zn^{2+} with an increase in fluorescence emission intensity. The original Zn^{2+} chemosensors TSQ[18] and Zinquin[19] (Figure 3-1a,b) were the first to be used to identify pools of free Zn^{2+} available for signaling. Since this time, small-molecule intensity probes with improved properties, notably ZPs,[20-23] ZnAFs,[24,25] and FluoZin-3[26,27] (Figure 3-1c-e), have been used extensively to study Zn^{2+} in signaling. These chemosensors contain a chelate moiety attached to a fluorophore such that, in the presence of Zn^{2+}, photoinduced electron transfer (PET) quenching, which occurs in the unbound probe, is disrupted to afford enhanced fluorescence emission. PET occurs when an electron from the nitrogen lone pair in the chelate moiety relaxes before fluorescence emission can occur; PET is disrupted when this lone pair is engaged in binding Zn^{2+}. ZPs, ZnAFs and FluoZin-3 are based on fluorescein, so they are quite bright. However, the majority contain aliphatic nitrogen ligands and thus suffer from protonation at physiological pH, which also disrupts PET quenching. The latest variants, ZP8 and ZnAF-2F, have improved pK_a properties and are useful over a broader

pH range. These probes generate 2-11-fold increases in fluorescence upon binding Zn^{2+}, depending on the efficiency of PET-quenching in the unbound state.

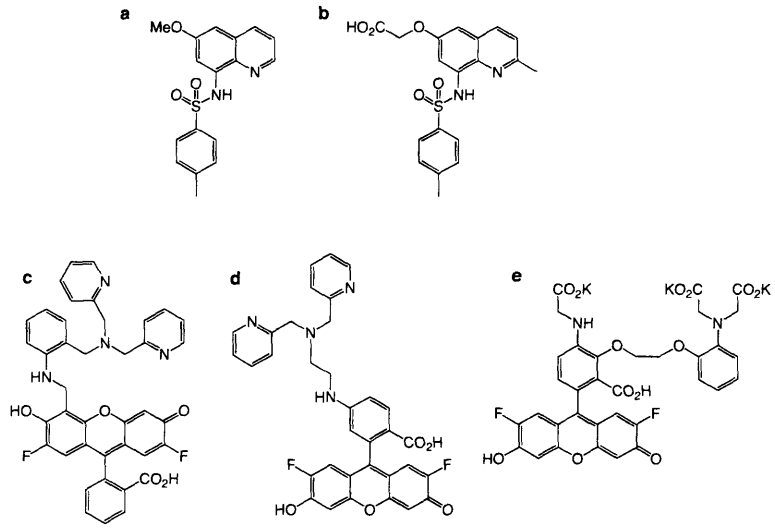

Figure 3-1. Structures of existing small-molecule Zn^{2+} chemosensors: (**a**) TSQ;[18] (**b**) Zinquin;[19] (**c**) ZP8;[20] (**d**) ZnAF-2F;[24] (**e**) FluoZin-3.[26]

Most peptide- and protein-based Zn^{2+} intensity sensors (Figure 3-2) have been inspired by natural Zn^{2+}-binding motifs. One protein-based sensor is an altered blue fluorescent protein (BFP, Figure 3-2a).[28] The BFP fluorophore comprises a dipyrrole unit of a porphyrin, which can bind Zn^{2+} in biological systems. Mutations were introduced in the protein to allow Zn^{2+} binding. This construct signaled Zn^{2+}-binding with a 2-fold fluorescence enhancement and a dissociation constant of 50 μM. In the Imperiali laboratory, zinc finger domains have been engineered with a single and small modification, an environment-sensitive dansyl fluorophore (Figure 3-2b).[29] When the dansyl fluorophore is appropriately placed in the sequence, it is solvent-exposed prior to Zn^{2+} binding but becomes packed into the hydrophobic core upon recognition of Zn^{2+}. This environment change results in an increase in fluorescence intensity and a shift in the emission wavelength. Several variants have been prepared with dissociation constants in the low pM to low nM range.[30] The large size of all of these peptide and protein probes can be prohibitive from a synthetic standpoint. Thus, Walkup and Imperiali generated a small, peptide-based Zn^{2+} chemosensor with an amino acid containing an 8-hydroxyquinoline moiety (Figure 3-2c).[31] However, this chemosensor exhibited weak fluorescence intensity. Finally, the most elegant protein-based sensing approach has been developed by the laboratories of Carol Fierke and

Richard Thompson.[32,33] These sensors are based on the enzyme carbonic anhydrase, which utilizes a Zn^{2+} co-factor. Apo-carbonic anhydrase variants sense Zn^{2+} by formation of a ternary complex with a fluorophore containing a sulfonamide moiety (Figure 3-2d). Certain sulfonamide fluorophores have a high affinity for Zn^{2+} bound in the carbonic anhydrase active site, and exhibit an increase in fluorescence intensity. Fierke and Thompson have generated a family of carbonic anhydrase-based Zn^{2+} sensors whose affinities span 7 orders of magnitude through modulation of the Zn^{2+} binding ligands and nearby residues. To overcome the limitation of ternary complex formation, a "reagentless" carbonic anhydrase-based sensor has been reported.[34]

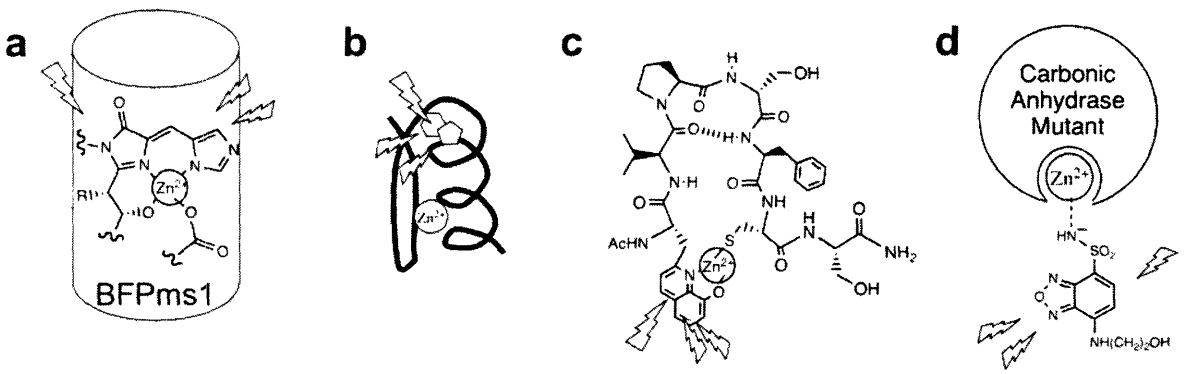

Figure 3-2. Schematic depictions of peptide and protein intensity-based Zn^{2+} chemosensors. (**a**) The site surrounding the BFP fluorophore is modulated to bind Zn^{2+} and trigger a fluorescence change.[28] (**b**) An environment-sensitive fluorophore incorporated into a side chain in a Zn^{2+} finger domain is buried in the hydrophobic pocket upon Zn^{2+} binding and exhibits in a fluorescence increase.[29] (**c**) A peptide-based chemosensor containing cysteine, the fluorophore 8-hydroxyquinoline, and a β-turn sequence to preorganize Zn^{2+} binding.[31] (**d**) A two-component system utilizing a carbonic anhydrase mutant and a sulfonamide-based fluorophore signals Zn^{2+} when the sulfonamide becomes deprotected upon binding.[32]

Ratiometric Zn^{2+} Chemosensors

Ratiometric chemosensors provide a means of internal calibration so that the analyte concentration can be determined independently of chemosensor concentration. These probes exhibit a shift in either excitation or emission wavelengths upon binding to the analyte; the Zn^{2+} concentration can then be determined from a ratio of excitation or emission wavelengths. Ratiometric probes are preferable over intensity-based probes because the emission of intensity-

based fluorescence probes is often affected by many other factors besides the concentration of Zn^{2+}. These variables include the intensity of the excitation source, the efficiency of the collection source, the distribution of the probe and the thickness of the optical section through which the image is collected.[35,36]

Currently, several examples of small-molecule ratiometric Zn^{2+} probes exist. Woodroofe and Lippard have coupled an additional fluorophore to Zn^{2+} probe as an internal standard (Figure 3-3a).[37] In this design, the linker between the Zn^{2+} chemosensor and the additional fluorophore is sensitive to esterases inside a cell; upon linker cleavage, the two fluorophores do not photophysically interact and are shown to colocalize inside cells. The Lippard laboratory has also developed two additional ratiometric chemosensors that are a hybrid between two fluorophores. In one case, the binding of Zn^{2+} causes a tautomerization between fluorescein and naphthofluorescein, which have distinct fluorescence properites (Figure 3-3b).[38] In the other case, the "rhodamine-like" fluorescence properties of the probe is disturbed upon Zn^{2+} binding to the nitrogen lone pair and the fluorescence behavior becomes "fluorescein-like" (Figure 3-3c).[39] Several probes have been developed based on an internal charge transfer (ICT) mechanism, such as IndoZin[27] (Figure 3-3d), FuraZin[27] (Figure 3-3e), and ZnAF-R2[40] (Figure 3-3f). This mechanism is complex but the main principle is that binding of Zn^{2+} influences the dipole moment of the fluorophore and changes the nature of the excited state. This most often results in changes in excitation wavelength, but can also exhibit changes in emission wavelength depending on the fluorophore. Additional interesting Zn^{2+} ratiometric fluorophores are 2-(2'-benzenesulfonamidophenyl)benzimidazole (Figure 3-3g), where Zn^{2+} disrupts excited state intramolecular proton transfer fluorescence quenching,[41] and related Zinbo-5 (Figure 3-3h), which can be excited by two-photon microscopy.[42]

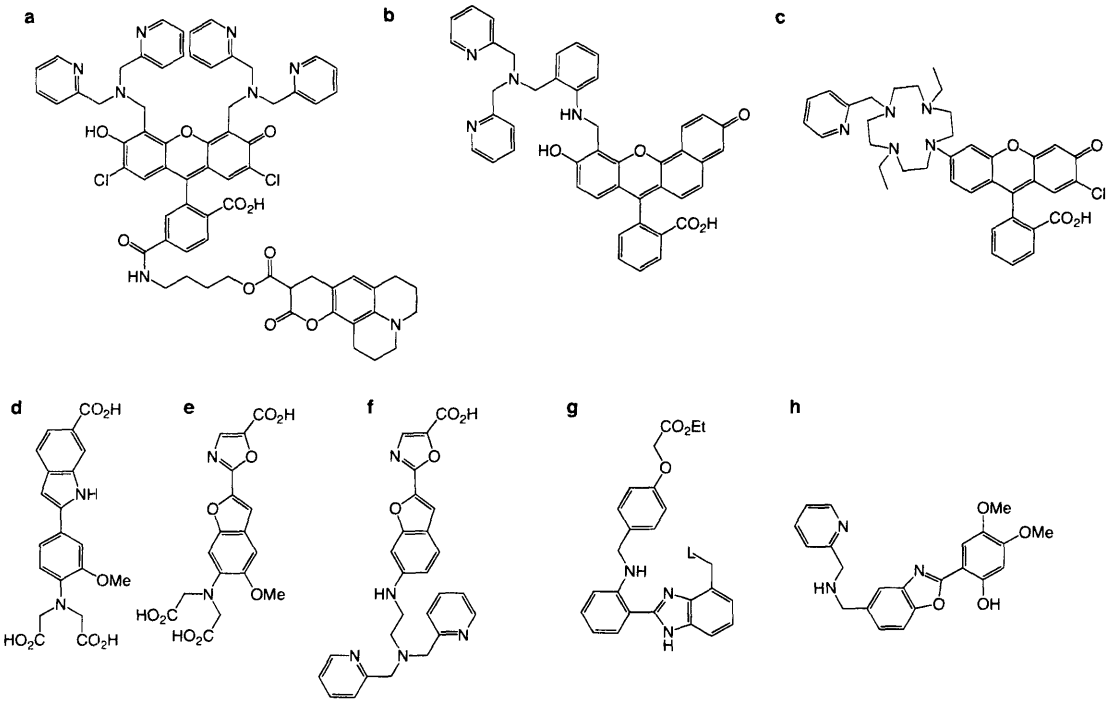

Figure 3-3. Structures of small-molecule ratiometric Zn^{2+} probes. (**a**) Coumazin;[37] (**b**) ZNP1;[38] (**c**) RF-1;[39] (**d**) IndoZin;[27] (**e**) FuraZin;[27] (**f**) ZnAF-R2;[40] (**g**) 2-(2'-benzenesulfonamidophenyl)-benzimidazole;[41] (**h**) Zinbo-5.[42]

Peptide and protein probes that operate via a FRET mechanism can be used to quantify Zn^{2+} with a ratio of excitation or emission wavelengths. These probes include donor and acceptor fluorophores whose relative distance is modulated upon Zn^{2+} binding, thereby altering the efficiency of energy transfer. Both metallothionein[43] (Figure 3-4a) and zinc finger domains[44] (Figure 3-4b) labeled with organic fluorophores have extremely low detection limits for Zn^{2+}. The metallothionein probe responds to Zn^{2+} loading without stoichiometry information, because there are multiple binding sites. The carbonic anhydrase approach mentioned previously has been extended to a FRET sensor by labeling of a carbonic anhydrase mutant with an acceptor fluorophore (Figure 3-4c).[36]

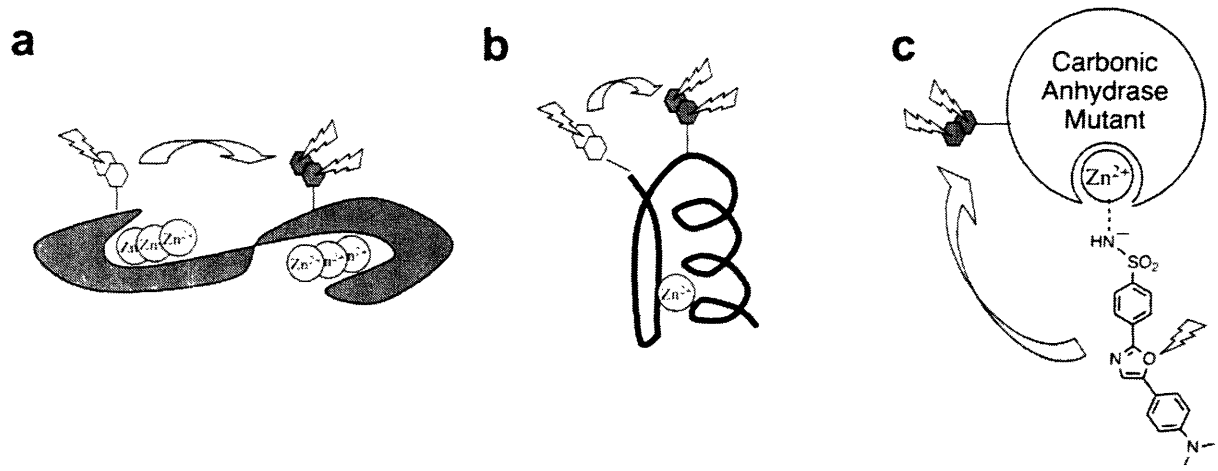

Figure 3-4. Peptide- and protein-based Zn^{2+} ratiometric chemosensors. (**a,b**) The distance between a pair of FRET fluorophores is altered upon Zn^{2+} binding to (**a**) metallothionein[43] and (**b**) a Zn^{2+} finger peptide;[44] (**c**) The fluorescence signal from the Zn^{2+}-bound sulfonamide can be transferred to a FRET acceptor on carbonic anhydrase.[36]

Importance of Tuning Probe Affinity

Quantifying free Zn^{2+} is only possible at Zn^{2+} concentrations at or near the dissociation constant of the chemosensor. Since the Zn^{2+} concentrations associated with signaling are unknown, it is important to be able to tune the affinity of a chemosensor for Zn^{2+}. With any probe, Zn^{2+} concentrations between 10% and 90% saturation can be quantified. When Zn^{2+} affinities are too tight, equilibrium is not maintained and the probe is completely bound under physiological conditions. Many of the currently available chemosensors are limited by their tight Zn^{2+} affinities (subnanomolar). There exist probes with micromolar affinity for Zn^{2+}, such as those based on Ca^{2+} chemosensors (FluoZin-3, FuraZin, IndoZin) where one carboxylate ligand has been removed.[27] However, the selectivity of these probes in the presence of physiological Mg^{2+} concentrations has not been sufficiently investigated. The ability to easily tune the affinity by modulating the ligands is critical and can be achieved by several means. For example, the ratiometric benzimidazole fluorophore reported by Fahrni[41] has been tuned over 6 orders of magnitude with 3 different probes by altering the chelating group denoted by L (Figure 3-3g). In addition, the Lippard laboratory has reported convergent syntheses to tune spectroscopic and chelate properties for their ZP[20] and newer ZS[45] probes. The modular nature of peptide synthesis allowed variants of the zinc-finger probes reported by Grant Walkup to be assembled with a

range of subnanomolar affinities. Genetic point-mutations were used to access the carbonic anhydrase family of probes; these probes have been developed to bind Zn^{2+} with affinities over several orders of magnitude up to 1 μM. However, these probes are quite large and must be manipulated by molecular biology methods. With the exception of the carbonic anhydrase probes, effective coverage over nanomolar concentrations of Zn^{2+} has not been achieved. Thus, optimized chemosensors are still needed to quantify nanomolar to micromolar Zn^{2+} concentrations.

Sox-Based Zn^{2+} Chemosensor Approach

Towards this end, the research presented herein is aimed at developing an addressable family of low molecular weight chemosensors with a range of Zn^{2+} affinities in the nM-μM range. These chemosensors would make it possible to determine Zn^{2+} concentration via analysis of the relative fluorescence intensities of multiple chemosensors with different affinities for Zn^{2+}. Alternatively, an additional fluorophore can be appended to any peptide in the family to give rise to a series of ratiometric Zn^{2+} chemosensors, enabling measurements of Zn^{2+} concentration independently of chemosensor concentration.

This new generation of chemosensors is smaller and more sensitive than the original design (Figure 3-3f) developed by Grant Walkup.[31] These peptide-based chemosensors exhibit tuned affinity for divalent zinc in the nM-μM range originating from the modular peptide architecture. An additional advantage of the peptide scaffold is that the fluorophore chosen need not form a completely selective 1:1 complex with Zn^{2+} because additional specificity determinants can be incorporated into the peptide sequence.

The basic design of the chemosensor peptides includes the Sox residue and a residue that affords an additional ligand for Zn^{2+} flanking a β-turn sequence, which pre-organizes the metal-ion binding site. The basic features of the design are represented in Figure 3-5. To tune the affinity, the additional ligand(s) and the β-turn sequence in the peptide are varied. Each peptide contains only six to eight amino acids. Two of these are serine residues, appended to the carboxy-terminus, to increase peptide solubility without interfering with metal binding. Further variation may be achieved through incorporation of an N-terminal module as a functionalized capping group instead of an amino acid derivative (Figure 3-5b). Preliminary experiments

involving adaptation of this modular Zn^{2+} sensing scaffold for FRET-based ratiometric sensing is also reported. In these probes, an additional fluorophore is appended on either side of the Zn^{2+} sensing motif.

Since these chemosensors are sufficiently polar not to be cell-permeable, they may be useful for detection of extracellular Zn^{2+} or as a diagnostic tool for medical or environmental samples. For applications in living cells, these chemosensors could be modified with additional modules that have been optimized in this laboratory to permeate cell membranes.[46]

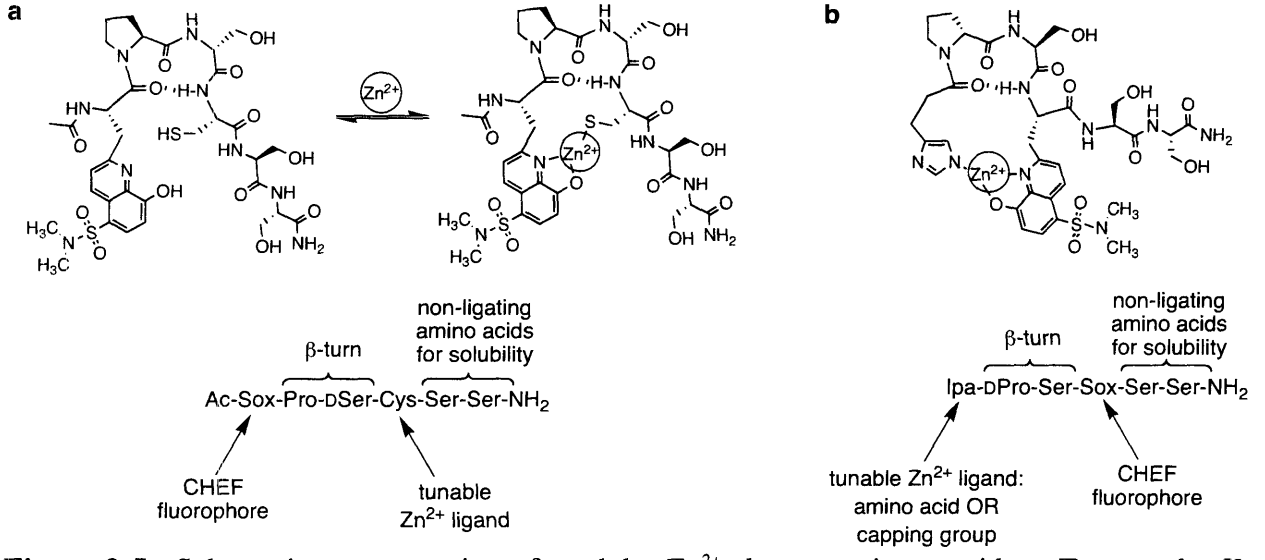

Figure 3-5. Schematic representation of modular Zn^{2+} chemosensing peptides. To tune the K_D for Zn^{2+}, the β-turn sequence, additional Zn^{2+} ligand, and the ligand arrangement are altered. Two of the general ligand arrangements used are pictured in **a** and **b**. The peptide in **b** has the additional flexibility that a functionalized capping group can be used as a ligand instead of an amino acid.

Results and Discussion

Background for Design Strategy

Initially, peptides similar to those containing Oxn or PhOxn amino acids reported previously from this laboratory[31,47] were synthesized with a 4-residue β-turn sequence sandwiched between Sox and an additional ligand for Zn^{2+}; for example, Ac-Sox-Val-DPro-Ser-Phe-Asp-Ser-Ser-NH_2 illustrates such a design. These 4-residue β-turn sequences were chosen because the *i* and *i*+3 residues have been important for maintaining β-turn conformations in the

absence of metal ions (see Chapter 1 for an explanation). However, peptides containing a 4-residue turn sequence and an additional ligand other than a cysteine exhibited complex binding equilibria. Thus, the sequence was pared down to the 2 critical residues, i+1 and i+2, to decrease the size and improve chelation with ligands in the i and i+3 positions.

Intensity-Based Peptide Chemosensor Design and Synthesis

Nineteen peptide sequences were designed, synthesized and characterized (Table 3-1). These peptides were synthesized via standard Fmoc SPPS. The identity of each of the peptides was confirmed by mass spectrometry and the purity was verified by RP-HPLC. These peptides differ in number and type of Zn^{2+}-binding ligands, ligand arrangement or β-turn sequence to modulate their affinity for Zn^{2+}.

Table 3-1. Zn^{2+} Chemosensors Peptide Sequences and Dissociation Constants

Peptide	Sequence[a]	Apparent K_D for 1:1 complex (nM)[b]	Complex(es) formed (Zn^{2+}:peptide)
P1	Ac-**Sox**-Pro-Ser-**Pen**-Ser-Ser-NH_2 [c]	9.6 ± 2.6	1:1
P2	**Ipa**-Gly-**Cys**-DPro-Gly-**Sox**-Ser-Ser-NH_2 [d]	11 ± 2	1:1
P3	Ac-**Sox**-Pro-Gly-**Cys**-Ser-Ser-NH_2	12 ± 1	1:1
P4	Ac-**Cys**-Pro-DSer-**Sox**-Ser-Ser-NH_2	15 ± 4	1:1
P5	Ac-**Sox**-Pro-DSer-**Cys**-Ser-Ser-NH_2	19 ± 5	1:1
P6	**Ipa**-Gly-**His**-DPro-Ser-**Sox**-Ser-Ser-NH_2 [d]	35 ± 5	1:1
P7	Ac-**Sox**-Pro-DSer-**pSer**-Ser-Ser-NH_2 [e]	130 ± 10	1:1
P8	Ac-**Sox**-Pro-DSer-**His**-Ser-Ser-NH_2	190	1:1 and 1:2
P9	**Ipa**-Pro-βPhe-**Sox**-Ser-Ser-NH_2 [d,f]	330	1:1 and 1:2
P10	**Ipa**-DPro-Gly-**Sox**-Ser-Ser-NH_2 [d]	360 ± 20	1:1
P11	**Ipa**-DPro-Ser-**Sox**-Ser-Ser-NH_2 [d]	530 ± 30	1:1
P12	Ac-**Sox**-Pro-DSer-**Glu**-Ser-Ser-NH_2	730 ± 80	1:1
P13	Ac-**Sox**-Pro-DSer-**Asp**-Ser-Ser-NH_2	910 ± 50	1:1
P14	**Ipa**-Pro-Gly-**Sox**-Ser-Ser-NH_2 [d]	990	1:1 and 1:2
P15	**Ipa**-Pro-DSer-**Sox**-Ser-Ser-NH_2 [d]	1100	1:1 and 1:2
P16	**Ipa**-Gly-Asn-**Sox**-Ser-Ser-NH_2 [d]	1600	1:1 and 1:2
P17	**Ipa**-Pro-Ser-**Sox**-Ser-Ser-NH_2 [d]	1900	1:1 and 1:2
P18	**Ipa**-Pro-βPhe-**Sox**-Ser-Ser-NH_2 [d,f]	3000	1:1 and 1:2
P19	Ac-**Sox**-Pro-DSer-Phe-Ser-Ser-NH_2	12000	1:1 and 1:2

[a] Ligating residues are indicated in bold, β-turn sequence is underlined.

[b] Obtained via direct fluorescence titration with $ZnCl_2$ in 50 mM Hepes (pH 7.0), 150 mM NaCl. Values reported with standard deviation are obtained from triplicate titrations with a peptide concentration near the K_D. Values without standard deviations are obtained via a single titration at [peptide] = 50 nM. K_D values are calculated by a global non-linear least-squares fit with the program Specfit/32.[48]

[c] Pen = β-dimethylcysteine; [d] Ipa = 3-(imidazol-4-yl)propionic acid; [e] pSer = phosphoserine;

[f] P9 and P18 each include one of the enantiomers of DL-βPhe.

The nineteen peptides contain thiolate, imidazole, phosphate or carboxylate ligands for Zn^{2+}. Several different β-turn sequences were investigated: type I (Pro-Ser, Gly-Asn), type II (Pro-DSer, Pro-Gly), type II' (DPro-Ser, DPro-Gly), and Pro-βPhe, which was inspired by turn sequences used in this laboratory for caged Zn^{2+} peptides.[49] Variation of the ligand orientation and number of ligands also altered the coordination environment.

Absorbance and Fluorescence Properties

In the presence of saturating $ZnCl_2$, the Sox peptides exhibit a maximum emission at 500 nm with a maximum excitation at 360 nm. In addition, these peptides maintain the striking luminescence properties of the fluorophore.[50] The extinction coefficient (ε_{max}) and quantum yield (Φ) values for representative chemosensor-Zn^{2+} complexes were determined following quantitative amino acid analysis (QAA) (Table 3-2). These representative chemosensors span the range of ligands and affinities for Zn^{2+}. The average of these ε_{max} and Φ values for representative peptides are 6200 M^{-1} cm^{-1} and 0.16, respectively; the 10% standard deviation results from the error in concentration of stock solutions determined by QAA. In the absence of Zn^{2+}, the quantum yields are less than 0.005, indicating a substantial 30-fold increase in fluorescence upon binding Zn^{2+}.

Table 3-2. Extinction Coefficient and Quantum Yield Values for Representative Peptides[a]

Peptide	$\varepsilon_{360\ nm}$ (M^{-1} cm^{-1})	$\Phi_{complex}$ [b]	$\Phi_{peptide}$ [b]
P3	5800	0.18	0.005
P6	5600	0.17	0.001
P10	5600	0.16	0.003
P12	7000	0.13	0.001
P13	6800	0.14	0.004

[a] Conditions: 50 mM Hepes (pH 7.0), 150 mM NaCl
[b] Relative to quinine sulfate (Φ_{360} = 0.55).

Summary of Binding Studies

Peptide binding characteristics were assessed via titrations with $ZnCl_2$ and Job plot analysis to determine the affinity and stoichiometry of complex formation. Titration data is fit with the program Specfit/32,[48] which analyzes multiwavelength data using an iterative method to obtain the association constant in terms of the $[Zn]_f$. Direct titrations were performed for all

peptide sequences under similar conditions for comparison purposes. Only dissociation constants for the 1:1 complex are listed in Table 3-1 and discussed in the following section because these depend the most heavily on the β-turn sequence and the additional Zn^{2+} ligand.

Binding Stoichiometry

Methods for assessing the binding stoichiometry are important to determine which chemosensors will be useful for quantifying Zn^{2+}. For the peptides listed in Table 3-1, four criteria were used to determine binding stoichiometry: a Job plot, a Scatchard plot, the model used for K_D calculation and the maximum fluorescence emission wavelength. To illustrate the conclusion from each method, data for peptides P13, which forms only a 1:1 Zn^{2+}:peptide complex, and P8, which forms both 1:1 and 1:2 complexes, are included. These data are representative of all peptide sequences synthesized. The first indication of exclusive 1:1 complex formation is a Job plot[51] that is symmetrical and exhibits a maximum at 0.5 mole fraction of Zn^{2+} (Figure 3-6a). However, a Job plot with a maxima at any other value besides 0.5 indicates formation of additional complexes; in the case of P13, a 1:2 Zn^{2+}:peptide complex is also formed because the maximum shifts to less than 0.5 (Figure 3-6b).[51] In addition, a change in the shape of the Job plot when a different emission wavelength is monitored is indicative of mixed complex formation.[51] The second criterion for 1:1 complex formation is a linear Scatchard plot of Zn^{2+} titration data (Figure 3-7).[51] Third, peptides forming a 1:1 complex exclusively throughout the course of a titration obtain a better fit with a 1:1 complexation model (Figure 3-8a). Addition of a 1:2 Zn^{2+}:peptide complex into the model fits the data for all other peptides (Figure 3-8b). Finally, the wavelength of maximum emission for a peptide forming only a 1:1 complex remains constant at 500 nm throughout a titration (Figure 3-9a). On the other hand, peptides forming 1:1 and 1:2 complexes exhibit shifts in the maximum emission wavelength from 475 nm to 500 nm as increasing amounts of Zn^{2+} are added (Figure 3-9b). This shift is observed because the 1:2 complex is also fluorescent, but demonstrates different photophysical properties.

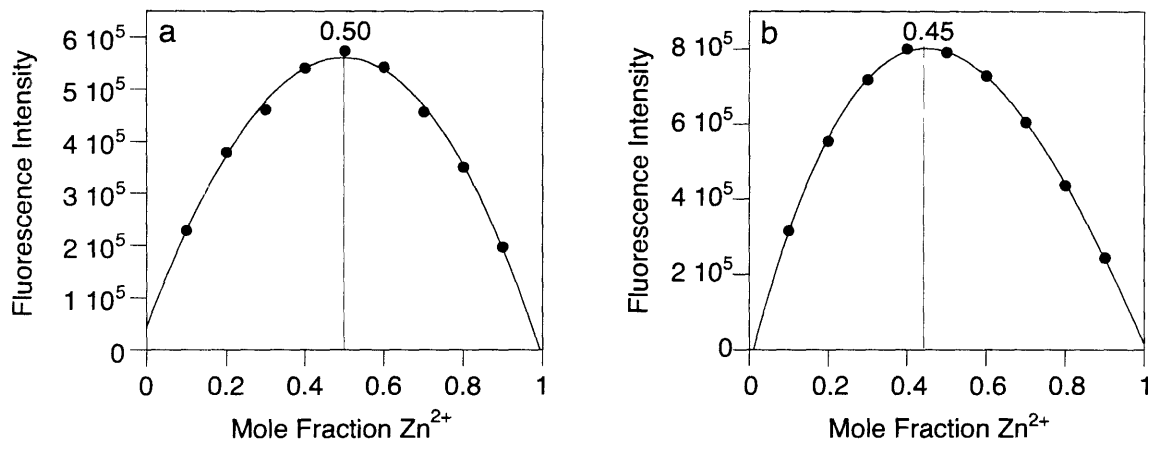

Figure 3-6. Job plots distinguish formation of a 1:1 complex from mixed complexes. (**a**) Job plot for a peptide which forms only 1:1 complexes, P13; (**b**) Job plot for a peptide which forms both 1:1 and 1:2 complexes, P8. The plots indicate the fluorescence intensity at 500 nm in 50 mM Hepes (pH 7.0), 150 mM NaCl. The total [peptide] + [$ZnCl_2$] = 0.98 μM.

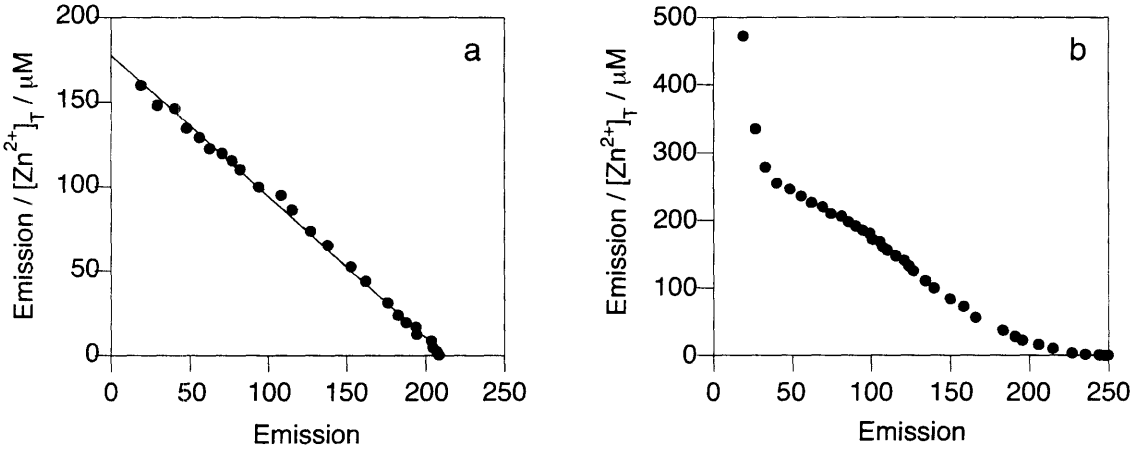

Figure 3-7. Scatchard plots distinguish formation of a 1:1 complex from mixed complexes. (**a**) Scatchard plot for a peptide which forms only 1:1 complexes, P13; (**b**) Scatchard plot for a peptide which forms both 1:1 and 1:2 complexes, P8. The plots indicate the fluorescence intensity at 500 nm. Titrations were performed with 500 nM peptide in 50 mM Hepes (pH 7.0), 150 mM NaCl. Data for entire titration is included.

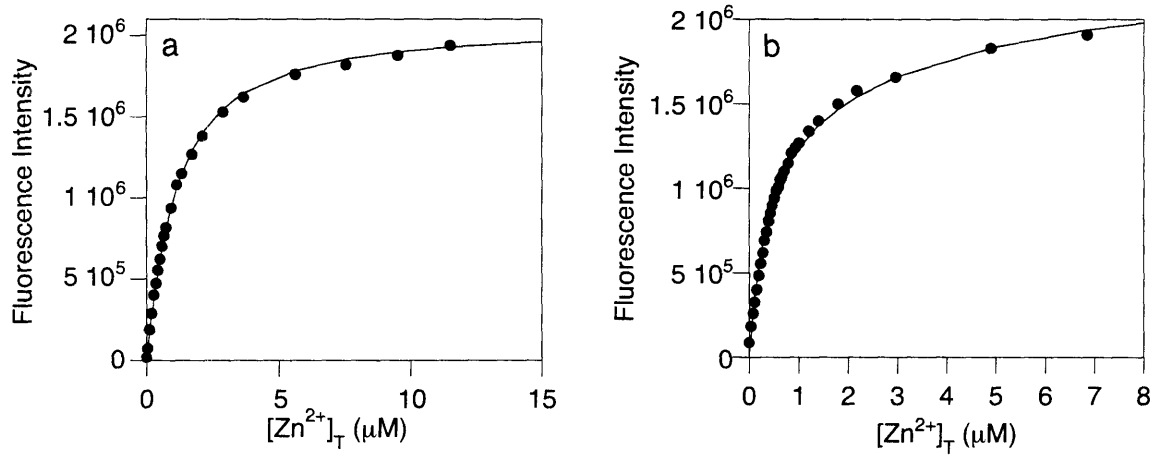

Figure 3-8. The complexation model that best fits the titration data indicates the type(s) of complex(es) formed. Fit obtained from titration data for (**a**) P13 using a 1:1 complexation model and (**b**) P8 using a 1:1 and 1:2 complexation model. With these models specified, a global non-linear least squares fit of the data was obtained via Specfit/32.[48] The plots indicate the fluorescence intensity at 500 nm. Titrations were performed with 500 nM peptide in 50 mM Hepes (pH 7.0), 150 mM NaCl. Data for entire titration is included.

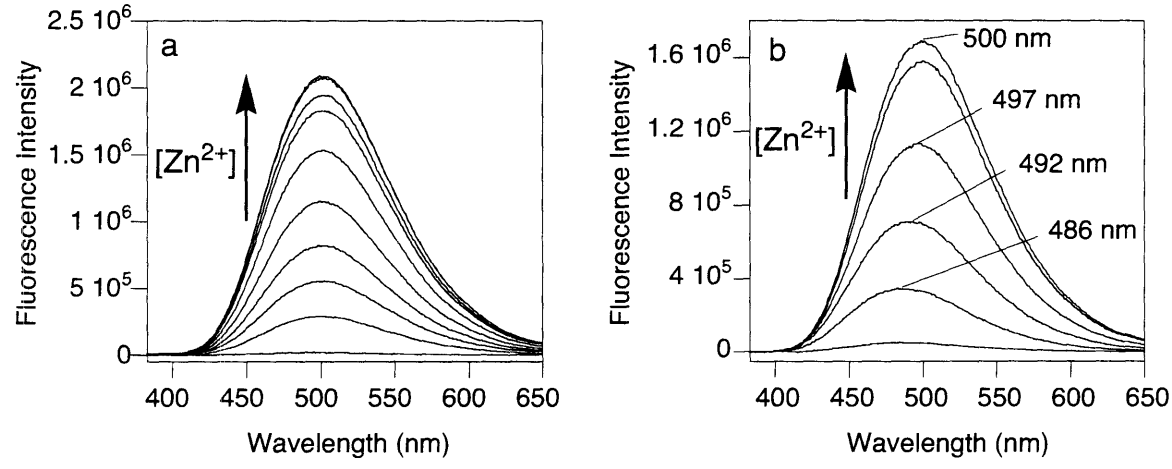

Figure 3-9. The behavior of the maximum emission wavelength during a titration distinguishes 1:1 complex formation from mixed complex formation. Spectra recorded for the titration of (**a**) P13 (emission maximum remains constant at 500 nm) and (**b**) P8 (emission maximum shifts during the titration). Only a few of the twenty-five data points collected are shown for clarity. Titrations were performed with 500 nM peptide in 50 mM Hepes (pH 7.0), 150 mM NaCl.

The rigid imidazole ligand was most sensitive to turn sequence modification and ligand arrangement; not all peptides synthesized with this ligand formed only 1:1 complexes. With the exception of P8, P15, P18 and P19, all peptides form only the 1:1 complex at peptide concentrations of 50 nM. Increasing the concentrations of peptides P9, P14, P16 and P17 resulted in formation of 1:2 complexes because any two given peptides are in closer proximity. A more favorable design exhibits a preference for 1:1 complex formation at high peptide concentrations, where chelation can outweigh the effect of concentration.

Of the nineteen peptides synthesized, eleven form 1:1 complexes at peptide concentrations in a useful range for biological experiments (low micromolar). For peptides that form mixed complexes, quantifying Zn^{2+} concentration is complicated by the fact that the relative concentrations of the 1:1 and 1:2 complexes change depending on both peptide and Zn^{2+} concentrations. Only the peptides that form 1:1 complexes (Table 3-3) will be further discussed, because they are the most useful. These eleven peptide sequences span two orders of magnitude in their dissociation constants. Since Zn^{2+} concentrations can be quantified from 10-90% saturation with a single chemosensor, these chemosensors are useful for monitoring Zn^{2+} concentrations over four orders of magnitude.

Table 3-3. Dissociation Constants for 1:1 Zn^{2+}:Peptide Complexes

Peptide	Zn^{2+} Ligands (N -> C)	Turn	Apparent K_D[a] (nM)
P1	**Sox**, Pen	Pro-DSer	9.6 ± 2.6
P2	Ipa, Cys, **Sox**	DPro-Gly	11 ± 2
P3	**Sox**, Cys	Pro-Gly	12 ± 1
P4	Cys, **Sox**	Pro-DSer	15 ± 4
P5	**Sox**, Cys	Pro-DSer	19 ± 5
P6	Ipa, His, **Sox**	DPro-Ser	35 ± 5
P7	**Sox**, pSer	Pro-DSer	130 ± 10
P10	Ipa, **Sox**	DPro-Gly	360 ± 20
P11	Ipa, **Sox**	DPro-Ser	530 ± 30
P12	**Sox**, Glu	Pro-DSer	730 ± 80
P13	**Sox**, Asp	Pro-DSer	910 ± 50

[a] Obtained via direct fluorescence titrations in triplicate. K_D values are calculated by a global non-linear least-squares fit with Specfit/32.[48]

Binding Trends

Inspection of the data presented in Table 3-3 allows the conclusion that the non-fluorophore Zn^{2+} ligand provides rough tuning of binding affinity. The affinity of a peptide for Zn^{2+} decreases along the following series: thiolate > two imidazoles > phosphate > one imidazole > carboxylate. This trend is expected based on the binding preferences of the Zn^{2+} ion, where "softer", or more polarizable, ligands are preferred.[2] The phosphate ligand appears out of order if solely a "soft" ligand explanation is invoked. The increased affinity of P7 for Zn^{2+} relative to the "softer" imidazole ligand may be due to the increased negative charge and/or the ability to bind as a bidentate ligand. The affinity of these peptides for Zn^{2+} spans two orders of magnitude through ligand variation.

Fine-tuning of binding affinity was possible through modification of the turn sequence and ligand arrangement. In general, a more flexible glycine residue in the turn sequence leads to a slightly tighter-binding peptide. Further, the ligand arrangement influences the Zn^{2+} affinity more strongly for imidazole ligands than for thiolate ligands. In addition, a peptide containing two imidazole ligands (P6) has significantly greater affinity over peptides containing a single imidazole ligand (P10, P11). However, the addition of an imidazole ligand to a cysteine-containing peptide barely changed the affinity (compare P2 to P4). The lack of increased affinity could be due to domination of the binding affinity by the thiolate donor or a result of the peptide adopting a conformation where the imidazole does not bind Zn^{2+}.

Implications for Further Tuning

The possibility of additional Zn^{2+} chemosensors with altered affinities is feasible through continued modification of this architecture considering the following trends. In general, affinity can be increased with "softer" ligands, a more flexible turn, and additional ligands. Affinity can be weakened with "harder" ligands and increased turn rigidity. While quantum mechanical forcefields exist for prediction of both ligand polarizability and energy-minimized structures, the necessary time and computing power for these calculations can be prohibitive. The structures of metal complexes of larger proteins can be minimized based on data from similar systems, but small peptides such as these chemosensors present a challenge. Therefore, synthesis and

characterization of each new chemosensor is necessary to empirically confirm the utility of each new design.

Influence of pH on Chemosensing Peptides

Because pH changes often accompany cellular signaling events,[52-54] it is important to investigate the effects of pH changes on both the chemosensor peptide and the chemosensor-Zn^{2+} complex. For this purpose, representative peptides of each ligand type were chosen. The fluorescence of all peptides in the absence of Zn^{2+} remain essentially unchanged between pH 4 and 10 (P10 is representative of all peptides in Figure 3-10). On the other hand, there is a dramatic change in the fluorescence intensity of the complex over the same pH range. All of the peptide-Zn^{2+} complexes are maximally fluorescent at and above pH 7 whereas the fluorescence of each peptide-Zn^{2+} complex is quenched below pH 5 (Figure 3-10). The pH profiles and p*K*a values calculated from these profiles (Table 3-4) differ slightly due to ligand variation. In particular, peptide P6 exhibits cooperative protonation of the two imidazole moieties; the pH profile shows an extremely sharp transition and fits to a 2-site model (Hill coefficient = 2, see Experimental). These probes all exhibit satisfactory pK_a values for cellular experiments.

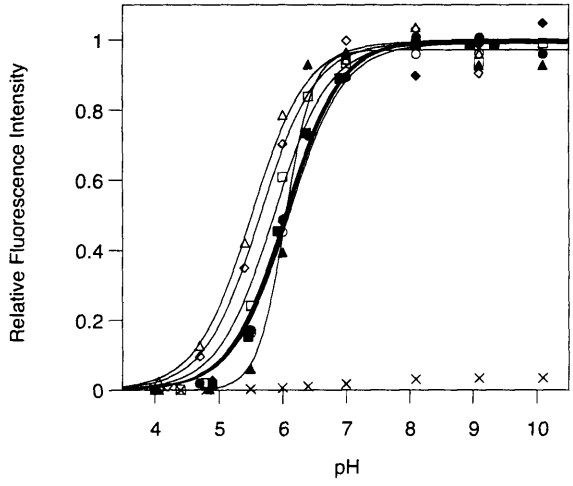

Figure 3-10. pH profiles of representative peptide and peptide-Zn^{2+} complexes. The fluorescence intensity at 500 nm is plotted for P10 (×) and the complexes Zn^{2+}-P1 (●), Zn^{2+}-P2 (■), Zn^{2+}-P5 (◆), Zn^{2+}-P6 (▲), Zn^{2+}-P7 (○), Zn^{2+}-P10 (□), Zn^{2+}-P12 (◇), Zn^{2+}-P13 (△). See experimental section for conditions and curve fit parameters.

Table 3-4. p*K*a's for chemosensor-Zn^{2+} complexes.

Peptide	Zn^{2+} Ligands Besides Sox	pK_a
P1	Pen	6.0
P2	Ipa, Cys	6.0
P5	Cys	6.1
P6	Ipa, His	6.0
P7	pSer	6.0
P10	His	5.8
P12	Glu	5.6
P13	Asp	5.5

Metal Competition Studies

To assess possible interference by relevant competing metal ions with the detection of Zn^{2+}, two separate experiments were performed: one to assess false positive responses where the competing ion forms a fluorescence complex with the chemosensor and another to identify false negative responses where the ability of the chemosensor to bind Zn^{2+} is compromised. In general, the metal-ion response variation between peptides can be explained as due to donor-atom preference for each metal ion.

Since metal ions besides Zn^{2+} are known to form fluorescent complexes with 8-hydroxyquinoline, including Mg^{2+} and Ca^{2+},[55] the fluorescence response of each chemosensor alone in the presence of each metal cation was investigated (Figure 3-11a). Only peptides containing "hard" carboxylate and phosphate donor ligands (P7, P12, P13) give a response with 1 mM Mg^{2+} and 1 mM Ca^{2+}. The response to Mg^{2+} is greater likely because the size of Mg^{2+} is more comparable to Zn^{2+} than that of Ca^{2+}.[2] P7 gives a substantial response to Mg^{2+} (50%) because Mg^{2+} has a particularly high affinity for phosphate, as seen by its frequent coordination to ATP and oligonucleotide sequences.[2]

The interference by Mg^{2+} and Ca^{2+} was investigated in greater depth for peptides P7, P12 and P13 by preliminary titrations. The dissociation constant of the P7-Mg^{2+} complex is roughly 10 mM, whereas the complexes of P12 and P13 with Mg^{2+} are at least two-fold weaker. In all cases, the Ca^{2+} complexes of these peptides have dissociation constants between 50 and 100 mM. The fluorescence properties of these complexes were discussed in Chapter 2; briefly, the Mg^{2+} complex is twice as bright and the Ca^{2+} complex 1.5 times as bright as the Zn^{2+} complex. With the exception of the P7-Mg^{2+} complex, one equivalent of Zn^{2+} added to the Mg^{2+} or Ca^{2+} complexes of these peptides shifts the emission wavelength maximum back to 500 nm,

suggesting that Zn^{2+} is able to efficiently compete with Ca^{2+} and Mg^{2+} binding when these ions are present at 1 mM. It is possible that a ratio of 485/500 nm could distinguish these complexes during analysis of an unknown sample.

Since many other metal ions do not form fluorescent complexes with 8-hydroxyquinoline, the fluorescence response of the peptide-Zn^{2+} complex in the presence of one equivalent of several additional metal ions was investigated (Figure 3-11b). In this study, K^+ does not interfere with fluorescence for any peptide-Zn^{2+} complex up to 1 mM K^+. For weaker Zn^{2+}-binding peptides, Mn^{2+} and Co^{2+} compete with Zn^{2+} binding by no more than 10% and 20%, respectively. Fe^{3+} interferes for peptides with "hard" oxygen donor atoms (P7, P12 and P13). Ni^{2+} causes significant quenching for peptides with imidazole and carboxylate ligands but has little affinity for peptides with thiolate and phosphate ligands. Cu^{2+} interferes with Zn^{2+}-binding for all peptides, and it entirely competes with Zn^{2+} for peptides containing thiolate ligands (P1, P2, P5).

With the exception of Ca^{2+}, Mg^{2+} and K^+, all metal ions investigated are unlikely to be present as free metal ions in biological systems. Regulatory proteins which bind copper[56] and zinc[57] ions sufficiently tightly to preclude the possibility of free amounts of these metals in the cytoplasm of *E. coli* have been discovered and, most likely, similar regulatory proteins for other metal ions exist in mammalian cells. For diagnostic purposes, a chemosensor can be chosen based on the lack of response to a competing metal ion in addition to the dissociation constant.

In addition, these chemosensors all form fluorescent complexes with Cd^{2+}. The concentration of Cd^{2+} in biological systems is subnanomolar[2] and thus it is unlikely to interfere with measurements in such systems. However, environmental and diagnostic applications exist for a Cd^{2+} chemosensor due to the toxicity of this metal ion. While Cd^{2+} forms complexes that are as fluorescent as the ones with Zn^{2+} for all peptides, the ability of P6 and P7 to differentiate between Zn^{2+} and Cd^{2+} is notable because such discrimination is rare. This discrimination may be explained by the size of Cd^{2+}, which is possibly too large to efficiently bind to all four ligands of P6. Also, Cd^{2+} is characterized as a "softer" metal ion than Zn^{2+}, which would disfavor phosphate coordination in P7. Though the trends described here favor the Zn^{2+} complexes, they imply that the peptide scaffold could be tuned for the specific detection of Cd^{2+} as well.

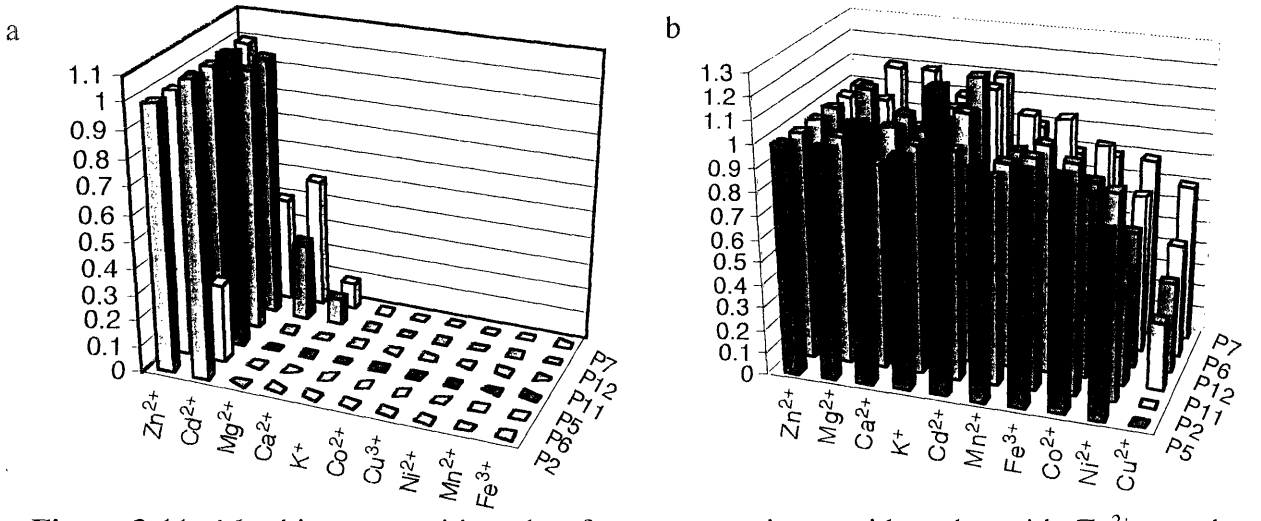

Figure 3-11. Metal ion competition plots for representative peptide and peptide-Zn^{2+} complexes, based on donor ligands. (**a**) Fluorescence intensity of peptides in the presence of various cations. (**b**) Fluorescence intensity of peptide plus 1 equivalent of Zn^{2+} in the presence of various cations. All metal ions were evaluated at one equivalent except Ca^{2+}, Mg^{2+} and K^{+}, which were used at 1 mM. Peptide concentrations were either 1 μM (P2, P5, P6 and P7) or 10 μM (P11, P12). Measurements were obtained in 50 mM Hepes (pH 7.0), 150 mM NaCl.

Probes of Zn^{2+} Concentration

For a given application, peptides spanning the range of affinities can be used to determine Zn^{2+} concentration within a defined range if one chemosensor gives a fluorescent response when another does not. To illustrate this approach, vials with different probes and varying concentrations of Zn^{2+} were prepared (Figure 3-12a). The observed fluorescence of each peptide at each of the three concentrations corresponds well with the data obtained from titrations (Figure 3-12b). Zn^{2+} concentrations can be narrowed into a range based on the responses of two or more peptides. This measurement does not require that the maximal fluorescence intensity be known, but only that one peptide does not give a response. For example, a solution that fluoresces in the presence of P5 but does not fluoresce in the presence of P7 would contain a Zn^{2+} concentration between roughly 50 and 200 nM. This method avoids many of the well-known difficulties associated with intensity-based measurements since the chemosensors are sufficiently similar to be compared under identical experimental conditions. Further, only very simple illumination equipment is required.

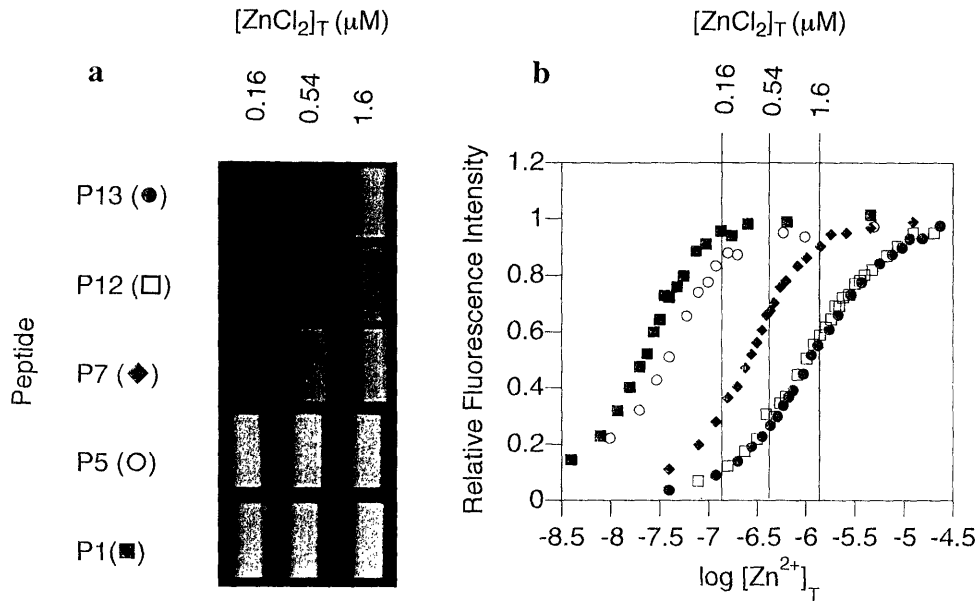

Figure 3-12. Visual representation of the range of Zn^{2+} affinities of five of the chemosensing peptides. (**a**) Vials were loaded with a 1 μM solution of the appropriate peptide and the indicated concentration of $ZnCl_2$ in 50 mM Hepes (pH 7.0), 150 mM NaCl. Vials were irradiated at 365 nm on a UV transilluminator. (**b**) Comparison of the fluorescence responses in **a** with the titration curves shows the probes behave as expected.

Investigation of Sox-Based Ratiometric Zn^{2+} Chemosensors

To enable Zn^{2+} concentration determination from a single chemosensor, both excitation and emission ratiometric chemosensors based on the Sox sensing strategy were examined. In both designs, an appropriate additional fluorophore is incorporated via amide bond formation into the peptide scaffold. Then, FRET is enabled between the additional fluorophore and Sox. To develop an emission ratiometric chemosensor, the additional fluorophore is chosen for reasonable overlap of the emission spectra with the excitation spectra of the Sox-Zn^{2+} complex, such that the energy is transferred to Sox upon Zn^{2+} binding (Figure 3-13a). To develop an excitation ratiometric chemosensor, an additional fluorophore is chosen whose excitation spectra overlap with the emission spectra of the Sox-Zn^{2+} complex (Figure 3-13b). The remainder of this chapter reports the choice of fluorophores for ratiometric sensing, the incorporation of these fluorophores into the peptide scaffold, and an investigation of the fluorescence properties of these new chemosensors.

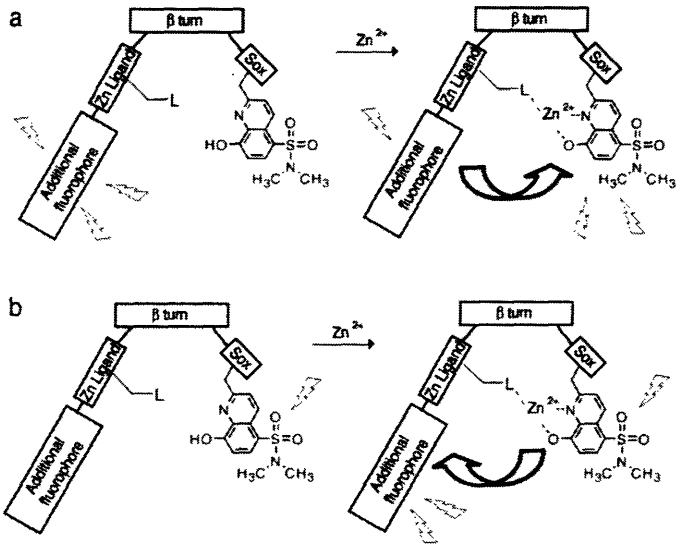

Figure 3-13. Schematic depictions of Sox-containing ratiometric chemosensors based on FRET. (**a**) In the emission ratiometric sensing strategy, energy from the additional fluorophore is transferred to the Sox-Zn^{2+} complex. A ratio of two different wavelengths in the emission spectra is used to determine Zn^{2+} concentration. (**b**) In the excitation ratiometric sensing strategy, energy from the Sox-Zn^{2+} complex is transferred to the additional fluorophore. A ratio of two different wavelengths in the excitation spectra is used to determine Zn^{2+} concentration.

Emission Ratiometric Chemosensors

Carbostyril 124 (cs124, Scheme 3-1) was chosen for the emission ratiometric chemosensor because it exhibits similar brightness to the Sox fluorophore. The cs124 fluorophore does not possess a handle for incorporation into peptide sequences. Thus, a soluble amino acid building block was synthesized by attaching cs124 to the side chain of glutamate (Scheme 3-1). Coupling of cs124 to Fmoc-Glu-OtBu was performed with the peptide coupling reagent HATU. Less reactive coupling agents such as PyBOP and diisopropylcarbodiimide were not effective. Deprotection of the *tert*-butyl group gave the final product, Fmoc-Glu(cs124)-OH in good yield. Upon conversion to an amide, the fluorescence properties of cs124 changed quite dramatically (Figure 3-14). Li and Selvin[58] reported the altered excitation spectra for a different cs124 amide construct, but the fluorescence emission properties were not noted. The emission of Fmoc-Glu(cs124)-OH shifted substantially relative to cs124 such that spectral overlap with the excitation of the P10-Zn^{2+} complex (Figure 3-12) enabled a FRET strategy.

Scheme 3-1. Synthesis of Fmoc-Glu(cs124)-OH

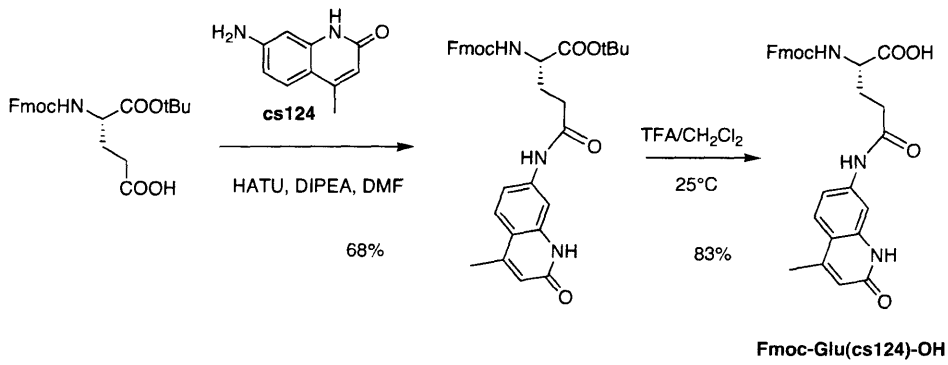

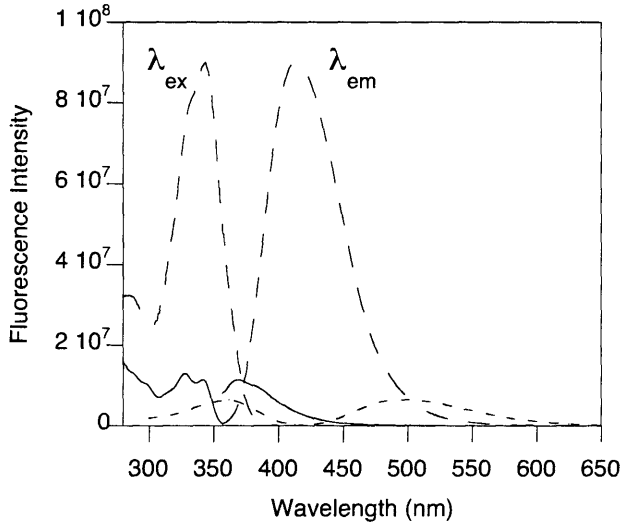

Figure 3-14. Excitation and emission spectra for cs124 (– –), Fmoc-Glu(cs124)-OH (—), and the P10-Zn^{2+} complex (- -). Spectra were obtained in 50 mM Hepes (pH 7.0), 150 mM NaCl with 10 μM of each species.

Fmoc-Glu(cs124)-OH was incorporated into three peptide sequences, based on Zn^{2+} chemosensors that formed 1:1 complexes (Table 3-5). Because incorporation of the additional fluorophore increases the hydrophobicity of these peptides, two arginine residues were included to increase solubility. These chemosensors contain either imidazole or carboxylate ligands for Zn^{2+} and the location of the cs124 moiety relative to the Zn^{2+} binding motif was varied. Peptides with thiolate ligands were avoided due to the possibility that ethanedithiol used in peptide cleavage cocktails might disrupt cs124 fluorescence via a Michael addition to the fluorophore.

Table 3-5. Sequences of Emission Ratiometric Zn^{2+} Chemosensors

Peptide	Sequence[a]	Apparent K_D for 1:1 complex (nM)[b]	Complex(es) formed (Zn^{2+}:peptide)
MDS32	Ac-*Glu(cs124)*-Ser-**His**-DPro-Gly-**Sox**-Arg-Arg-NH_2	ND	1:1 and 1:2
MDS33	**Ipa**-DPro-Gly-**Sox**-Ser-Ser-*Glu(cs124)*-Arg-Arg-NH_2	640	1:1
MDS34	Ac-**Sox**-Pro-DSer-**Asp**-Ser-Ser-*Glu(cs124)*-Arg-Arg-NH_2	2500	1:1

[a] Ligating residues are indicated in bold, additional fluorophore in italics. β-turn sequence is underlined.

[b] Obtained via direct fluorescence titration. Values reported are obtained from a single titration where [peptide] = 500 nM in 50 mM Hepes (pH 7.0), 150 mM NaCl. K_D values are calculated from a fit of the emission ratio 500/369 nm as described in the Experimental section.

Energy transfer between the two fluorophores can be observed by monitoring the emission at 500 nm at different excitation wavelengths for these two peptides in the presence of Zn^{2+}. Since cs124 itself does not emit at 500 nm, the carbostyril bands present in the excitation spectrum at 328 nm and 342 nm indicate energy transfer to the Sox-Zn^{2+} complex (Figure 3-15a). Further, this spectrum also shows that the emission of the peptide at 500 nm is 2.5 times greater when excited at 342 nm versus 368 nm (where Sox can be selectively excited). This difference is also illustrated by emission spectra of MDS32 and the MDS32-Zn^{2+} complex at different excitation wavelengths (Figure 3-15b). This figure also shows the ratiometric response to Zn^{2+} when the probe is excited at 342 nm.

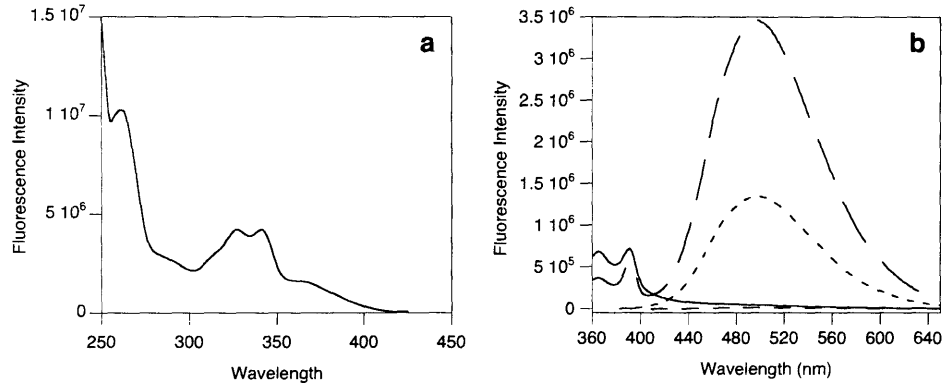

Figure 3-15. Evidence of FRET for peptide MDS32. (**a**) Excitation spectra of MDS32 for emission at 500 nm. (**b**) Emission spectra with excitation at 342 nm for MDS32 (—) and MDS32-Zn^{2+} (— —), and with excitation at 368 nm for MDS32 (– –) and MDS32-Zn^{2+} (- -). Spectra were obtained in 50 mM Hepes (pH 7.0), 150 mM NaCl.

To characterize more carefully the response of these probes to Zn^{2+}, titrations were conducted (Figure 3-16). As the concentration of Zn^{2+} is increased, the emission band due to cs124 at 369 nm decreases with a concomitant increase in the emission band due to the Sox-Zn^{2+} complex. Both the magnitude of the decrease in the 369 nm emission band and the maximum emission intensity at 500 nm varies between peptides. These results are consistent with a FRET mechanism based on the varied distance between the cs124 amino acid and Zn^{2+}-binding motif. During the course of a Zn^{2+} titration, MDS32 exhibited a slight shift (5 nm) in the emission intensity at 500 nm indicative of mixed complex formation; on the other hand, titrations of MDS33 and MDS34 revealed 1:1 complex formation. The ratio of fluorescence intensities (500/369 nm) could be fit for MDS33 and MDS34 to determine dissociation constants; a representative fit is shown in Figure 3-17. These dissociation constants (Table 3-5) correlate with those for the peptides P10 and P13, upon which they were based, respectively.

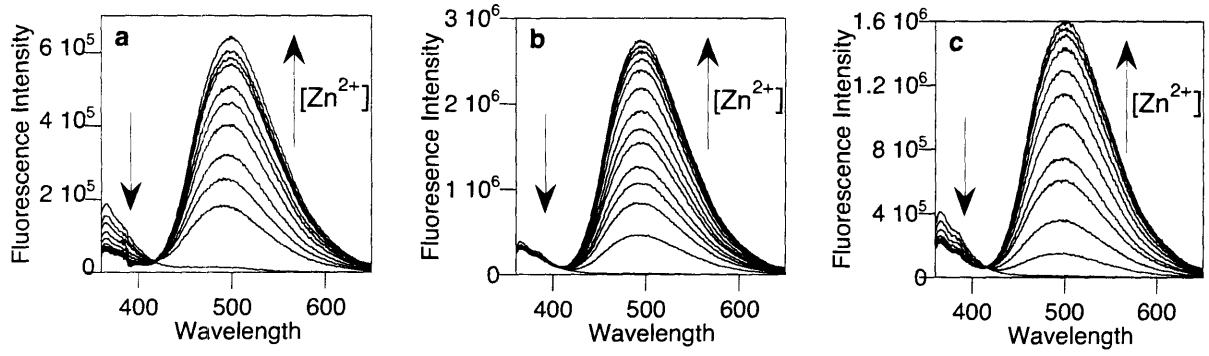

Figure 3-16. Effect of increasing concentrations of Zn^{2+} on fluorescence spectra of (**a**) MDS32; (**b**) MDS33; (**c**) MDS34. Titrations were performed in 50 mM Hepes (pH 7.0), 150 mM NaCl.

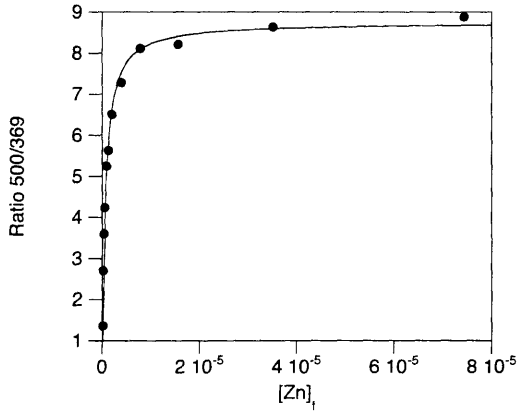

Figure 3-17. Representative fit of the 500/369 nm emission ratio for MDS33.

The FRET mechanism is corroborated by the complexes of these peptides with Cd^{2+} and Cu^{2+}. Cd^{2+} affords a similar response to Zn^{2+}. On the other hand, addition of high concentrations of Cu^{2+} resulted in the same fluorescence decrease at 369 nm, but no increase at 500 nm was observed due to the quenching effect of Cu^{2+} on Sox.

Preliminary investigations of pH sensitivity showed that the unbound probes exhibit a decrease in fluorescence at 369 nm in response to increasing the pH from 6.5 to 8.0. The bound probes do not exhibit a fluorescence change in this range. Since Sox has a small quantum yield in the absence of Zn^{2+}, it is possible that the pH sensitivity of the cs124 fluorescence emission band are due to changes in protonation state of the unbound Sox fluorophore. Thus, these probes will

be useful in a controlled environment that is not sensitive to pH fluctuations. The ratiometric response can easily be calibrated for each peptide to determine Zn^{2+} concentration.

Excitation Ratiometric Chemosensors

To afford an alternative approach and enable longer-wavelength readouts, an excitation ratiometric chemosensor containing Bodipy-R6G (Figure 3-18) was investigated. This approach was inspired by the work of Fierke and Thompson (Figure 3-4c).[36] Bodipy-R6G exhibits reasonable overlap with Sox at its excitation wavelength, 528 nm, and exhibits an unusually large Stokes' shift for Bodipy fluorophores (19 nm). Thus, the emission wavelength of Bodipy-R6G (547 nm) should be observable independent of Sox. The Bodipy-R6G succinimidyl ester was used to cap the free amine terminus of purified peptides in solution. The designed sequences vary the distance between the Bodipy fluorophore and the Zn^{2+}-binding motif (Table 3-6).

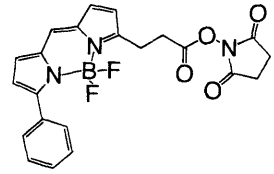

Figure 3-18. Structure of BodipyR6G succinimidyl ester

Table 3-6. Sequences of Excitation Ratiometric Zn^{2+} Chemosensors

Peptide	Sequence
MDS35	*BodipyR6G*-Gly-Ser-**Sox**-Pro-DSer-**Asp**-NH_2
MDS36	*BodipyR6G*-Ahx-Ser-Gly-**Sox**-Pro-DSer-**Asp**-NH_2

Energy transfer between the two fluorophores can be observed by a lack of fluorescence emission intensity at 500 nm when the probe is excited at 360 nm. The photophysics of these probes are a bit less straightforward because BodipyR6G can also be excited at 360 nm. However, addition of Zn^{2+} results in a decrease in fluorescence emission of BodipyR6G, indicating that the Sox-Zn^{2+} complex is quenching the fluorophore. This quenching is reversible upon addition of EDTA. The band at 360 nm appears to be an exception to the quenching, but this band is due to the contribution from emission of the Sox-Zn^{2+} complex (Figure 3-19). The

Bodipy fluorophore experiences less of a quenching effect by the Sox-Zn^{2+} complex in MDS36 when it is placed further away from the Zn^{2+}-binding site. This quenching is reversible upon addition of EDTA. Similarly to the emission ratiometric probes, these probes are sensitive to pH in the 6.5-8.0 range, due to deprotonation of the Sox fluorophore. Unfortunately, determination of binding constants from these data was problematic because the Bodipy fluorophore photobleaches but the Sox-Zn^{2+} complex does not. Thus, a more stable fluorophore is necessary for an excitation ratiometric probe.

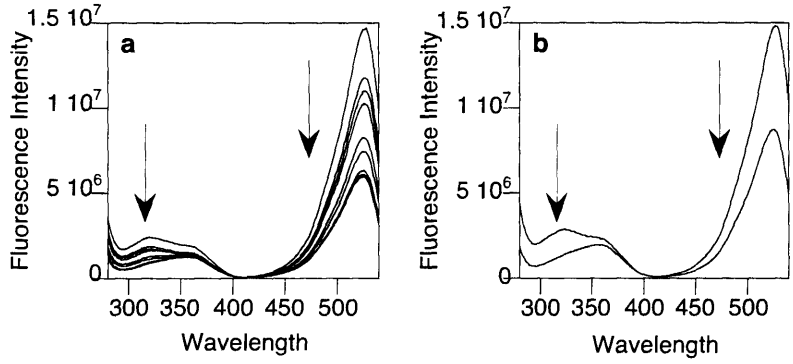

Figure 3-19. Effect of increasing Zn^{2+}concentrations on the fluorescence excitation spectra (547 nm) of (**a**) MDS35; (**b**) MDS36. Spectra were obtained in 50 mM Hepes (pH 7.0), 150 mM NaCl.

Conclusion

The non-natural amino acid Sox has been used as a modular building block in peptide sequences that bind Zn^{2+} in the nanomolar range where few useful Zn^{2+} chemosensors currently exist. The affinity for Zn^{2+} was tuned by variation of the ligands, scaffold, and turn sequence of the peptide. This tuning generated eleven peptide sequences that bind to Zn^{2+} in a 1:1 complex with affinities spanning 10 nM to 1 μM (Table 3-3). These chemosensors are individually useful to study Zn^{2+} concentrations over four orders of magnitude where the chemosensor is between 10% and 90% saturated. The general trends gleaned from these binding constants have implications for further tuning to generate new chemosensors. Compared to existing chemosensors for Zn^{2+}, the ease of tuning the Zn^{2+} affinity by altering the scaffold is superior. The brightness of these Sox-based chemosensors is the same order of magnitude as Zinbo-5 and

ZNP-1, but is 20-30-fold dimmer than those based on fluorescein and rhodamine (ZPs, ZnAFs, RF-1).

Under conditions for biological experiments, these probes are not compromised by pH or relevant competing metal ions. For diagnostic experiments, chemosensors from this family can be chosen based on their Zn^{2+}-affinity as well as their metal ion preferences. Finally, the chemosensors can easily be used to determine Zn^{2+} concentration, if the peptide concentration is unknown, when one chemosensor gives a positive response and another does not. For Zn^{2+} concentration determination via internal calibration with a single chemosensor, ratiometric chemosensors have been developed. These ratiometric probes are not optimal at this time but these examples illustrate that this modular scaffold is amenable to ratiometric sensing strategies.

Future Directions

To further develop the ratiometric Zn^{2+} sensing approach, the additional fluorophore should be placed farther from the Zn^{2+}-sensing motif so that it is only influenced by the strong fluorescence of the Sox-Zn^{2+} complex and not the weak fluorescence of the unbound Sox fluorophore. For the excitation ratiometric sensing strategy, an acceptor fluorophore with closely-matched with yet distinct from the fluorescence properties of the Sox-Zn^{2+} complex and with less susceptibility to photobleaching is necessary.

Acknowledgements

I am indebted to Dr. Dierdre Pearce for the idea to develop such a family of chemosensors with a range of Zn^{2+} affinities with the Sox fluorophore. Her preliminary design ideas included a few of the ligands I have chosen. I thank her for experimental advice via e-mail. I would also like to thank Dr. Kathy J. Franz for many helpful discussions and Dr. Robert A. Binstead of Spectrum Software Associates for assistance with the Specfit/32 program. Research grants were provided by the NSF (CHE-9996335 and a graduate research fellowship). The NMR spectrometers at MIT were provided by a grant from the NSF (DBI-9729592 and CHE-9808061) and NIH (1S10RR13886-01).

Experimental

Synthetic Procedures

All chemicals were obtained from Aldrich and all peptide synthesis reagents were obtained from Novabiochem, with the exception of trifluoroacetic acid (peptide synthesis grade, Perseptive Biosystems). Glass-backed thin layer chromatography plates were obtained from EM Science (silica gel 60 F_{254}, 0.25 micron thickness) and visualized by UV. Proton nuclear magnetic resonance spectra were recorded on a Varian 300 MHz instrument. Chemical shifts are reported relative to a value of 2.50 for DMSO.

Fmoc-Glu(cs124) tert-butyl ester

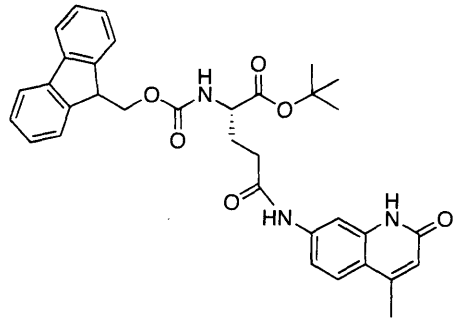

Fmoc-Glu-OtBu (126 mg, 0.30 mmol), and HATU (126 mg, 0.33 mmol) were dissolved in DMF (4.5 ml) and then diisopropylethylamine (78 µl, 0.33 mmol) was added. The reaction was stirred for 5 minutes and carbostyril 124 (60 mg, 0.33 mmol) was added. The reaction was followed by TLC and found to be complete after 26 hours. The reaction mixture was diluted with ethyl acetate (100 ml), washed with water (3 x 20 ml) and brine (2 x 15 ml). The organic layer was dried ($MgSO_4$) and the solvent was removed under reduced pressure. The mixture was redissolved in dichloromethane with sonication and purified by flash chromatography (silica, ethyl acetate/acetic acid, 99:1) to yield a white solid (109 mg, 68%). TLC R_f = 0.83 (silica, dichloromethane/methanol, 4:1), R_f = 0.33 (silica, ethyl acetate/acetic acid, 99:1), R_f = 0.61 (silica, dichloromethane/methanol, 9:1). ^{1}H NMR (300 MHz, DMSO-d_6) 11.52 (s, 1 H), 10.18 (s, 1 H), 7.88 (d, J = 7 Hz, 2 H), 7.77 (d, J = 2 H, 1 H), 7.59 (d, J = 8 Hz, 2 H), 7.40 (t, J = 7 Hz, 2 H), 7.26-7.40 (m, 3 H), 6.23 (s, 1 H), 4.20-4.33 (m, 3 H), 3.94-4.00 (m, 1 H), 2.42-2.60 (m, 2 H), 2.36 (s, 3H), 2.00-2.10 (m, 1 H), 1.80-1.90 (m, 1 H), 1.40 (s, 9 H).

Fmoc-Glu(cs124)-OH

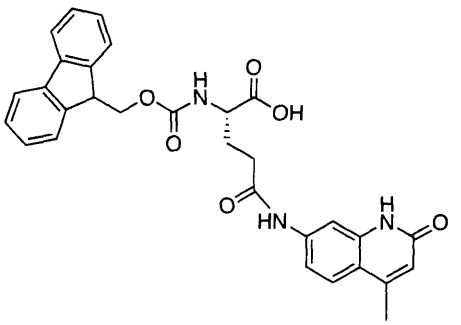

Fmoc-Glu(cs124)-OtBu (34 mg, 0.06 mmol) was dissolved in dichloromethane (3 ml) and triisopropylsilane (290 µl, 1.42 mmol) was added, followed by trifluoroacetic acid (3 ml). The mixture was stirred for 2 hours at 25°C. The solvent was removed under a stream of air. The silane was removed by rotary evaporation three times with dichloromethane. The solid was dried under high vacuum overnight to yield a white solid (25 mg, 83%). TLC R_f = 0.0 (silica, ethyl acetate/acetic acid, 99:1). ^{1}H NMR (300 MHz, DMSO-d_6) 11.50 (s, 1 H), 10.17 (s, 1 H), 7.87 (d, J = 8 Hz, 1 H), 7.67 (s, 1 H), 7.66-7.72 (m, 2 H), 7.59 (d, J = 9 Hz, 1 H), 7.39 (t, J = 7 Hz, 2 H), 7.26-7.33 (m, 3 H), 6.22 (s, 1 H), 4.19-4.31 (m, 2 H), 3.96-4.30 (m, 1 H), 2.42-2.47 (m 2 H), 2.34 (s, 1 H), 2.02-2.16 (m, 1 H), 1.80-1.94 (m, 1 H).

Peptide Synthesis

Peptides were synthesized using standard Fmoc amino acid protection chemistry on Fmoc-PAL-PEG-PS resin (0.2 mmol equiv.). All Fmoc-protected amino acids were purchased from Novabiochem, and resin was purchased from Advanced Chem Tech. All couplings of Fmoc-protected amino acids to the resin were carried out with benzotriazole-1-yl-oxy-tris-pyrrolidino-phosphonium hexafluorophosphate (PyBOP) and diisopropylethylamine (DIPEA) to generate the activated ester. The resin was swelled in dichloromethane (5 min.) then DMF (5 min.) prior to synthesis. All amino acids other than Sox and cysteine were added by the following representative procedure: removal of the Fmoc group (20% piperidine solution in DMF, 3 x 5 min.), wash (DMF, 5 x 1 min.), coupling (Fmoc-Xaa-OH/PyBOP/DIPEA, 6:6:6, 0.15 M amino acid in DMF, 45 min.), rinse (DMF, 2 x 1 min; DCM, 2 x 1 min.). To couple the Sox residue, double coupling with 2 equivalents was used (Fmoc-Sox-OH/PyBOP/DIPEA, 2:2:2, 0.15 M amino acid in DMF, 2 x 120 min.). To couple cysteine, the pentafluorophenyl ester was used

(Fmoc-Cys(Trt)-OPfp/DIPEA, 6:6, 0.15 M amino acid in DMF, 30 min.) After addition of the final residue, the peptide was either capped with an acetyl group (HOBt/acetic anhydride, 14:10, in DMF/CH_2Cl_2, 9:1) or imidazolyl propionic acid (PyBOP/3-imidazolyl propionic acid, 6:6, in DMF/NMP, 1:1). Following capping, a final deblock cycle (20% piperidine in DMF, 3 x 5 min.) was performed to cleave any aryl ester formed. The resin was dried under high vacuum overnight prior to a two hour cleavage with one of the following mixtures: for peptide containing a thiol moiety, trifluoroacetic acid/triisopropylsilane/water/ethanedithiol (94:1:2.5:2.5), otherwise, trifluoroacetic acid/triisopropylsilane/water (95:2.5:2.5). The resulting solution was concentrated, and the peptide precipitated by addition of cold 1:1 diethyl ether:hexanes solution. The pellet was triturated with cold 1:1 ether:hexanes (3 x 1.5 ml for 15 mg resin), redissolved in water, filtered and lyophilized overnight. Peptides were purified by preparatory reverse-phase C_{18} HPLC, and only fractions containing a single peak by analytical HPLC (C_{18}) with the correct mass were used for analytical experiments.

Representative Procedure for Coupling BodipyR6G to Purified Peptides

Following purification, the unprotected peptide was dissolved in 0.1 M sodium bicarbonate pH 8.3 (200 μl). The amount of peptide in this solution was determined to be 8.0 mM by UV/VIS (ε_{355} = 8247 M^{-1} cm^{-1} in 0.1 M NaOH with 1 mM Na_2EDTA). To this solution, Bodipy-R6G (1.50 mg, 3.3 μmol, 2 eq., Molecular Probes) dissolved in anhydrous DMSO (100 μl) was added and the reaction was left to shake gently for 1 hour. The mixture was purified by preparatory HPLC (C_{18}; solvent A = water, 0.002% v/v TFA; solvent B = MeCN, 0.002% v/v TFA, 5 min. 7% B followed by linear gradient 7-50% B over 30 min. followed by 10 min. 50% B).

Peptide Characterization Data

Peptide	Sequence	Mol. Formula	HPLC T_R (min)	*m/z* (z+) Calcd	*m/z* (z+) found[d]
P1	Ac-Sox-Pro-DSer-Pen-Ser-Ser-NH_2	$C_{35}H_{51}N_9O_{13}S_2$	23.4[a]	870.3 (+1)	870.3
P2	Ipa-Gly-Cys-DPro-Gly-Sox-Ser-Ser-NH_2	$C_{38}H_{52}N_{12}O_{13}S_2$	25.0[b]	949.3 (+1)	949.5
P3	Ac-Sox-Pro-Gly-Cys-Ser-Ser-NH_2	$C_{32}H_{45}N_9O_{12}S_2$	22.3[a]	812.3 (+1)	812.3
P4	Ac-Cys-Pro-DSer-Sox-Ser-Ser-NH_2	$C_{33}H_{47}N_9O_{13}S_2$	26.0[a]	842.3 (+1)	842.3
P5	Ac-Sox-Pro-DSer-Cys-Ser-Ser-NH_2	$C_{33}H_{47}N_9O_{13}S_2$	24.5[a]	842.3 (+1)	842.1
P6	Ipa-Gly-His-DPro-Ser-Sox-Ser-Ser-NH_2	$C_{42}H_{56}N_{14}O_{14}S$	21.4[b]	1013.4 (+1)	1013.4
P7	Ac-Sox-Pro-DSer-pSer-Ser-Ser-NH_2	$C_{33}H_{48}N_9O_{17}PS$	21.3[a]	906.3 (+1)	906.4
P8	Ac-Sox-Pro-DSer-His-Ser-Ser-NH_2	$C_{36}H_{49}N_{11}O_{13}S$	21.1[a]	876.3 (+1)	876.3
P9	Ipa-Pro-βPhe-Sox-Ser-Ser-NH_2	$C_{40}H_{50}N_{10}O_{11}S$	25.4[b]	879.3 (+1)	879.4
P10	Ipa-DPro-Gly-Sox-Ser-Ser-NH_2	$C_{33}H_{44}N_{10}O_{11}S$	21.4[b]	789.3 (+1)	789.3
P11	Ipa-DPro-Ser-Sox-Ser-Ser-NH_2	$C_{34}H_{46}N_{10}O_{12}S$	19.5[a]	819.3 (+1)	819.3
P12	Ac-Sox-Pro-DSer-Glu-Ser-Ser-NH_2	$C_{35}H_{49}N_9O_{15}S$	21.2[a]	868.3 (+1)	868.3
P13	Ac-Sox-Pro-DSer-Asp-Ser-Ser-NH_2	$C_{34}H_{47}N_9O_{15}S$	21.8[a]	854.3 (+1)	854.1
P14	Ipa-Pro-Gly-Sox-Ser-Ser-NH_2	$C_{33}H_{44}N_{10}O_{11}S$	20.1[a]	789.3 (+1)	789.3
P15	Ipa-Pro-DSer-Sox-Ser-Ser-NH_2	$C_{34}H_{46}N_{10}O_{12}S$	23.0[a]	819.3 (+1)	819.5
P16	Ipa-Gly-Asn-Sox-Ser-Ser-NH_2	$C_{32}H_{43}N_{11}O_{12}S$	18.9[a]	806.3 (+1)	806.3
P17	Ipa-Pro-Ser-Sox-Ser-Ser-NH_2	$C_{34}H_{46}N_{10}O_{12}S$	19.7[a]	819.3 (+1)	819.3
P18	Ipa-Pro-βPhe-Sox-Ser-Ser-NH_2	$C_{40}H_{50}N_{10}O_{11}S$	26.2[b]	879.3 (+1)	879.4
P19	Ac-Sox-Pro-DSer-Phe-Ser-Ser-NH_2	$C_{39}H_{51}N_9O_{13}S$	24.4[a]	886.3 (+1)	886.3
MDS32	Ac-Glu(cs124)-Ser-His-DPro-Gly-Sox-Arg-Arg-NH_2	$C_{59}H_{81}N_{21}O_{15}S$	26.6[b]	679.2 (2+)	678.8
MDS33	Ipa-DPro-Gly-Sox-Ser-Ser-Glu(cs124)-Arg-Arg-NH_2	$C_{60}H_{83}N_{21}O_{16}S$	26.7[b]	462.5 (3+)	462.8
MDS34	Ac-Sox-Pro-DSer-Asp-Ser_2-Glu(cs124)-Arg-Arg-NH_2	$C_{61}H_{86}N_{20}O_{20}S$	29.2[b]	726.3 (2+)	726.2
MDS35a	Gly-Ser-Sox-Pro-DSer-Glu-NH_2	$C_{32}H_{45}N_9O_{13}S$	22.2[a]	796.3 (+1)	796.3
MDS35	BODIPYR6G-Gly-Ser-Sox-Pro-DSer-Glu-NH_2	$C_{50}H_{58}BF_2N_{11}O_{14}S$	37.9[c]	1118.3 (+1)	1118.3
MDS36a	Ahx-Ser-Gly-Sox-Pro-DSer-Glu-NH_2	$C_{58}H_{56}N_{10}O_{14S}$	23.9[c]	909.4 (+1)	909.4
MDS36	BODIPYR6G-Ahx-Ser-Gly-Sox-Pro-DSer-Glu-NH_2	$C_{56}H_{69}BF_2N_{12}O_{15}S$	39.0[c]	1231.5 (+1)	1231.5

[a] 5 min. 7% B followed by linear gradient 7-70% B over 30 min.
[b] 5 min. 10% B followed by linear gradient 10-50% B over 30 min.
[c] 5 min. 7% B followed by linear gradient 7-50% B over 30 min.
[d] ES-MS data were collected on a PE Biosystems Mariner mass spectrometer.

Instrumentation

High-Performance Liquid Chromatography (HPLC): Waters 400 and 600 systems (solvent A = water, 0.1% v/v TFA; solvent B = MeCN, 0.1% v/v TFA). Columns used: C_{18} analytical, Beckman Ultrasphere ODS, 5 μm, 150 x 4.6 mm; C_{18} preparatory, YMC-Pack Pro, 5 μm, 250 x 20 mm.

Electrospray Mass Spectrometer: Applied Biosystems Mariner mass spectrometer

UV-Vis Spectrophotometer: Beckman DU 7500.

Fluorimeter: Fluoromax 2 from Jobin Yvon (λ_{ex} = 360 nm or 400 nm, λ_{em} = 485 nm).

Preparation of Buffers and Stock Solutions

All solutions were prepared polyproplyene that was rinsed with 10% HNO_3 and Milli-Q (Millipore) water. Care was taken that none of the solutions used for assays came in contact with metal or glass during handling. Assays were performed in 50 mM Hepes (pH 7.0), 150 mM NaCl. This buffer solution was prepared using high purity chemicals (SigmaUltra) and Milli-Q water. The buffer was treated by passage through a column of Chelex resin (Na^+ form, Biotechnology Grade, BioRad) to remove trace metal impurities and the pH adjusted to 7.0. For pH adjustment, 1 M solutions of acid and base were prepared using Milli-Q grade water using high purity hydrochloric acid solution (Baseline, Seastar Chemicals) and sodium hydroxide (99.998+%, Aldrich). All metal ion stock solutions were prepared from high purity chloride salts. The concentration of zinc(II) chloride, magnesium(II) chloride, calcium(II) chloride and cadmium(II) chloride solutions were determined by titration with a standardized solution of EDTA (Aldrich) in the presence of an Eriochrome Black T (Aldrich).[59] Stock solutions of other metal chlorides were prepared by weight. Stock solutions of the peptides were prepared in Milli-Q (Millipore) water. Based on the extinction coefficient of 5-(*N*,*N*-dimethylsulfonamido)-8-hydroxy-2-methylquinoline (ε_{355} = 8247 M^{-1} cm^{-1} in 0.1 M NaOH, 1 mM Na_2EDTA), peptide stock solution concentrations were determined on a Beckman DU 7500 Spectrophotometer from an average of the values from four separate solutions, each prepared using a different volume of the stock solution. For MDS32, MDS33 and MDS34, there exists significant contribution at 355 nm from cs124, so ε_{370} = 6542 M^{-1} cm^{-1} was used to quantify stocks. For MDS35 and MDS35, stock solutions were prepared in methanol and stored at –80°C, and their concentrations were determined based on the BodipyR6G chromophore (ε_{528} = 70,000 M^{-1} cm^{-1}). Peptide stock solutions were stored at 4°C, with the exception of thiol-containing peptides, which were stored at –80°C. Peptides containing cs124 or BodipyR6G were protected from light.

Extinction Coefficient and Quantum Yield Determination

Extinction coefficients and quantum yields were determined for representative peptide sequences in 50 mM Hepes (pH 7.0), 150 mM NaCl. For these experiments, peptide stock solution concentrations were determined by quantitative amino acid analysis (QAA). ε_{max} values were determined by plotting absorbance at 360 nm versus concentration for four separate solutions

with peptide concentrations between 20 and 60 μM and 1 mM $ZnCl_2$. Quantum yield values were determined using quinine sulfate dihydrate (Fluka, puriss. for fluorescence) in 0.1 M H_2SO_4 as a standard (Φ = 0.55). The absorbance and integrated fluorescence intensity of a 4 μM solution of each peptide with 200 μM $ZnCl_2$ was compared to a 4 μM solution of quinine sulfate with 360 nm excitation. The calculated Φ assumes that the refractive index of 0.1 M H_2SO_4 is identical to that of 50 mM Hepes (pH 7.0), 150 mM NaCl. Since the error associated with QAA and Φ of quinine sulfate are at least 10%, the error in ε and Φ are no less than 10%.

K_D Determination

Fluorescence titrations were performed on a Fluoromax 2 from Jobin Yvon, with λ_{ex} = 368 nm, slit widths = 5 nm. The titrations were carried out in triplicate by adding aliquots of $ZnCl_2$ to a peptide solution of known concentration. Dissociation constants were determined by a global non-linear least-squares fit of the data with the program Specfit/32,[48] with the exception of MDS32, MDS33 and MDS34. The dissociation constants of these peptides were determined from a ratio of emission intensities at 500/369 nm. The concentration of the peptide-Zn^{2+} complex was determined from the fraction of the maximum fluorescence ratio attained at each data point:

$$[pep - Zn^{2+}] = \frac{f}{f_{total}}[pep]_{total}$$

Then the $[Zn]_{free}$ is determined by:

$$[Zn^{2+}]_f = [Zn^{2+}]_t - [pep - Zn^{2+}]$$

Then a plot of the emission ratio versus $[Zn^{2+}]_f$ is made and fit by the following equation using KaleidaGraph (Origins, v3.6) software:

$$R = \frac{R_{max}[Zn^{2+}]_f}{[Zn^{2+}]_f + K_D}$$

Influence of pH

The following buffers were prepared containing 150 mM NaCl, passed through a Chelex column and adjusted to the desired pH with ultrapure acid and base solutions: 50 mM Mes (pH 5.5 and

6.0, Fluka Biochemika), 50 mM Hepes (pH 7.0 and 8.1, SigmaUltra), 50 mM Ches (pH 9.1 and 10.1, Fluka Biochemika). For readings below pH 5.5, Chelex-treated solutions of 150 mM NaCl adjusted to pH 4 and 4.7 were prepared and the pH of the solution was recorded after the fluorescence measurement. Fluorescence spectra of peptides (1 μM if $K_{D,Zn}$ < 200 nM or 10 μM if $K_{D,Zn}$ > 200 nM) were recorded without and with 1 equiv. Zn^{2+}. The emission intensity at 500 nm was extracted and data were normalized to an average of the maximum fluorescence readings. To determine the pK_a for each chemosensor, the data were fit to the following equation:

$$F = \frac{F_{max}}{1 + 10^{(pK_a - pH)*h}}$$

The Hill Coefficient (h) was fixed to a 1 binding site model (h = 1) for all peptides except P6, for which a 2-binding site model (h = 2) was used.

Metal Ion Competition

The fluorescence response of the peptides (1 μM if $K_{D,Zn}$ < 200 nM or 10 μM if $K_{D,Zn}$ > 200 nM) and peptide-Zn^{2+} complexes to 5 mM K^+, 1 mM Mg^{2+}, 1 mM Ca^{2+} and 1 equivalent Mn^{2+}, Co^{2+}, Cu^{2+}, Ni^{2+}, Fe^{3+}, and Cd^{2+} was investigated in 50 mM Hepes (pH 7.0), 150 mM NaCl. The emission intensity at 500 nm was extracted and compared to the value of fluorescence intensity at 500 nm for the Zn^{2+} complex.

References

(1) Vallee, B. L.; Falchuk, K. H. The biochemical basis of zinc physiology. *Physiol. Rev.* **1993**, *73*, 79-118.

(2) Frausto da Silva, J. J. R.; Williams, R. J. P. *The Biological Chemistry of the Elements: the Inorganic Chemistry of Life*; 2nd ed.; Oxford University Press: Oxford, 2001.

(3) Frederickson, C. J. Imaging zinc: old and new tools. *Sci. STKE* **2003**, *2003*, pe18.

(4) Berg, J. M.; Shi, Y. The galvanization of biology: a growing appreciation for the roles of Zn^{2+}. *Science* **1996**, *271*, 1081-1085.

(5) Beyersmann, D.; Haase, H. Functions of zinc in signaling, proliferation and differentiation of mammalian cells. *BioMetals* **2001**, *14*, 331-341.

(6) Maret, W. Crosstalk of the group IIa and IIb metals calcium and zinc in cellular signaling. *Proc. Natl. Acad. Sci. USA* **2001**, *98*, 12325-12327.

(7) Frederickson, C. J.; Bush, A. I. Synaptically released zinc: physiological functions and pathological effects. *BioMetals* **2001**, *14*, 353-366.

(8) Frederickson, C. J.; Suh, S. W.; Silva, D.; Frederickson, C. J.; Thompson, R. B. Importance of zinc in the central nervous system: the zinc-containing neuron. *J. Nutr.* **2000**, *130*, 1471S-1483S.
(9) Cuajungco, M. P.; Lees, G. J. Zinc metabolism in the brain: relevance to human neurodegenerative disorders. *Neurobiol. Dis.* **1997**, *4*, 137-169.
(10) Grodsky, G. M.; Schmid-Formby, F. Kinetic and quantitative relationships between insulin release and ^{65}Zn efflux from perifused islets. *Endocrinology* **1985**, *117*, 704-710.
(11) Formby, B.; Schmid-Formby, F.; Grodsky, G. M. Relationship between insulin release and ^{65}Zn efflux from rat pancreatic islets maintained in tissue culture. *Diabetes* **1984**, *33*, 229-234.
(12) Qian, W.-J.; Gee, K. R.; Kennedy, R. T. Detection of secretion from single pancreatic β-cells using extracellular fluorogenic reactions and confocal fluorescence microscopy. *Anal. Chem.* **2003**, *75*, 3136-3143.
(13) Kikuchi, K.; Komatsu, K.; Nagano, T. Zinc sensing for cellular application. *Curr Opin. Chem. Biol.* **2004**, *8*, 182-191.
(14) Kimura, E.; Aoki, S. Chemistry of zinc(II) fluorophore sensors. *BioMetals* **2001**, *14*, 191-204.
(15) Burdette, S. C.; Lippard, S. J. Coordination chemistry for the neurosciences. *Coord. Chem. Rev.* **2001**, *216-217*, 333-361.
(16) Lim, N. C.; Freake, H. C.; Brükner, C. Illuminating zinc in biological systems. *Chem. Eur. J.* **2005**, *11*, 38-49.
(17) Jiang, P.; Guo, Z. Fluorescent detection of zinc in biological systems: recent development on the design of chemosensors and biosensors. *Coord. Chem. Rev.* **2004**, *248*, 205-229.
(18) Frederickson, C. J.; Kasarkis, E. J.; Ringo, D.; Frederickson, R. E. A quinoline fluorescence method for visualizing and assaying the histochemically reactive zinc (bouton zinc) in the brain. *J. Neurosci. Methods* **1987**, *20*, 91-103.
(19) Zalewski, P. D.; Forbes, I. J.; Betts, W. H. Correlation of apoptosis with change in intracellular labile Zn(II) using Zinquin(2-methyl-8-*p*-toluenesulphonamido-6-quinolyloxy)acetic acid, a new specific fluorescent-probe for Zn(II). *Biochem J.* **1993**, *296*, 403-408.
(20) Chang, C. J.; Nolan, E. M.; Jaworski, J.; Okamoto, K.; Hayashi, Y.; Sheng, M.; Lippard, S. J. ZP8, a neuronal zinc sensor with improved dynamic range; imaging zinc in hippocampal slices with two-photon microscopy. *Inorg. Chem.* **2004**, *43*, 6774-6779.
(21) Burdette, S. C.; Frederickson, C. J.; Bu, W.; Lippard, S. J. ZP4, an improved neuronal Zn^{2+} sensor of the Zinpyr family. *J. Am. Chem. Soc.* **2003**, *125*, 1778-1787.
(22) Burdette, S. C.; Walkup, G. K.; Spingler, B.; Tsien, R. Y.; Lippard, S. J. Fluorescence sensors for Zn^{2+} based on a fluorescein platform: synthesis, properties and intracellular distribution. *J. Am. Chem. Soc.* **2001**, *123*, 7831-7841.
(23) Walkup, G. K.; Burdette, S. C.; Lippard, S. J.; Tsien, R. Y. A new cell-permeable fluorescent probe for Zn^{2+}. *J. Am. Chem. Soc.* **2000**, *122*, 5644-5645.
(24) Hirano, T.; Kikuchi, K.; Urano, Y.; Nagano, T. Improvement and biological applications of fluorescent probes for zinc, ZnAFs. *J. Am. Chem. Soc.* **2002**, *124*, 6555-6562.
(25) Hirano, T.; Kikuchi, K.; Urano, Y.; Higuchi, T.; Nagano, T. Highly zinc-selective fluorescent sensor molecules suitable for biological applications. *J. Am. Chem. Soc.* **2000**, *122*, 12399-12400.

(26) Gee, K. R.; Zhou, Z.-L.; Qian, W.-J.; Kennedy, R. Detection and imaging of zinc secretion form pancreatic β-cells using a new fluorescent zinc indicator. *J. Am. Chem. Soc.* **2002**, *124*, 776-778.
(27) Gee, K. R.; Zhou, Z.-L.; Ton-That, D.; Sensi, S. L.; Weiss, J. H. Measuring zinc in living cells. A new generation of sensitive and selective fluorescence probes. *Cell Calcium* **2002**, *31*, 245-251.
(28) Barondeau, D. P.; Kassman, C. J.; Tainer, J. A.; Getzoff, E. D. Structural chemistry of a green fluorescent protein Zn biosensor. *J. Am. Chem. Soc.* **2002**, *124*, 3522-3524.
(29) Walkup, G. K.; Imperiali, B. Design and evaluation of a peptidyl fluorescent chemosensor for divalent zinc. *J. Am. Chem. Soc.* **1996**, *118*, 3053-3054.
(30) Walkup, G. K.; Imperiali, B. Fluorescent chemosensors for divalent zinc based on zinc finger domains. enhanced oxidative stability, metal binding affinity, and structural and functional characterization. *J. Am. Chem. Soc.* **1997**, *119*, 3443-3450.
(31) Walkup, G. K.; Imperiali, B. Stereoselective synthesis of fluorescent α-amino acids containing oxine (8-hydroxyquinoline) and their peptide incorporation in chemosensors for divalent zinc. *J. Org. Chem.* **1998**, *63*, 6727-6731.
(32) Fierke, C. A.; Thompson, R. B. Fluorescence-based biosensing of zinc using carbonic anhydrase. *BioMetals* **2001**, 205-222.
(33) Thompson, R. B.; Peterson, D.; Mahoney, W.; Cramer, M.; Maliwal, B. P.; Suh, S. W.; Frederickson, C. J.; Fierke, C. A.; Herman, P. Fluorescent zinc indicators for neurobiology. *J. Neurosci. Methods* **2002**, *118*, 63-75.
(34) Thompson, R. B.; Maliwal, B. P.; Feliccia, V. L.; Fierke, C. A.; McCall, K. Determination of picomolar concentrations of metal ions using fluorescence anisotropy: biosensing with a "reagentless" enzyme transducer. *Anal. Chem.* **1998**, *70*, 4717-4723.
(35) *Fluorescent and Luminescent Probes for Biological Activity*; 2nd ed.; Mason, W. T., Ed.; Academic Press: San Diego, CA, 1999.
(36) Thompson, R. B.; Cramer, M. L.; Bozym, R.; Fierke, C. A. Excitation ratiometric fluorescence biosensor for zinc ion at picomolar levels. *J. Biomed. Optics* **2002**, *7*, 555-560.
(37) Woodroofe, C. C.; Lippard, S. J. A novel two-fluorophore approach to ratiometric sensing of Zn^{2+}. *J. Am. Chem. Soc.* **2003**, *125*, 11458-11459.
(38) Chang, C. J.; Jaworski, J.; Nolan, E. M.; Sheng, M.; Lippard, S. J. A tautomeric zinc sensor for ratiometric fluorescence imaging: application to nitric oxide-induced release of intracellular zinc. *Proc. Natl. Acad. Sci. USA* **2004**, *101*, 1129-1134.
(39) Burdette, S. C.; Lippard, S. J. The rhodafluor family. an initial study of potential ratiometric fluorescent sensors for Zn^{2+}. *Inorg. Chem.* **2002**, *41*, 6816-6823.
(40) Maruyama, S.; Kikuchi, K.; Hirano, T.; Urano, Y.; Nagano, T. A novel, cell-permeable, fluorescent probe for ratiometric imaging of zinc ion. *J. Am. Chem. Soc.* **2002**, *124*, 10650-10651.
(41) Henary, M. M.; Wu, Y.; Fahrni, C. J. Zinc(II)-selective ratiometric fluorescent sensors based on inhibition of excited-state intramolecular proton transfer. *Chem. Eur. J.* **2004**, *10*, 3015-3025.
(42) Taki, M.; Wolford, J. L.; O'Halloran, T. V. Emission ratiometric imaging of intracellular zinc: design of a benzoxazole fluorescent sensor and its application in two-photon microscopy. *J. Am. Chem. Soc.* **2004**, *126*, 712-713.

(43) Hong, S. H.; Maret, W. A fluorescence resonance energy transfer sensor for the beta-domain of metallothionein. *Proc. Natl. Acad. Sci. USA* **2003**, *100*, 2255-2260.
(44) Godwin, H. A.; Berg, J. M. A fluorescent zinc probes based on metal-induced peptide folding. *J. Am. Chem. Soc.* **1996**, *118*, 6514-6515.
(45) Nolan, E. M.; Lippard, S. J. The zinspy family of fluorescent zinc sensors: synthesis and spectroscopic investigations. *Inorg. Chem.* **2004**, *43*, 8310-8317.
(46) Carrigan, C. N.; Imperiali, B. The engineering of membrane-permeable peptides. *Anal. Biochem.* **2005**, in press.
(47) Jotterand, N.; Pearce, D. A.; Imperiali, B. Asymmetric synthesis of a new 8-hydroxyquinoline-derived α-amino acid and its incorporation in a peptidyl sensor for divalent zinc. *J. Org. Chem.* **2001**, *66*, 3224-3228.
(48) *SPECFIT/32 for Windows*, 3.0; Spectrum Software Associates: Marlborough, MA,
(49) Hyun, S., Massachusetts Institute of Technology, S.M. 2003.
(50) Pearce, D. A.; Jotterand, N.; Carrico, I. S.; Imperiali, B. Derivatives of 8-hydroxy-2-methylquinoline are powerful prototypes for zinc sensors in biological systems. *J. Am. Chem. Soc.* **2001**, *123*, 5160-5161.
(51) Connors, K. A. *Binding Constants: The Measurement of Molecular Complex Stability*; John Wiley and Sons, Inc.: New York, 1987.
(52) Llopis, J.; McCaffery, J. M.; Miyawaki, A.; Farquhar, M. G.; Tsien, R. Y. Measurement of cytosolic, mitochondrial, and Golgi pH in single living cells with green fluorescent proteins. *Proc. Natl. Acad. Sci. USA* **1998**, *95*, 6803-6808.
(53) Li, J.; Eastman, A. Apoptosis in an interleukin-2-dependent cytotoxic T lymphocyte cell line is associated with intracellular acidification. Role of the Na(+)/H(+)-antiport. *J. Biol. Chem.* **1995**, *270*, 3203-3211.
(54) Shepherd, R. M.; Henquin, J. C. The role of metabolism, cytoplasmic Ca^{2+}, and pH-regulating exchangers in glucose-induced rise of cytoplasmic pH in normal mouse pancreatic islets. *J. Biol. Chem.* **1995**, *270*, 7915-7921.
(55) Seitz, W. R. Fluorescence Derivatization. In *CRC Critical Reviews in Analytical Chemistry*; CRC Press: Boca Raton, FL, 1980; Vol. 8, p 367-404.
(56) Rae, T. D.; Schmidt, P. J.; Pufahl, R. A.; Culatta, V. C.; O'Halloran, T. V. Undetectable intracellular free copper: the requirement of a copper chaperone for superoxide dismutase. *Science* **1999**, *284*, 805-808.
(57) Outten, C. E.; O'Halloran, T. V. Femtomolar sensitivity of metalloregulatory proteins controlling zinc homeostasis. *Science* **2001**, *292*, 2488-2492.
(58) Li, M.; Selvin, P. R. Luminescent polyaminocarboxylate chelates of terbium and europium: the effect of chelate structure. *J. Am. Chem. Soc.* **1995**, *117*, 8132-8138.
(59) Basset, J.; Denney, R. C.; Jeffery, G. H.; Mendham, J. *Vogel's Textbook of Quantitative Inorganic Analysis*; William Clowers: London, 1978.

Chapter 4:

Versatile and Sensitive Fluorescent Chemosensors of Protein Kinase Activity: Design and Optimization

A portion of the work described in this chapter has been published in:
Shults, M. D.; Imperiali, B. Versatile fluorescence probes of protein kinase activity. *J. Am. Chem. Soc.* **2003**, 125, 14248-14249.

A portion of the introduction has been submitted for publication.
Rothman, D. R.; Shults, M. D.; Imperiali, B. Chemical approaches for investigating phosphorylation in signal transduction networks, submitted.

Introduction

Within cellular signaling, protein phosphorylation is the post-translational modification most frequently used to regulate protein activity.[1-3] Phosphorylation is tightly regulated by the actions of protein kinase and protein phosphatases, which perform phosphorylation and dephosphorylation reactions, respectively.[4] Protein kinases are the most abundant enzyme class, encoded for by 1 out of every 50 human genes.[2] These enzymes catalyze the transfer of the γ-phosphoryl from ATP to a free hydroxyl group in a peptide or protein substrate (Figure 4-1). This hydroxyl group is the side chain of a serine, threonine or tyrosine amino acid in eukaryotes. The activity of each kinase is controlled by its phosphorylation state, subcellular localization, and binding interactions within protein complexes.[1] Several serious human diseases, including many cancers[5], result from aberrant phosphorylation. For this reason, protein kinase regulation constitutes a crucial area for therapeutic development.[6,7]

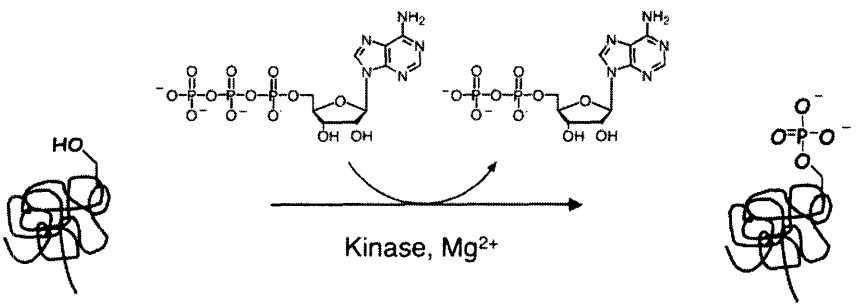

Figure 4-1. The reaction catalyzed by protein kinases.

Detecting Protein Kinase Activity

Tools to study protein kinases are invaluable for investigating the details of signal transduction. Chemosensors for kinase activity would provide a means to screen inhibitor candidates for therapeutics and chemical biology. In addition, these assays could be used to determine competitive substrates to identify cellular phosphorylation motifs and improved kinase substrates. Further, chemosensors for monitoring kinase activities in cell extracts and in living cells will be useful for unraveling complex signaling cascades and for understanding the roles of individual kinases in human disease.

The most common assay for protein kinase activity is a radioactivity-based assay where phosphoryl transfer from [γ-^{32}P]ATP to a peptide or protein substrate is quantified by scintillation counting. Whereas ^{32}P-based assays can be general and sensitive, they require special handling and are not practical for high-throughput applications. In addition, sub-physiological ATP concentrations are required (10-50 μM) to avoid overdiluting the [γ-^{32}P]ATP. Such "ATP-starved" conditions diminish the absolute activity of most kinases, which limits the resolution and sensitivity of radioactivity-based kinase assays. On the other hand, probes based on fluorescence are ideal due to their sensitivity and compatibility with standard instrumentation. To date, a variety of discontinuous and continuous fluorescence assays for protein kinase activity have been reported. The next sections will highlight existing technologies in both categories and discuss the merits and drawbacks of each.

Discontinuous Fluorescence Kinase Activity Assays

Discontinuous assays require that an aliquot of the reaction mixture be removed prior to analysis of the reaction product. These assays are typically broadly applicable to any kinase of interest. A multitude of diverse sensing strategies exist, so only the most widely-used and creative assays will be discussed here, including assays that 1) utilize specific detection of the incipient phosphate via a phospho-specific antibody or a metal chelate, 2) take advantage of differential protease sensitivity upon phosphorylation, 3) quantify product formation following separation from the substrate, and 4) monitor ATP or ADP concentrations. These assays use a variety of methods for fluorescent readout: fluorescence intensity, a ratio of fluorescence intensities, fluorescence polarization, and even luminescence.

A fluorescence intensity signal can be generated by a phospho-specific antibody when it is attached to a Eu^{3+}-chelate[8,9] or fluorescence bead[10] (Figure 4-2a). Alternatively, a phospho-specific antibody can be used in a fluorescent enzyme-linked immunosorbent assay (ELISA)-based approach.[11,12] ELISA-based assays utilize a secondary antibody (that recognizes the phospho-specific antibody) which is coupled to an enzyme which performs a fluorogenic reaction. This coupled enzyme approach in particular allows for signal amplification, which improves sensitivity. However, these aforementioned assays require separation of unbound antibody from the reaction mixture.

Homogeneous assays are desirable due to fewer processing steps and can be achieved with labeled phospho-specific antibodies when the kinase substrate is also labeled. Following phosphorylation when the antibody and substrate are bound, energy transfer between the two labels is achieved. These labels can be two fluorophores that undergo fluorescence resonance energy transfer (FRET)[13] or a singlet oxygen generator coupled to an acceptor whose fluorescence is modulated by singlet oxygen[14] (Figure 4-2b).

An alternative approach for a homogeneous assay is the use of fluorescence polarization (FP). In this technique, the tumbling rate of a fluorophore is measured; a fluorophore attached to a large construct tumbles more slowly than a fluorophore attached to a small construct. Thus, when a fluorescently-labeled phosphopeptide binds to a large reagent such as a phospho-specific antibody, the change in FP can be measured. Typically, these assays are performed as competition immunoassays such that a fluorescently-labeled tracer phosphopeptide is displaced by the kinase reaction product to afford a larger signal change (Figure 4-2c).[15,16] A further extension of this design is to displace a tracer that complements an enzyme fragment to restore activity (Figure 4-2d).[17]

Because the use of phospho-specific antibodies is expensive and can be poor for detecting serine/threonine phosphorylation, synthetic receptors based on metal chelates have been developed for phosphoamino acid recognition (Figure 4-2e). The phosphate group is a well-known chelating moiety, with a preference for oxophilic metal ions, such as Ca^{2+}, Mg^{2+}, Zn^{2+}, Fe^{3+} and Eu^{3+}. Synthetic metal chelates have been used to detect phosphopeptides via both fluorescence intensity changes[18,19] and fluorescence polarization.[20-22] Some of these approaches require separation of the phosphorylated product from the reaction mixture. Further, the assays that operate in a homogeneous format are restricted in both ATP concentration (to prevent ATP-binding to the receptor) and in additional chelate concentrations (to prevent the metal ion from being stripped from the receptor).

As an alternative to specific recognition of the incipient phosphate, fluorescent discrimination of substrate peptide and product phosphopeptide can be accomplished when these peptides are differentially processed by a secondary enzyme. These approaches were inspired by fluorogenic protease assays, and designed such that phosphorylation disrupts recognition by a protease. Proteases cleave the substrate peptide preferentially to either liberate latent

fluorophore[23] or to disrupt FRET between fluorophores on opposite sides of the peptide substrate[24] (Figure 4-2f). In these examples, the product phosphopeptide is nonfluorescent or exhibits FRET, respectively.

Phosphorylation also modulates the electrophoretic mobility of a substrate. Thus, fluorescently-labeled peptide substrates can be separated from the phosphorylated products by gel[25] or capillary[26,27] electrophoresis to quantify product formation (Figure 4-2g). In these examples, separation is time consuming and low throughput.

Finally, ATP consumption by the kinase can be monitored. Remaining ATP can be detected via a luminescence reaction[28] or newly-formed ADP can be detected with a specific aptamer-based sensor[29] (Figure 4-2h). These sensors can be problematic for kinases with ATPase activity.

The range of discontinuous approaches, many of which are commercially available, has afforded assays for nearly every kinase target. Assays can be chosen based on the desired reaction conditions, instrumentation, and expertise. These assays can be quite sensitive due to signal amplification, processing steps to reduce background fluorescence, or unlimited size and complexity of reagents. In addition, some of the assays can be adapted for use with protein substrates for the target kinase, which can be helpful if the target kinase does not efficiently phosphorylate peptides or when a good peptide substrate is not known. However, most of the sensing approaches are not compatible with physiological concentrations of ATP and are not selective for the target kinase; thus endogenous kinase activities can only be detected by first immunopurifying the kinase from a cell lysates, with the notable exception of single-cell assays via capillary electrophoresis.[26,27] Further, the processing steps that increase sensitivity of these assays are time consuming, low-throughput and do not allow kinetic, real-time information for each measurement.

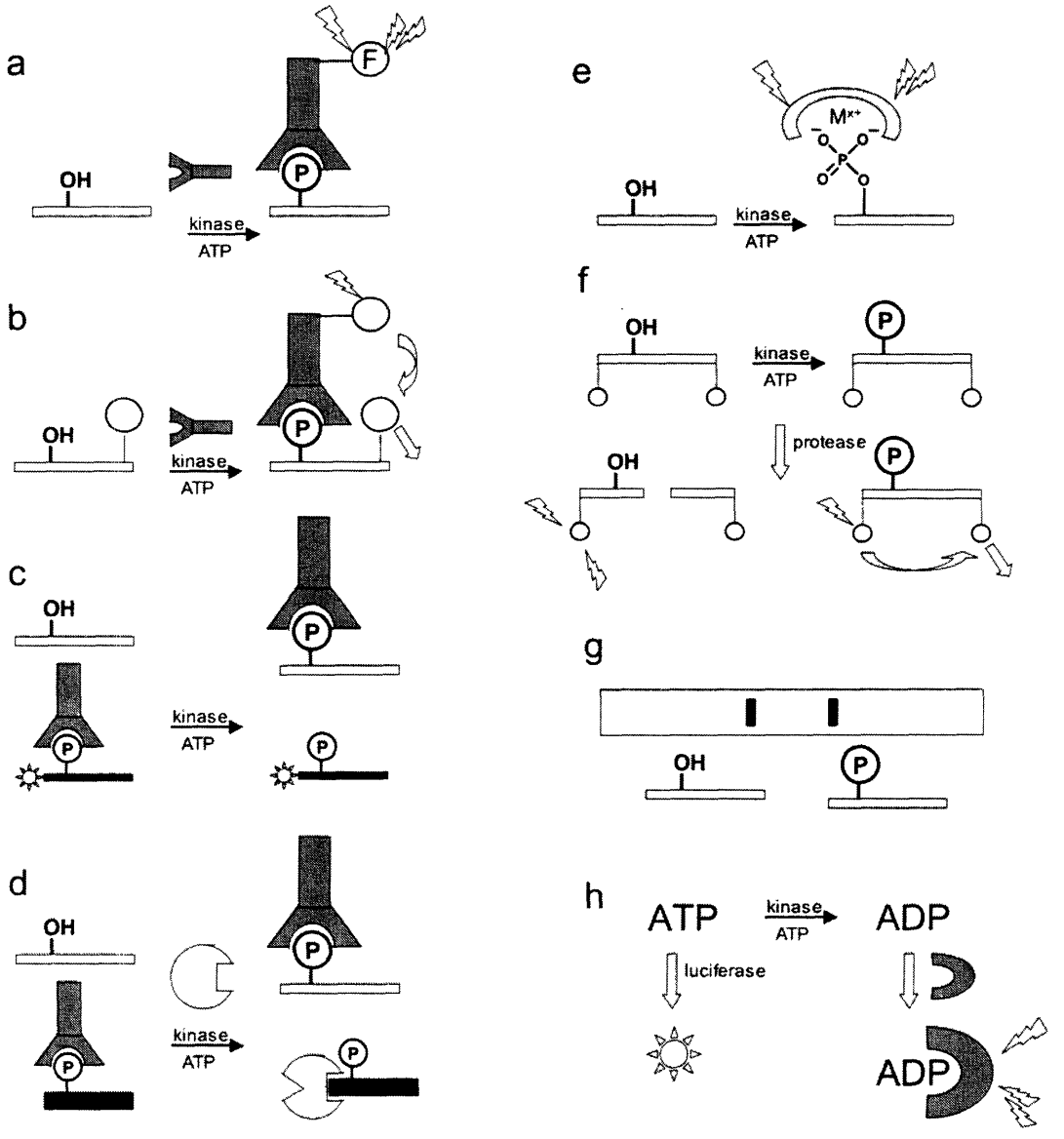

Figure 4-2. Examples of discontinuous assays for protein kinase activity. (**a**) Labeled antibodies are utilized to detect phosphoproduct formation. (**b**) Energy transfer between labels on substrate and antibody in proximity reveals phosphoproduct formation.[13,14] (**c**) Phosphoproduct disrupts binding of fluorescently-labeled tracer peptide to antibody, which is measured by a change in fluorescence polarization.[15,16] (**d**) Phosphoproduct liberates a peptide fragment that complements an inactive enzyme; then a fluorogenic reaction catalyzed by the active enzyme reports product formation.[17] (**e**) A metal chelate recognizes phosphoproduct via either fluorescence intensity changes or fluorescence polarization changes. (**f**) Phosphorylation renders a peptide resistant to protease digestion as measured by FRET;[24] (**g**) Reaction progress is quantified by electrophoretic separation. (**h**) Conversion of ATP to ADP can be quantified by specific reagents for either molecule.[28,29]

Continuous Fluorescence Kinase Activity Assays

On the other hand, continuous assays allow the reaction to be easily monitored while it is proceeding without additional experimental effort. Systems designed to exhibit fluorescence changes upon phosphorylation allow for a continuous readout in real time and enable facile kinetic analyses and *in vivo* imaging. In addition, these assays are typically compatible with cell lysates, living cells, physiological ATP concentrations, and high-throughput analysis. These strategies all generate a change in fluorescence upon phosphorylation either via dual fluorophore (by FRET) or single fluorophore approaches. Both protein- and peptide-based chemosensors have been designed (Figure 4-3). These approaches will be discussed below, and their properties are demonstrated in Table 4-1.

Continuous Protein-Based Kinase Activity Probes

FRET-based probes include donor and acceptor fluorophores whose relative distance is modulated upon probe phosphorylation, thereby altering the efficiency of energy transfer and thus the fluorescence signal. Protein kinase assays based upon FRET most commonly include appropriate pairs of donor and acceptor fluorophores that are derived from the *Aequorea victoria* fluorescent proteins (AFPs), although small-molecule fluorophores are also used (Figure 4-3a-c). Chemosensors based on both increases and decreases in FRET efficiency have been reported and the magnitude of the fluorescence changes significantly affects sensitivity and utility. Endogenous proteins exhibiting a phosphorylation-dependent conformational change have been employed to develop fluorescence-based chemosensors of kinase activity (Figure 4-3a,b).[30-33] A more general approach involves a modular design, which includes a peptide substrate for a target kinase, a linker region, and a phosphopeptide recognition domain such as a phosphotyrosine-binding SH2 domain (Figure 4-3c).[34-40] Upon phosphorylation, the phosphopeptide binds to its cognate recognition domain, which alters the distance between the flanking AFPs to afford a fluorescence response. These modular probes can in principle be used for any kinase by modifying the substrate sequence and corresponding binding domain.

An alternative strategy involves a single-fluorophore protein construct that has been developed using a circularly-permuted AFP (cpAFP).[41] cpAFPs are created by linking the N- and C-termini of an AFP and making a disconnection at an alternate location in the sequence.

Substrate and phosphopeptide recognition modules are then appended to the new N- and C-termini. Sensing is achieved when phosphorylation affords intramolecular binding, which modifies the conformation of the AFP, affording a fluorescence change (Figure 4-3d). In principle, several different kinase activities can be monitored simultaneously with this approach due to the variety of AFPs with different spectral properties that are available. However, only one of the three cpAFPs attempted to date was found to be useful. Additionally, this probe exhibited a decrease in fluorescence intensity upon substrate peptide phosphorylation, which is less desirable than an increase in signal, since the loss of signal could be mistaken for photobleaching.

Careful characterization of the properties of the protein-based probes, such as phosphorylation stoichiometry and fluorescence changes upon complete phosphorylation, can be challenging. It has been noted that some probes respond even in the absence of a phosphorylatable residue in the substrate sequence. The size of AFPs (often significantly larger than other sensor domains) and their ability to be phosphorylated may also complicate predictable changes in FRET, signal characterization, and recognition. Finally, the small fluorescence changes limit the sensitivity of these probes.

Continuous Peptide-Based Kinase Activity Probes

Synthetic environment-sensitive and chelation-sensitive fluorophores have been successfully incorporated into peptide-based probes for detecting kinase activities. Generally, a sequence of amino acids recognized by the target kinase is incorporated into a substrate peptide next to the residue to be phosphorylated, while the fluorophore is placed on the other side with an optional linker.

Environment-sensitive fluorophores (also called solvatochromic dyes) exhibit a change in their fluorescence properties (both intensity and maximum emission wavelength) due to the polarity of the immediate environment. Introduction of a phosphoryl group in proximity to the fluorophore then alters the local polarity and results in a fluorescence change (Figure 4-3e). Many researchers have attached environment-sensitive fluorophores to amino acid side chains one to five residues from the phosphorylation site, but this distance usually yields low sensitivity.[42-45] However, attachment of the solvatochromic dye directly to the peptide backbone

on the N-terminus of the residue to be phosphorylated has provided a strikingly sensitive probe for PKC when the solvatochromic 7-nitrobenz-2-oxa-1,3-diazole (NBD) is used.[46]

Chelation-sensitive fluorophores utilize biologically-available metal ions, such as Ca^{2+} or Mg^{2+}, to aid in sensing phosphorylation. A chelation-enhanced fluorescence (CHEF) chemosensing strategy has exploited elevated Ca^{2+} levels that activate PKC with appropriate positioning of a Ca^{2+} indicator fluorophore for effective metal-binding following phosphorylation (Figure 4-3f).[47] The alternative use of Mg^{2+} in this case would enable a general approach since Mg^{2+} is present in low millimolar concentrations in the cytoplasm. However, an attempt to modify the Ca^{2+}-based probes for Mg^{2+}-chelation to sense PKA activity was unsuccessful.[48]

These existing peptide-based approaches have not yet been proven general for application to additional kinases. It is likely that many kinases are more sensitive to large fluorophores adjacent to the phosphorylation site.

Table 4-1. Properties of individual continuous fluorescent sensors of protein kinase activity

Sensor	Target Kinase	Mechanism	λ_{ex} (nm)	λ_{em} (nm)	Signal change[a]	Ref.
Protein-based						
ART	PKA	FRET	380 (BGFP)	450/510 (RGFP)	22% ↓	30
Picchu	Abl/EGFR	FRET	433 (CFP)	475/527 (YFP)	60% ↑	31
KCP-1	PKC	FRET	405 (GFP^2)	530/500 (EYFP)	50% ↑	33
Rh-CrkΔ-Fl	Abl	FRET	490 (fluorescein)	580/520 (rhodamine)	20% ↓	32
Umezawa						
Phocus	IR	FRET	440 (CFP)	535/480 (YFP)	15-20% ↑	34
Aktus	Akt	FRET	↓	↓	10% ↑	35
Cyan sinphos	IR	AFP conformational change			10% ↓	41
Tsien						
AKAR	PKA	FRET	440 (ECFP)	535/480 (Citrine/EYFP)	25-50% ↑	37
CrkII-based reporter	Abl	FRET	↓	↓	15-30% ↑	38
Src-reporter	Src	FRET			25-30% ↓	38
EGFR-reporter	EGFR	FRET			25-35% ↑	38
CKAR	PKC	FRET	440 (mCFP)	535/480 (mYFP)	15-20% ↓	39
BKAR	Akt	FRET	↓	↓	10-25% ↓	40
Peptide-based						
Lawrence						
NBD-based	PKC	Environment-sensitive	520	540	2.5-fold ↑	47
Ca^{2+}-based	PKC	CHEF	490	525	3.6-fold ↑	46

[a]Fluorescence increase for protein-based probes reported as range visualized by maximally stimulating target kinase in vivo. Fluorescence increase for peptide-based probes reported as fluorescence difference between phosphorylated peptide and substrate peptide. [b]↑ = fluorescence increase; ↓ = fluorescence decrease

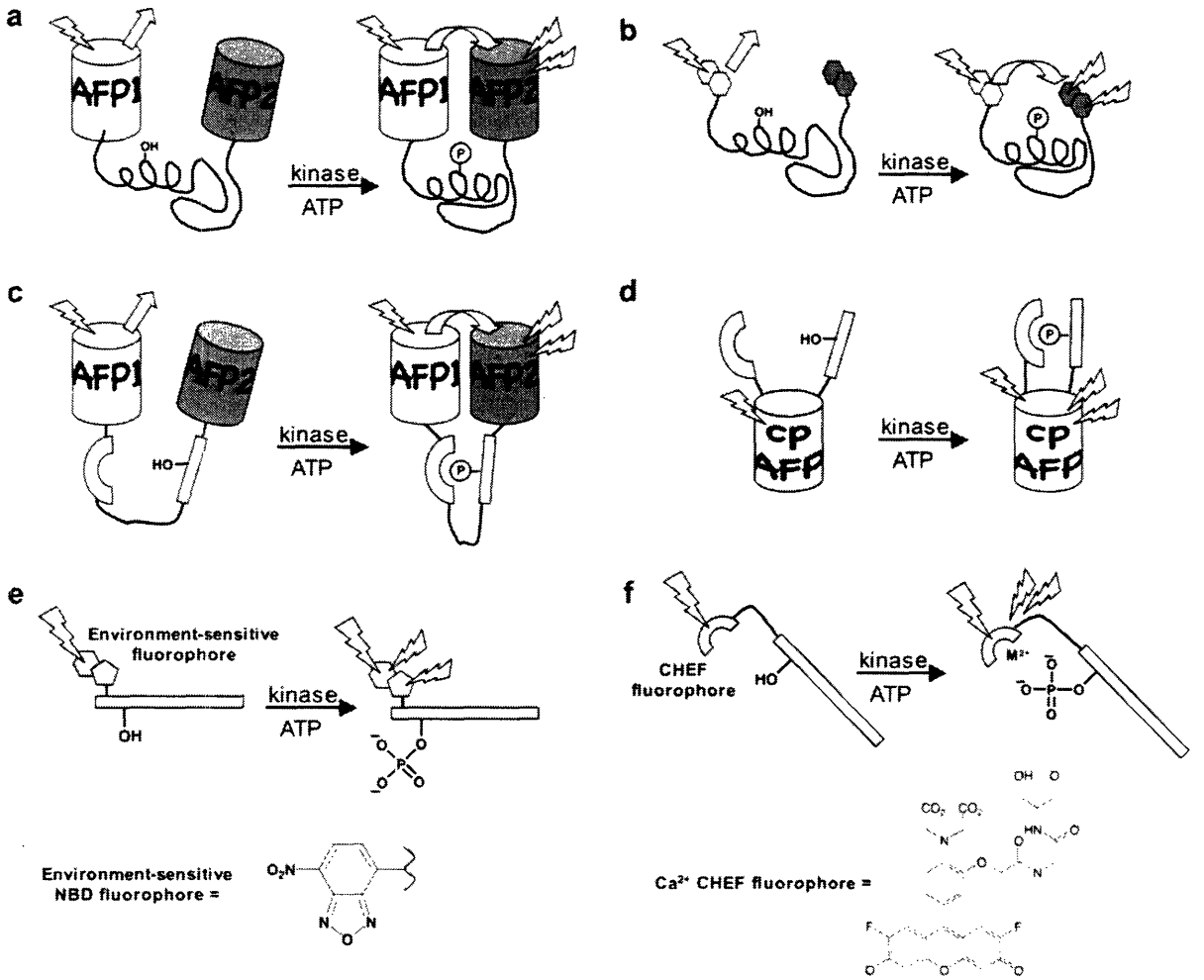

Figure 4-3. Fluorescence response generation for continuous assays of protein kinase activity. (**a,b**) A protein that undergoes a conformational change upon phosphorylation which alters the distance between (**a**) AFPs appended to the N- and C-terminus,[30,31,33] or (**b**) Two small molecule fluorophores.[32] (**c**) A modular sensor with two AFPs flanking a phosphorylation recognition domain, linker and substrate sequence for the target kinase. Intramolecular binding of the phosphoamino acid to the recognition domain alters the distance between the two AFPs.[34,37,38] (**d**) A phosphorylation recognition domain and substrate sequence for the target kinase appended at the newly-generated N- and C-termini of cpAFP, such that the conformation of the AFP is altered upon phosphorylation.[41] (**e**) Phosphorylation alters the local environment of an adjacent fluorophore and changes its fluorescence intensity.[47] (**f**) Appropriate placement of chelation-sensitive fluorophores relative to the phosphorylation site on a peptide substrate results in both metal ion binding and fluorescence increase upon phosphorylation.[46]

Ideal Characteristics for a Chemosensor of Kinase Activity

Since the ultimate goal is to understand kinases signaling in the complex environment of the cell, chemosensors with substantial improvements over existing approaches are highly desirable. In addition to the characteristics of an ideal chemosensor discussed in Chapter 1, kinase chemosensors should measure the catalytic competence of the target kinase in a complex environment consisting of phosphate-containing species and related kinases. In addition, the strategy should be broadly applicable to any kinase but not involve radioactivity, specialized antibodies or multiple handling steps. Further, probe design should afford a fluorescence increase upon phosphorylation without the need for separating substrate and product for analysis and to allow for a continuous readout in real time. The magnitude of this increase should be large for high sensitivity. Finally, the probe should exhibit good reactivity with the target kinase at physiological substrate concentrations (low micromolar) to minimize reactivity with off-target kinases and perturbation of cellular signaling process.

This chapter will detail a versatile phosphorylation chemosensing strategy that is general for detection of serine, threonine and tyrosine phosphorylation. These probes utilize a CHEF mechanism with the nonnatural amino acid Sox and physiological Mg^{2+} concentrations. Each chemosensor comprises a small sensing module appended either the C- or N-terminal to the serine, threonine or tyrosine of an optimized peptide substrate for the target kinase. The sensing module contains a 2–3 residue β-turn element to preorganize Mg^{2+}-binding between the Sox fluorophore and the incipient phosphate. In addition, the Mg^{2+}-binding affinity of the product phosphopeptide is shown to be much greater than the substrate peptide, which results in a large fluorescence increase upon phosphorylation. Optimization of the β-turn sequence to improve the fluorescence increase and reactivity towards the target kinase is reported. Details of the chemosensing mechanism will be presented, along with recommendations for the generation of addition chemosensors. Finally, preliminary experiments towards high-throughput and biological applications will be introduced.

Results:

Substrate Design and Synthesis

Chemosensor design begins from an optimized peptide substrate from the literature. The important residues for kinase recognition are preserved on one side of the residue to be phosphorylated. The sensing module is positioned on the other side of the serine, threonine, or tyrosine from this optimized peptide substrate, and includes the Sox amino acid and a β-turn sequence (Figure 4-4). A two-residue β-turn sequence is used for chemosensors of the serine/threonine kinase activity, while an additional residue is necessary in the β-turn for sensing tyrosine phosphorylation to allow for chelation between Sox and the large phosphotyrosine side chain.

Several important kinases were targeted for development of chemosensors: protein kinase C (PKC),[49] cAMP-dependent protein kinase (PKA),[50,51] Akt,[52,53] mitogen-activated protein kinase-activated protein kinase-2 (MK2),[54,55] Pim2,[56] and Abl[57]. Initially, peptide substrates were synthesized for PKC, PKA and Abl (PKC-S1, PKC-S2, PKA-S1, Abl-S1; Table 4-2) to evaluate the scope of this design strategy. Then, the β-turn sequences of the PKC and PKA probes were optimized for signal and reactivity. This knowledge was applied to generate additional kinase chemosensors for the serine/threonine kinases Pim2, Akt, and MK2.

Substrate peptides (e.g. PKC-S1) and corresponding product phosphopeptides (e.g. PKC-P1) were synthesized by Fmoc SPPS. Standard protocols were used, with two special considerations for these chemosensing peptides. First, peptides with a C-terminal sensing module should contain a C-terminal glycine residue to suppress diketopiperazine formation during synthesis. Also, an additional deblock cycle must be performed following acetyl capping of all peptides to cleave any Sox aryl ester formed. All peptides are purified to >95% by HPLC and identified by electrospray mass spectrometry.

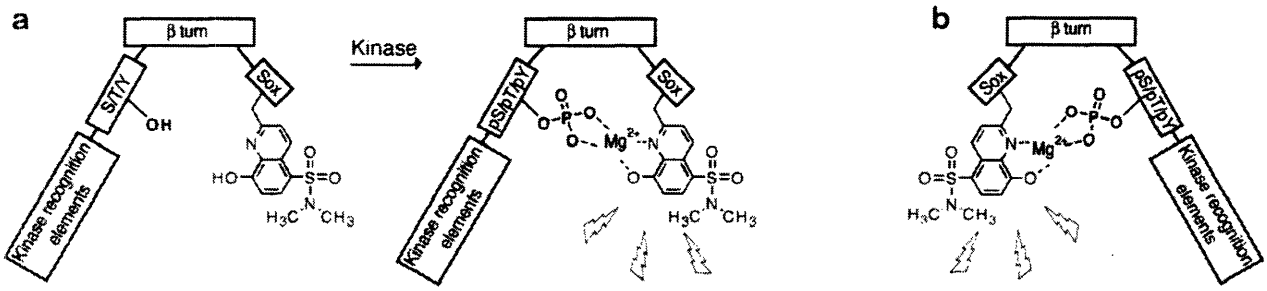

Figure 4-4. Design of fluorescent chemosensors of protein kinase activity. The chemosensor peptide contains three important design modules: critical kinase specificity determinants, the chelation-enhanced fluorophore (CHEF) Sox, and a β-turn to preorganize Mg^{2+}-binding between Sox and the incipient phosphate. Phosphorylation increases the affinity of the peptide for Mg^{2+} and the fluorescent signal is generated by chelation of Mg^{2+}. The kinase recognition elements may be placed on either (**a**) the C-terminus or (**b**) the N-terminus of the serine, threonine or tyrosine residue to be phosphorylated.

Fluorescence Properties

The absorption and fluorescence properties of the Mg^{2+}-Sox complex were introduced in Chapter 2. To summarize, the absorbance band at 360 nm gives rise to a fluorescence emission at 485 nm.

The ε_{max} and quantum yield (Φ) values for the Sox-Mg^{2+} complex were determined with the peptide MK2-P1. The UV-Vis spectra of the Mg^{2+} and Zn^{2+} complexes of MK2-P1 are identical, thus the ε_{max} for the Mg^{2+} complex is identical to that reported for Zn^{2+}-chemosensing peptides (6200 M^{-1} cm^{-1}, Chapter 3). The quantum yield of the Mg^{2+} complex is 0.34, which is twice that of the Zn^{2+} complex. The quantum yield for the unbound form (Φ = 0.004) was reported in Chapter 3.

Chemosensing Mechanism

These chemosensors exhibit a change in fluorescence upon phosphorylation due to an order of magnidue difference in Mg^{2+} affinities between the substrate and product peptides, as illustrated by the Mg^{2+}-titration curves of PKC-S2 and PKC-P2 (Figure 4-5a). Importantly, the magnitude of the fluorescence increase depends on the concentration of Mg^{2+}, and an increase is observed over a wide range of Mg^{2+} concentrations. Thus, a change in fluorescence upon phosphorylation will occur with a variety reaction conditions. Notably, a substantial fluorescence

increase is observed for both *in vitro* kinase reaction conditions (10 mM, Figure 6b) and free cytoplasmic Mg^{2+} (0.5 – 5 mM).[58]

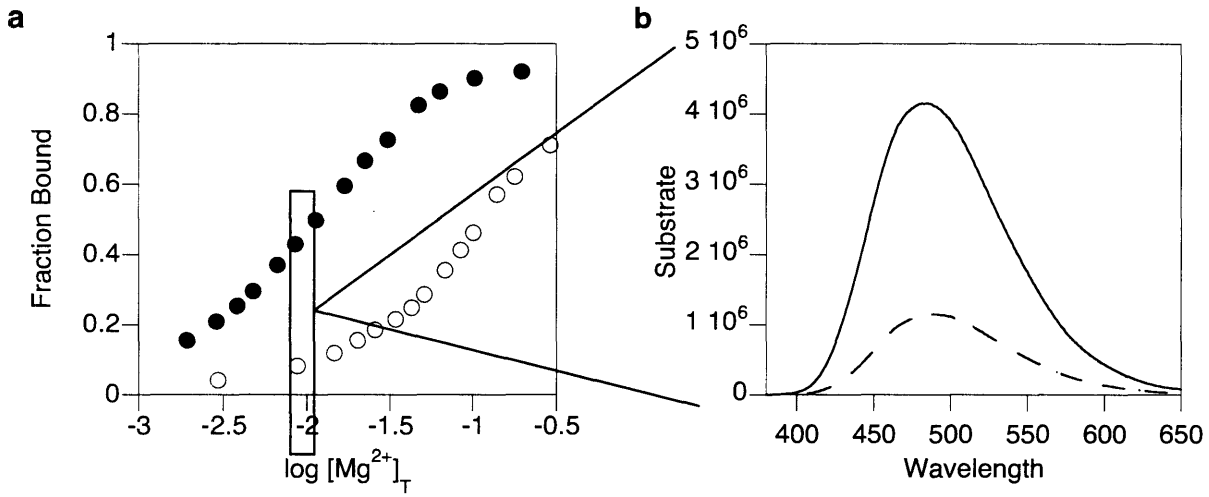

Figure 4-5. Origin of the difference in fluorescence intensity between substrate peptide and product phosphopeptide. (a) Mg^{2+} titration curves for PKC-P2 (●) and PKC-S2 (○) in 20 mM Hepes (pH 7.4), 150 mM NaCl. (b) Fluorescence spectra of PKC-P2 (–) and PKC-S2 (--) with 10 mM $MgCl_2$ in 20 mM Hepes (pH 7.4), 150 mM NaCl.

The magnitude of the fluorescence increase depends most strongly on the Mg^{2+} concentration, but it is also influenced by temperature, instrumentation, high concentrations of other metal ions, and species that chelate Mg^{2+}. The ability to chemically synthesize the product phosphopeptide allows empirical determination of the fluorescence increase for facile adaptation of the assay to a variety of assay conditions and Mg^{2+} concentrations.

Magnitude of the Fluorescence Increase

Fluorescence increase values for first generation PKC, PKA and Abl substrates (PKC-S1, PKC-S3, PKA-S1, Abl-S1; Table 4-2) illustrate that the chemosensing strategy detects serine, threonine and tyrosine phosphorylation with excellent sensitivity. In addition, the design is compatible with both a C- or N-terminal kinase recognition motif. These first-generation substrates utilized a Pro-Gly or Gly-Pro β-turn. However, certain kinases have strong requirements for residues in the –1 and +1 positions relative to the phosphorylation site. For

example, PKA-S1 is a poor substrate for PKA because the glycine residue replaces a preferred leucine residue at the -1 position ($K_M \sim 40$ μM, $V_{max} \sim 0.3$ μmol/min/mg). Thus, reactivity must be taken into consideration when designing a substrate. To improve and generalize the approach, we evaluated probe sensitivity with an additional recognition element in the β-turn sequence.

Inclusion of a leucine residue in the β-turn sequence to create the PKA chemosensor PKA-S2 resulted in both a larger fluorescence increase and improved reactivity with PKA. This chemosensor exhibited maximum fluorescence emission at 474 nm instead of at 485 nm, which indicates formation of mixed complexes with Mg^{2+} (stoichiometry evaluated as in Chapter 3). Mixed complex formation is not problematic for chemosensing when the peptide concentration is significantly below the Mg^{2+} concentration, since the ratio of complexes remains constant when the metal ion concentration is constant. However, 1:1 complexes should afford a larger fluorescence increase.

With one residue in the β-turn fixed for kinase recognition, the stereochemistry at proline was varied in an attempt to obtain a larger fluorescence increase. Both PKC and PKA substrates were synthesized with D-proline in the turn sequence (PKC-S4 and PKA-S3). For PKC chemosensors, which contain an N-terminal sensing module and glycine in the –1 position, Pro gave the largest fluorescence increase. On the other hand, for PKA chemosensors, which contain a C-terminal sensing module and leucine in the +1 position, D-Pro gives the largest fluorescence increase. In addition, the product phosphopeptide PKA-P3 exhibited maximum fluorescence intensity at 485 nm, indicating only 1:1 complex formation.

In order to evaluate the application of these design principles to other kinase substrates, substrates for Pim2, Akt, and MK2 were synthesized. The trend observed for the best PKA chemosensor was confirmed, because the largest fluorescence increase for a Pim2 chemosensor was obtained with D-Pro in the C-terminal sensing module. When the chemosensors Akt-S1 and MK2-S1 were designed utilizing this optimized Xaa-D-Pro β-turn sequence, they exhibited the most substantial fluorescence increases to date.

The best β-turn sequence for serine phosphorylation was also optimal for threonine phosphorylation with a C-terminal sensing module. This was determined by comparing the fluorescence spectra of Akt-P2 and a similar phosphopeptide where a proline residue was used in

the β-turn (Ac-ARKRERAYpTF-Pro-Sox-Gly-NH_2, Akt-P3). Not only did Akt-P3 exhibit less fluorescence at 485 nm, but it also formed mixed complexes ($\lambda_{em,max}$ = 474 nm).

To improve the affinity of the product phosphopeptide for magnesium, an additional chelating aspartate residue was incorporated in the sensing module, either one (PKC-S5) or two (PKC-S6) residues from Sox. This additional chelating moiety does increase the fluorescence intensity of the product phosphopeptide, but it also increases the Mg^{2+} affinity of the substrate peptide. As such, it did not generate a more substantial fluorescence increase over the closely-related peptide PKC-S4. Notably, though PKC-S5 and PKC-S6 do not have the largest fluorescence increase of all PKC chemosensors, the useful fluorescence increase suggests that the Sox-based chemosensing approach will be compatible with acidic residues.

Table 4-2. Peptide substrate sequences and fluorescence increases with 10 mM Mg^{2+}

Substrate	Residue to be phosphorylated	Location of sensing module	Sequence[a]	Fold Fluorescence Increase[b]
PKC-S1	Ser	N	Ac-Sox-Pro-G**S**FRRR-NH_2	5.7
PKC-S4	Ser	N	Ac-Sox-DPro-G**S**FRRR-NH_2	3.0
PKC-S2	Thr	N	Ac-Sox-Pro-G**T**FRRR-NH_2	3.8
PKC-S5	Ser	N	Ac-Asp-Sox-DPro-G**S**FRRR-NH_2	3.0
PKC-S6	Ser	N	Ac-Asp-Gly-Sox-DPro-G**S**FRRR-NH_2	2.7
PKA-S1	Ser	C	Ac-LRRA**S**-Gly-Pro-Sox-NH_2	2.5
PKA-S2	Ser	C	Ac-LRRA**S**L-Pro-Sox-NH_2	4.0
PKA-S3	Ser	C	Ac-LRRA**S**L-DPro-Sox-Gly-NH_2	5.5
Abl-S1	Tyr	N	Ac-Sox-Pro-Gly-I**Y**AAPFAKKK-NH_2	3.6
Pim2-S1	Ser	C	Ac-ARKRRRHP**S**G-DPro-Sox-Gly-NH_2	3.7
Pim2-S2	Ser	C	Ac-ARKRRRHP**S**G-Pro-Sox-Gly-NH_2	3.2
Akt-S1	Ser	C	Ac-ARKRERAY**S**F-DPro-Sox-Gly-NH_2	10
Akt-S2	Thr	C	Ac-ARKRERAY**T**F-DPro-Sox-Gly-NH_2	6.0
MK2-S1	Ser	C	Ac-AHLQRQL**S**I-DPro-Sox-Gly-NH_2	12

[a] The portion of the peptide sequence obtained from the literature is indicated by one-letter amino acid codes, with the residue to be phosphorylated in bold. [b] Assay conditions: 20 mM Hepes (pH 7.4), 10 mM $MgCl_2$, 0.1 mM EGTA, λ_{ex} = 360 nm, 3 nm excitation and emission slit widths. Fluorescence increase is determined by dividing the fluorescence of the phosphopeptide (10 μM) at 485 nm by the fluorescence of the substrate peptide (10 μM) at 485 nm.

Origin of the Large Fluorescence Increase

To assess the relationship between phosphopeptide affinity for Mg^{2+} and fluorescence increase, the Mg^{2+} dissociation constants of a few peptides spanning the range of fluorescence increases were determined. Binding affinities were assessed by Mg^{2+} titrations (Figure 4-6) and fit to a 1:1 binding model utilizing Specfit/32[59]; these peptides fulfill the criteria for 1:1 complexes from Chapter 3. Inspection of the dissociation constants for MK2-P1, PKC-P1, and Akt-P1 (Table 4-3), allows the conclusion that a product phosphopeptide with higher affinity for Mg^{2+} results in a more sensitive probe. To maintain constant ionic strength near the K_D, 150 mM NaCl was included in the buffer. Since the K_D depends on the ionic strength[60] and addition of Mg^{2+} rapidly increases the ionic strength, inclusion of 150 mM NaCl ensures that accurate comparison between peptides are made. The dissociation constants of the substrate peptides are challenging to measure, because it is difficult to maintain constant ionic strength for K_D values greater than 100 mM and thus to compare binding affinities. It is likely that the Sox residue itself is the only contributor to the binding of the substrate peptides to Mg^{2+} in the absence of an additional chelating residue.

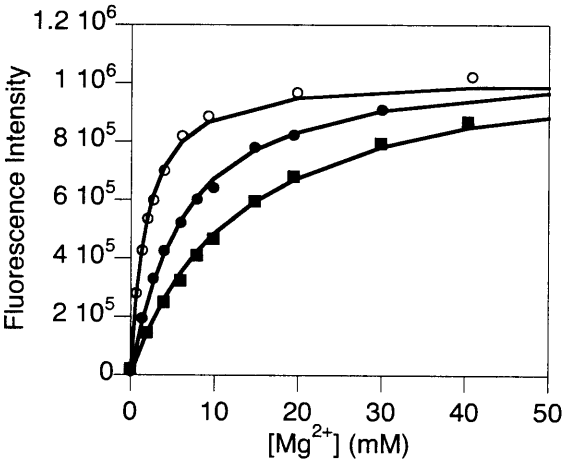

Figure 4-6. Mg^{2+} titration curves for MK2-P1 (○), Akt-P1 (●) and PKC-P1 (■). Fluorescence intensities at 485 nm were extracted from spectra obtained in 20 mM Hepes (pH 7.4), 150 mM NaCl. Fits were obtained by Specfit/32.[59]

Table 4-3. Apparent dissociation constants for select phosphopeptide-Mg^{2+} complexes

Peptide	Apparent K_D (mM)[a]	Fluorescence increase[b]
PKC-P1	12 ± 2	5.7
Akt-P1	6.8 ± 0.4	10
MK2-P1	1.8 ± 0.3	12

[a] Values reported are an average ± std dev for triplicate titrations, each performed by adding aliquots of a standardized $MgCl_2$ solution to peptide (1 μM) in 20 mM Hepes (pH 7.4), 150 mM NaCl. Dissociation constants were obtained from experimental data with the program Specfit/32.[59]

[b] Fluorescence increase is determined by dividing the fluorescence of the phosphopeptide (10 μM) at 485 nm by the fluorescence of the substrate peptide fluorescence (10 μM) at 485 nm in 20 mM Hepes (pH 7.4), 10 mM $MgCl_2$, 0.1 mM EGTA.

Fluorescence Increase Quantifies Product Formation

When a substrate peptide is incubated with a target kinase, an increase in fluorescence over time is observed as expected (Figure 4-7a). The magnitude of the increase was confirmed to correspond with the values reported in Table 4-2 for complete phosphorylation of PKC-S1 and Abl-S1 with their respective kinases.

The fluorescence intensity at any intermediate time is the sum of the contributions from both substrate and product peptides. At time t, the fluorescence intensity (I) can be determined from:

$$I(t) = f_S S(t) + f_P P(t) \qquad (1)$$

where $S(t)$ is the amount of substrate (μM), $P(t)$ is the amount of product (μM), f_S is the fluorescence intensity per μM of substrate, and f_P is fluorescence intensity per μM of product. The constants f_P and f_S are determined empirically under the desired assay conditions by obtaining the slope of fluorescence intensity versus concentration of P and S, respectively. It is imperative that the fluorescence signal for each substrate peptide and product phosphopeptide is linear with respect to concentration. These constants depend on the concentration of Mg^{2+} and the Mg^{2+} affinity of each peptide. Because the concentration of peptide used is significantly lower than the Mg^{2+} dissociation constant, the fraction of peptide bound to Mg^{2+} is constant regardless of peptide concentration. However, measured fluorescence is nonlinear when the

absorbance is significantly greater than 0.05.[61] In practice, if the range of peptide concentrations investigated includes concentrations greater than 30 μM, 400 nm should be used as the excitation wavelength for the entire experiment.

The amount of substrate and product at time *t* are related by:

$$S(t) + P(t) = S_0 \tag{2}$$

where S_0 is the initial amount of substrate. The amount of product formed at time *t* is determined by substituting equation (2) into (1):

$$P(t) = \frac{I(t) - f_S S_0}{f_P - f_S} \tag{3}$$

In addition to confirming that the fluorescence intensity upon 100% turnover matched that for synthetic phosphopeptide, the ability of equation (3) to predict the extent of product formation at time *t* by fluorescence measurements was investigated. Subjection of aliquots of the reaction mixture to HPLC (Figure 5-7b) and electrospray mass spectrometry analysis (Figure 4-7c) confirmed that product turnover can be quantified by fluorescence (Table 4-4).

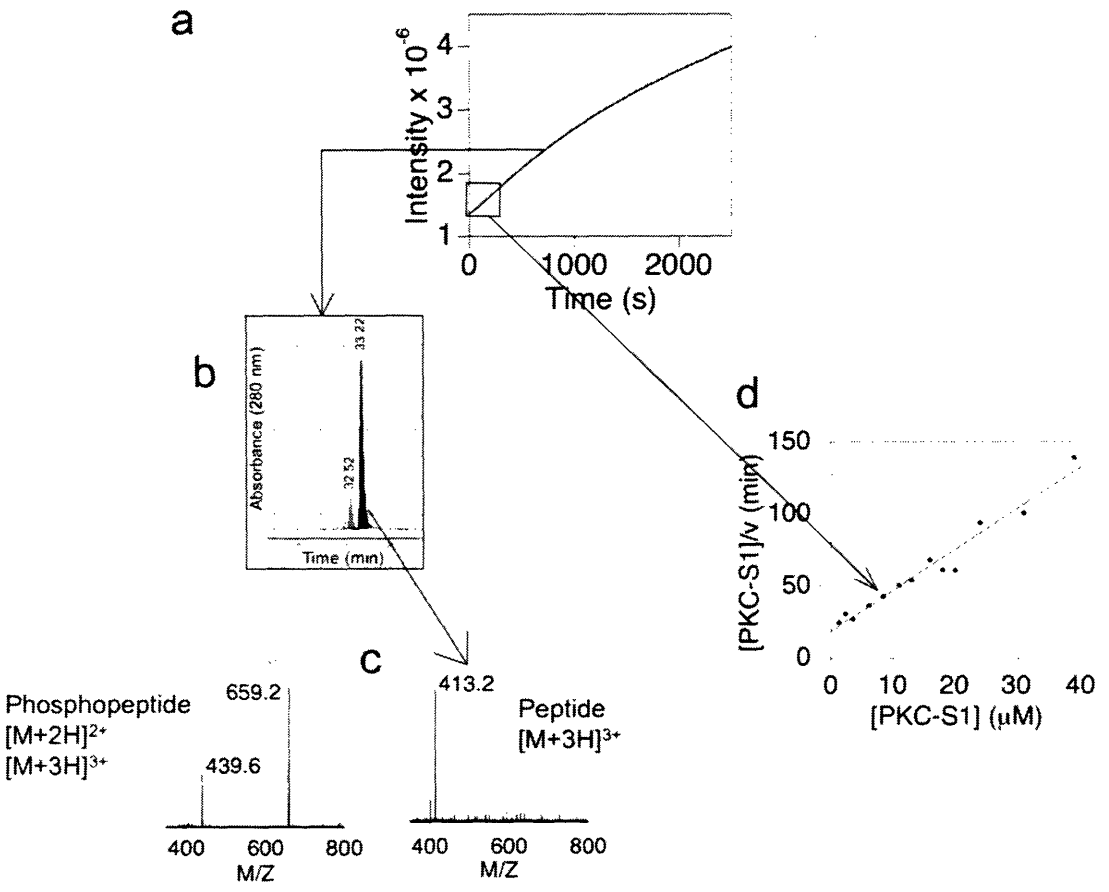

Figure 4-7. Confirmation of product formation and calculation of kinetic parameters from the continuous fluorescence response of the peptide chemosensor during a kinase reaction. (**a**) Fluorescence intensity over the reaction time-course of PKC-S1 (10 μM) with PKC_{α}; (**b**) HPLC of aliquot from reaction mixture at 700 s; (**c**) ESI-MS spectra of each peak from the HPLC plot in (b); (**d**) A representative Hanes plot of initial slopes data for this substrate where one point was obtained from the data in (a).

Table 4-4. HPLC and ESI- MS verification and quantification of product formation observed by fluorescence.

Kinase Substrate	Initial [Substrate] (μM)	Reaction Time	Substrate			Product					
			HPLC T_R (min)	*m/z* (z+)		HPLC T_R (min)	*m/z* (z+)		Concentration (μM)		
				Found	Calcd		Found	Calcd	Fluor-escence[c]	HPLC[d] 228 nm	HPLC[d] 280 nm
PKA-S2	46 μM	300 s	26.2[a]	587.8 (2+)	587.8	25.0[a]	627.8 (2+)	627.8	1.6	1.3	1.9
PKA-S2	7.8 μM	700 s	25.6[a]	587.8 (2+)	587.8	24.4[a]	627.8 (2+)	627.8	3.4	3.3	3.5
PKA-S2	7.8 μM	18 min	26.0[a]	587.8 (2+)	587.8	24.8[a]	627.8 (2+)	627.8	4.6	4.4	4.8
PKC-S1	30 μM	12 min	33.2[b]	413.2 (3+)	413.2	32.5[b]	659.2 (2+)	659.2	3.3	3.2	4.7

[a] HPLC gradient: 10 min. 15% B followed by linear gradient 15-50% B over 30 min. [b] HPLC gradient: 10 min. 0% B, linear gradient 0-10% B over 2 min. followed by linear gradient 10-50% B over 30 min. [c] Calculated by equation (3). [d] Calculated from the integrated area on the HPLC trace where total area equals S_0.

Determination of Kinetic Parameters for Chemosensors

The continuous nature of the Sox-based kinase assay allows initial rates to be determined from a single reaction mixture without extra effort to isolate and process aliquots. An additional benefit of the Sox-based chemosensing strategy is the compatibility with millimolar concentrations of ATP, which is significantly above the K_M for this substrate and allows an ATP-independent K_M to be calculated for the peptide substrate.

To obtain K_M and V_{max} for each substrate by fluorescence, the initial fluorescence increase (boxed in Figure 9a) needs to be converted to a product formation rate. Since the initial velocity of the reaction is the amount of product formed over time, taking the derivative of equation (3) with respect to time gives:

$$v = \frac{dP(t)}{dt} = \frac{\frac{dI(t)}{dt}}{f_P - f_S} \tag{4}$$

This equation accounts for a fluorescence increase due to product formation and a slight decrease in fluorescence over time due to substrate consumption. The initial slope of the reaction, $dI(t)/dt$, is measured within the first 10% of substrate turnover for several substrate concentrations between 0.5 and 5 × K_M. A linear fit of a Hanes plot ([S]/v vs. [S]) is used to find K_M and V_{max} (Figure 4-7d), where the X-intercept is $-K_M$, the slope is $1/V_{max}$. Hanes plot analysis was chosen because the data does not need to be weighted compared to Lineweaker-Burke analysis. In addition, this plot emphasizes higher substrate concentrations, where any error in substrate concentration produces only a small error in the rate.[62]

The kinetic parameters for optimized chemosensors are listed in Table 4-5. Importantly, the K_M and V_{max} values illustrate that these peptides are good substrates for their respective enzymes. The K_M values for most peptides are in good agreement with the reported K_M for the kinase recognition motif. Values are not available for threonine phosphorylation, but weaker phosphorylation of threonine by PKC (PKC-S2) has been noted for many substrate sequences,[63] and equivalent threonine phosphorylation by Akt (Akt-S2) was expected.[64] Peptides PKA-S2,

PKA-S3, and Abl-S1 have significantly different values from the literature. The improved K_M values for PKA-S2 and PKA-S3 is most likely due to a difference in ATP concentrations. The poorer K_M for Abl-S1 is likely because an important glutamate residue at the –3 position[65] was substituted with a proline residue as part of the β-turn. In general, comparison with K_M values from the literature demonstrates that the reporter motif does not interfere with reactivity of the substrate.

Table 4-5. Kinetic parameters for select kinase chemosensors

Substrate	K_M (μM)[a]	V_{max} (μmol min^{-1} mg^{-1})[a]	K_M (μM) literature	Ref.
PKC-S1	8.6 ± 2.9	5.9 ± 1.9	10	[66]
PKC-S2	23 ± 3	2.3 ± 0.6	--	
PKA-S2	1.8 ± 0.5	3.7 ± 1.6	16	[67]
PKA-S3	2.9 ± 0.6	6.3 ± 0.5	16	[67]
Akt-S1	3.8 ± 0.2	0.59 ± 0.14	8.8	[68]
Akt-S2	2.9	0.59	--	
MK2-S1	21 ± 2	2.3 ± 0.2	31	[69]
Abl-S1	26 ± 5	9.3 ± 0.5	4.0	[65]

[a] Values reported are from triplicate Hanes plots with substrate concentrations 0.5–5 × K_M.

Substrate specificity

As a preliminary assessment of the selectivity of some of these probes, PKC-S1, PKA-S3, Akt-S1, and MK2-S1 were assayed against recombinant PKC_α and PKA. PKC_α phosphorylated its designed substrate but also MK2-S1, and PKA phosphorylated PKA-S3 and to a slight extent, Akt-S1 (Figure 4-8). These measured selectivities likely parallel those for the substrates upon which these chemosensors were based.

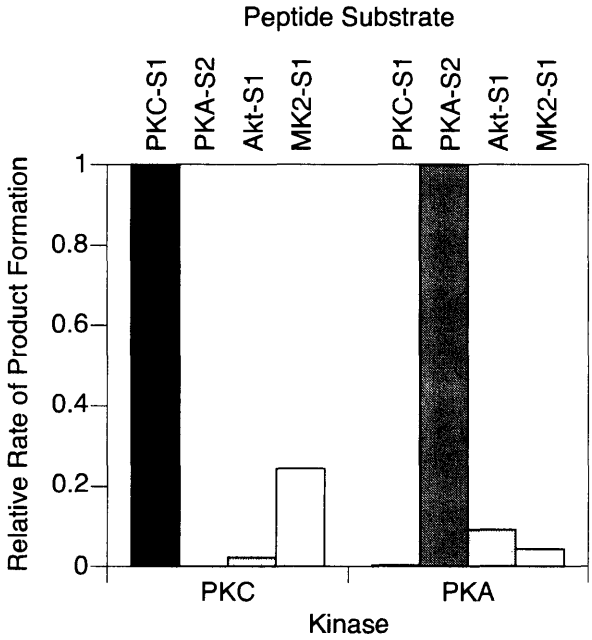

Figure 4-8. Cross-reactivity of peptide substrates with PKC_{α} and PKA. The rate of product formation was determined from equation (4) and was normalized to the designed substrate for each kinase.

Influence of Relevant Metal Ions on Kinase Chemosensing Ability

The ability of other biologically-relevant metal ions to compromise detection of kinase activity was investigated. In these experiments, the concentrations of all components were chosen to resemble physiological conditions: 10 μM peptide, 10 mM Mg^{2+}, and physiological concentrations or higher of other metal ions.[70] The fluorescence intensity of both the substrate peptide (Figure 4-9a) and the product phosphopeptide (Figure 4-9b) was investigated 1) in the absence of Mg^{2+} to detect fluorescence complexes (possible for Ca^{2+} and Zn^{2+}), and 2) in the presence of Mg^{2+} to detect quenched complexes (possible for all other metal ions).

With the exception of Zn^{2+}, no metal ions interfere at physiological concentrations. Even so, the response to Zn^{2+} is less than 20%. Fluorescence values for the substrate peptide with all metal ions in the presence of Mg^{2+} are within error due to low total fluorescence. The quenching effect of NaCl on the product phosphopeptide is a result of increased ionic strength, which alters the Mg^{2+} dissociation constant.

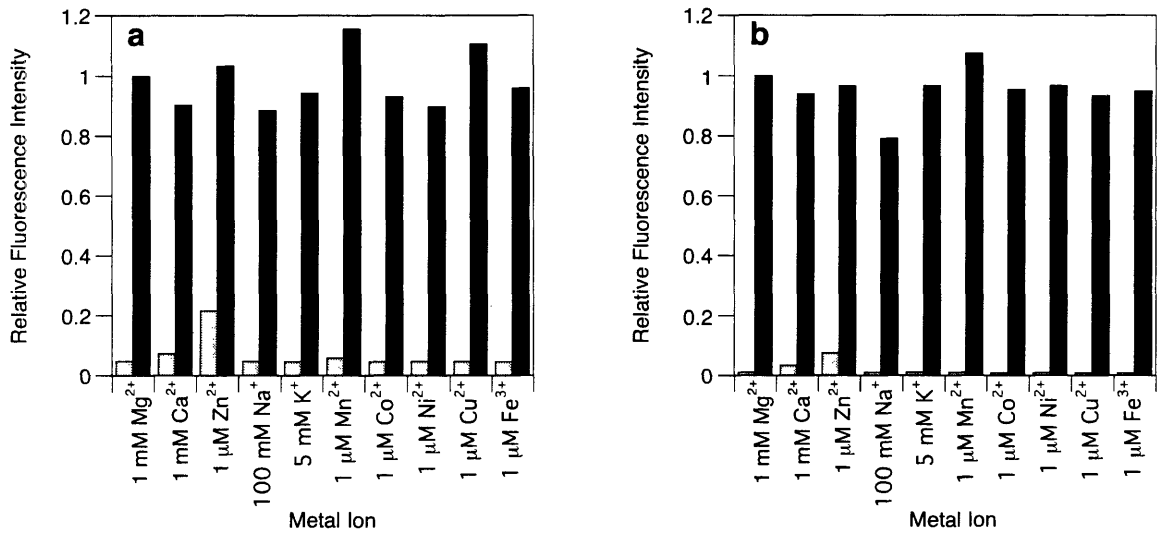

Figure 4-9. Effect of physiological metal ions on kinase chemosensors. Peptides (**a**) PKA-S2 and (**b**) PKA-P2 (10 μM each) were evaluated with the indicated metal ion concentrations in the presence and absence of $MgCl_2$ (10 mM). Fluorescence intensity for each measurement is plotted relative to the complex with 10 mM Mg^{2+}.

Finally, some kinases require significantly higher concentrations of Mn^{2+} for *in vitro* activity (e.g. EGFR), so the fluorescence of substrate and product peptides were tested with 1 mM Mn^{2+}. The probes are much less sensitive under these conditions; Mn^{2+} quenches substrate fluorescence by 70% and product fluorescence by 95% such that phosphorylation results in a 30% fluorescence decrease.

Application to High-Throughput Kinase Inhibitor Screening

To illustrate the immediate utility of these probes in high-throughput screening applications, the chemosensor PKC-S2 was used to interrogate PKC inhibition. Commercially available PKC inhibitors with distinctly different inhibitory constants (IC_{50}) were chosen: bisindolylmaleimides I (GF109203X), IV and V. In high-throughput 96-well plate format, three different doses of each inhibitor were tested against PKC. The initial fluorescence increase of each reaction was normalized against the fluorescence increase in the absence of inhibitor. The PKC-S2 assay easily detects that bisindolylmaleimide I is the most potent PKC inhibitor, as expected (Figure 4-10). Additional high-throughput applications include analysis of kinase activity in crude cell lysates, which will be discussed in the next chapter.

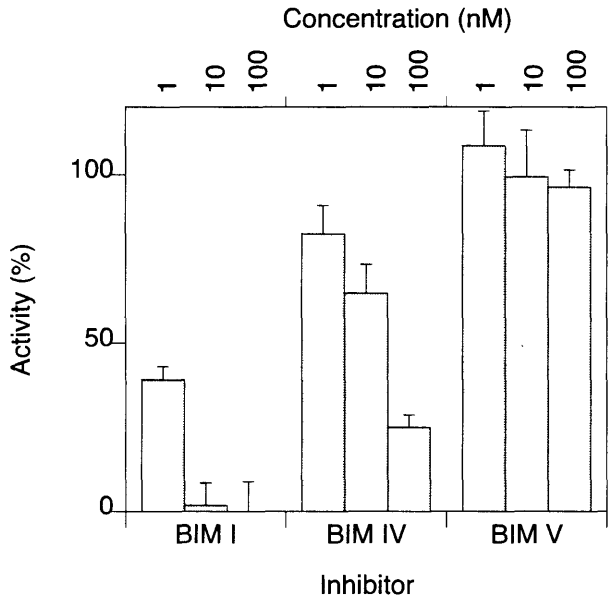

Figure 4-10. Influence of varying concentrations BIM I, BIM IV, and BIM V on PKC_{α} activity.

Discussion

The successful design of fluorescent chemosensors of protein kinase activity containing the Sox amino acid is reported. The versatility of the approach allows generation of probes for both serine/threonine and tyrosine kinases with recognition residues on either the N- or C-terminus. Compared to other sensors for kinase activity, Sox-based probes are easily synthesized and their use is incredibly straightforward, without complicated handling steps.

Many general conclusions can be drawn from the fluorescence increase values in Table 4-2. First, the fluorescence increase for phosphorylation of serine, threonine and tyrosine is quite large (3–12-fold) across the range of 14 probes synthesized. Even sub-optimal designs give larger fluorescence increases than any other probe reported to date. The chemosensing strategy is compatible with acidic residues and additional proline residues in the kinase recognition motif (Pim2-S1). The fluorescence increase for each chemosensor depends on the residue to be phosphorylated; serine affords the largest increase in fluorescence, followed by threonine and tyrosine. The flexibility of the phosphoserine side chain as compared to phosphothreonine and phosphotyrosine likely improves the propensity for chelate formation.

The β-turn is the other important factor that determines the magnitude of the fluorescence increase. Kinase recognition is crucial for excellent reactivity; one recognition element must remain fixed in the turn sequence for serine/threonine kinase chemosensors, thus the stereochemistry at proline is used to tune the fluorescence increase. The fluorescence increase trends for these kinase chemosensors suggest that Mg^{2+} prefers a type II β-turn, either Xaa-DPro or Pro-Gly. The fact that Xaa-DPro gives a larger fluorescence increase than a turn containing glycine suggests that Mg^{2+} prefers a rigid β-turn. This differentiates the coordination preferences of Mg^{2+} from those of Zn^{2+}, which might be expected because Mg^{2+} prefers octahedral coordination geometry whereas Zn^{2+} prefers tetrahedral.

From the chemosensors presented herein, optimal design recommendations can be made for all serine/threonine kinase chemosensors containing N-terminal kinase recognition elements and for a subset of serine/threonine kinase chemosensors containing C-terminal kinase recognition elements (with Gly in the –1 position) (Figure 4-11a). Kinase substrates with a C-terminal recognition elements with a residue other than Gly at the –1 position need to be further investigated. The type II β-turn that is optimal in the PKA, Akt, MK2 and Pim2 substrates is not possible when the –1 position is fixed with an L-amino acid; either Pro-Xaa (Type I) or DPro-Xaa (Type II') remain as options.

Optimal peptide chemosensors for PKC, PKA, Akt, MK2, Pim2 are shown in Figure 4-11b. To generate additional probes, the best design principles presented herein (Figure 4-11a) can be applied and then the fluorescence increase can be determined empirically.

While the design principles for serine and threonine phosphorylation were investigated in most depth herein, one chemosensor for a tyrosine kinase was developed (Abl-S1). Tyrosine kinase chemosensor design requires an additional element in the β-turn sequence, and it is likely that similar optimization to that performed for serine/threonine kinases will lead to improved probes for tyrosine kinase activity,

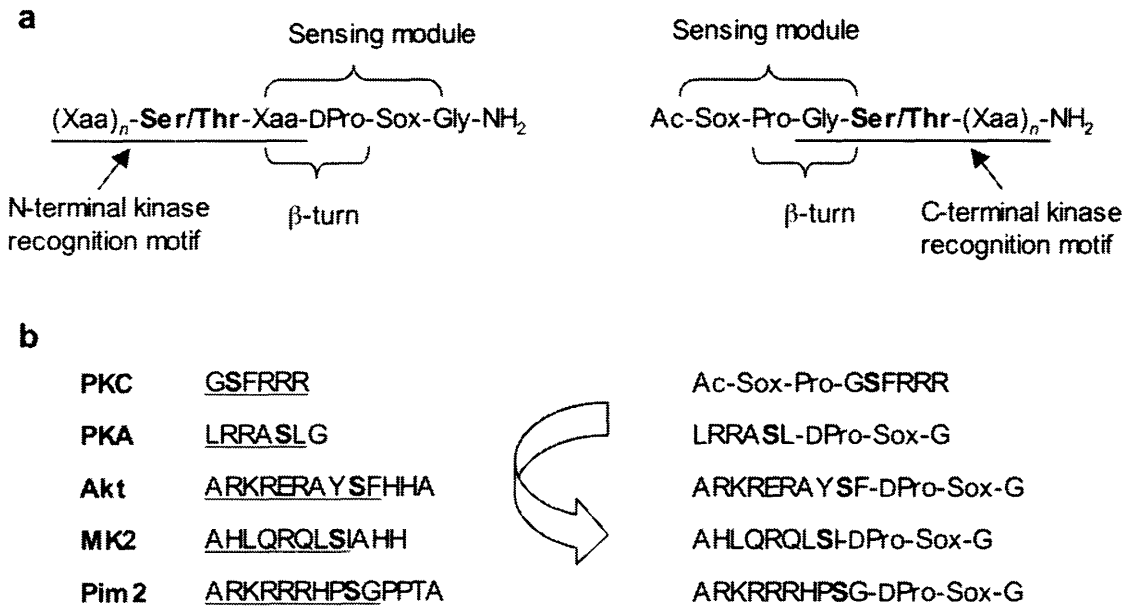

Figure 4-11. Optimized kinase chemosensor design based on results presented herein for serine/threonine phosphorylation. (**a**) The critical kinase specificity determinants in the chemosensor peptide sequence are derived from an optimized peptide substrate, including one residue in the sensing module as part of the β-turn sequence. (**b**) Specific optimized peptide substrates from the literature are converted to kinase chemosensors as described in (a). The residues to be phosphorylated are indicated in bold.

A method for determining the kinetic parameters from fluorescence data has been established and validated. The K_M and V_{max} values determined for the optimized chemosensors show that these probes are good substrates for their respective kinases. Desirable kinetic parameters aid probe sensitivity, as large V_{max}/K_M ratios result in faster turnover and thus a larger fluorescence slope. High-throughput assays are even more facile than determination of kinetic parameters because the slopes can be compared without converting to turnover.

The chemosensing approach should be adaptable to studying kinases in living cells. The chemosensing strategy is compatible with physiological Mg^{2+} concentrations and is not influenced by other biologically-available metal ions. The fluorescence of Sox is similar to that of NBD in water, which has been used by the Lawrence laboratory[47] to visualize kinase activity in cells. A necessary first step will be to investigate the utility of these chemosensors in cell extracts, which will be undertaken in Chapter 5.

Conclusion

In conclusion, we have developed a widely applicable, continuous fluorescence assay for protein kinase activity. In contrast with other existing sensing methodologies, this assay is extremely versatile, straightforward and exhibits a large signal increase. The ability to chemically synthesize the product phosphopeptide enables careful characterization of the fluorescence behavior and substrate turnover. In addition, the stable fluorescence of the Sox-Mg^{2+} complex permits a continuous assay, which obviates problems with the termination steps of endpoint assays. In general, the substantial fluorescence changes of these peptide-based probes will be important for sensing the activity of less abundant endogenous kinases. A mere 1% turnover corresponds to a 5–10% fluorescence increase, which is easily measured under the prescribed conditions.

The β-turn sequence in the sensing module was optimized for improved reactivity and sensitivity by incorporating an additional amino acid recognition element and evaluating which isomer of proline affords the largest fluorescence increase. The large signal increase is compatible with all types of kinase peptide substrates but does vary depending on the requirements of the target kinase, including 1) the residues nearby the Mg^{2+} chelating moiety; 2) the type of residue to be phosphorylated and 3) the presence of additional chelating residues.

The ability to quantify substrate turnover by fluorescence allowed determination of the kinetic parameters for each substrate. The kinase chemosensing peptides have similar kinetic parameters to the optimal peptides for these kinases, which indicates that the sensing module does not affect specific activity. The best design principles determined were easily applied to additional peptide chemosensors, suggesting that a chemosensor for any kinase can be developed based on the results presented herein. These probes are immediately applicable to high-throughput screening assays.

Assays utilizing Sox-based chemosensors offer many advantages over discontinuous assays of protein kinase activity. Importantly, real-time analysis of reaction progress is possible. In addition, handling steps to separate incompatible reaction components or to manipulate the substrate are not required to analyze reaction outcome. Even discontinuous assays that are

homogeneous and allow for a simple one-step quenching procedure are not compatible with physiological ATP concentrations and complex reaction mixtures.

The Sox-based chemosensors share several common advantages of continuous probes of protein kinase activity and are superior in some regards. They are compatible with physiological ATP concentrations and complex reaction components. As readily-synthesized peptide-based probes, they are amenable to *in vitro* studies with recombinant kinases. On the other hand, protein-based probes are more useful for work in living cells due to the effort to isolate the sensor following expression. Similar to the modular AFP-based probes, Sox-based chemosensors can be easily modified for analysis of any desired kinase by altering the kinase recognition motif. The brightness of the Sox-based probes is comparable to that of NBD, and is roughly an order of magnitude dimmer than the Ca^{2+} CHEF probes and protein-based constructs. While the Sox-based probes are limited in their ability to accommodate residues on both sides of the phosphorylation site, modular expressible probes suffer limitations on the sequence to be phosphorylated due to the requirement for intramolecular binding of this sequence to the recognition domain. In addition to the aforementioned advantages, the most important advantage of the Sox-based chemosensing strategy is the dramatic fluorescence increase, rendering these probes the most sensitive.

Future Directions

Further improvements in sensitivity, reactivity, specificity and scope will increase the utility of all probes. To augment sensitivity of the chemosensing strategy in general, a brighter fluorophore with red-shifted fluorescence is desirable, especially considering that AFP-based probes are extremely bright and excited in the visible spectrum. Such a fluorophore may be possible by designing additional aromatic rings onto the Sox chromophore. In addition, such a probe with an alternate excitation and emission wavelength could be used in concert with a probe containing Sox for simultaneous imaging of two kinase activities.

The specificity and reactivity of these probes could be optimized by incorporation of recognition elements on both the C- and N-terminus of the phosphorylation site. This would likely afford a better substrate for Abl. For this purpose, modifying an amino acid side chain with the Sox chromophore will be investigated.

Incorporation of Sox into full-length protein substrates[71] would provide a means to study kinases that do not effectively phosphorylate peptide substrates. Additionally, the generation of protein-based probes would allow inclusion of docking domains to improve specificity when current peptide substrates are nonspecific.

In addition to high-throughput screening in solution, these chemosensors could also be immobilized in arrays for diagnostics or proteomics research. For cellular studies, functionalities such as peptide transduction domains, targeting peptide sequences, or additional fluorophores as internal standards can be readily incorporated.

These versatile and powerful chemosensors provide tools for researchers studying the roles of protein kinases in signal transduction. The design principles presented herein provide guidelines for the generation of additional probes. The application of these probes to high-throughput screening and cellular studies should aid in signal transduction research.

Acknowledgements

I would like to thank Professor Barbara Imperiali for Figure 4-3 and for her creativity, which turned a frustrating result in the Zn^{2+}-chemosensing project into an elegant approach for assaying kinase activities. I would also like to thank Eugenio Vazquez for helpful discussions and Jebrell Glover for verifying the equations presented in this chapter. This research was supported by the National Institutes of Health (GM64346 Cell Migration Consortium, P50-068762 Cell Decision Processes Center) and the National Science Foundation (CHE-9996335).

Experimental

Peptide Synthesis

Peptides were synthesized using standard Fmoc amino acid protection chemistry on Fmoc-PAL-PEG-PS resin (Applied Biosystems, 0.2 mmol equiv). All Fmoc-protected amino acids and coupling reagents were purchased from Novabiochem. Couplings of Fmoc-protected amino acids to the resin were carried out with either 1) 1-benzotriazolyoxytris(pyrrolidino)phosphonium hexafluorophosphate (PyBOP), 1-hydroxybenzotriazole (HOBt) and diisopropylethylamine (DIPEA) or 2) *O*-(7-azabenzotrazol-1-yl)-1,1,3,3-tetramethyluronium hexafluorophosphate (HATU) and DIPEA to generate the activated ester. The resin was swelled in dichloromethane (5 min.) then DMF (5 min.) prior to synthesis. All amino acids other than the Sox, phosphoserine, phosphothreonine and phosphotyrosine were added by the following representative procedure: removal of the Fmoc group (20% piperidine solution in DMF, 3 x 5 min.), wash (DMF, 5 x 1 min.), coupling (amino acid/PyBOP/DIEA, 6:6:6, 0.05 M in DMF, 30 min.), rinse (DMF, 2 x 1 min; DCM, 2 x 1 min.). To couple the Sox residue, double coupling with 2 equivalents each time was used (Fmoc-Sox-OH/PyBOP/DIPEA, 2:2:2, 0.15M in DMF, 2 x 30 min.). When Sox was coupled after a proline residue, longer coupling times were used (120 min). To couple the phosphoamino acid residues, HATU was used (Fmoc-Xaa(PO(OBzl)OH)-OH/HATU/DIPEA, 3:3:3, 0.05 M in DMF, 30 min.), with care to avoid an excess of HATU because this often leads to capping of the N-terminus with a guanidinium moiety. After addition of the final residue, the peptide was acetyl-capped (pyridine/acetic anhydride, 20:20, 0.15 M in DMF, 30 min.), and a final deblock cycle (20% piperidine in DMF, 3 x 5 min.) was performed to cleave any Sox aryl ester formed. The resin was dried under high vacuum overnight prior to a 2.5-hour cleavage with trifluoroacetic acid/triisopropylsilane/water (95:2.5:2.5, 40 μl/mg resin for substrate peptides and 140 μl/mg resin for product phosphopeptides). The resulting solution was concentrated under a stream of nitrogen. The pellet was triturated with cold 1:1 ether:hexanes (3 x 1.5 ml for 15 mg resin), redissolved in 50:50 water/acetonitrile, filtered and lyophilized overnight. Peptides were redissolved in water containing 0.1% TFA and were purified by preparatory reverse-phase HPLC (C_{18}) to greater than 95% (confirmed by analytical HPLC, C_{18}). Peptide identities were confirmed by electrospray mass spectrometry (ESI-MS).

Peptide Characterization Data

Peptide	Sequence	Mol. Formula	HPLC T_R (min)	*m/z* (z+) calcd	*m/z* found
PKC-S1	Ac-Sox-Pro-Gly-Ser-Phe-Arg-Arg-Arg-NH_2	$C_{53}H_{80}N_{20}O_{13}S$	26.7[a]	413.2 (+3)	413.2
PKC-P1	Ac-Sox-Pro-Gly-pSer-Phe-Arg-Arg-Arg-NH_2	$C_{53}H_{81}N_{20}O_{16}PS$	25.7[a]	659.3 (+2)	659.2
PKC-S2	Ac-Sox-Pro-Gly-Thr-Phe-Arg-Arg-Arg-NH_2	$C_{54}H_{82}N_{20}O_{13}S$	22.8[b]	417.9 (+3)	417.9
PKC-P2	Ac-Sox-Pro-Gly-pThr-Phe-Arg-Arg-Arg-NH_2	$C_{54}H_{83}N_{20}O_{16}PS$	21.6[b]	666.3 (+2)	666.3
PKC-S4	Ac-Sox-DPro-Gly-Ser-Phe-Arg-Arg-Arg-NH_2	$C_{53}H_{80}N_{20}O_{13}S$	30.05[a]	413.2 (+3)	413.2
PKC-P4	Ac-Sox-DPro-Gly-pSer-Phe-Arg-Arg-Arg-NH_2	$C_{53}H_{81}N_{20}O_{16}PS$	28.77[a]	659.2 (+2)	659.2
PKC-S5	Ac-Asp-Sox-DPro-Gly-Ser-Phe-Arg-Arg-Arg-NH_2	$C_{57}H_{85}N_{21}O_{16}S$	29.05[a]	451.5 (+3)	451.5
PKC-P5	Ac-Asp-Sox-DPro-Gly-pSer-Phe-Arg-Arg-Arg-NH_2	$C_{57}H_{86}N_{21}O_{19}PS$	27.86[a]	478.4 (+3)	478.2
PKC-S6	Ac-Asp-Gly-Sox-DPro-Gly-Ser-Phe-Arg-Arg-Arg-NH_2	$C_{59}H_{88}N_{22}O_{17}S$	28.92[a]	470.6 (+3)	470.5
PKC-P6	Ac-Asp-Gly-Sox-DPro-Gly-pSer-Phe-Arg-Arg-Arg-NH_2	$C_{59}H_{89}N_{22}O_{20}PS$	28.16[a]	497.4 (+3)	497.2
PKA-S1	Ac-Leu-Arg-Arg-Ala-Ser-Gly-Pro-Sox-NH_2	$C_{47}H_{75}N_{17}O_{13}S$	28.92[a]	559.8 (+2)	559.7
PKA-P1	Ac-Leu-Arg-Arg-Ala-pSer-Gly-Pro-Sox-NH_2	$C_{47}H_{76}N_{17}O_{16}PS$	28.68[a]	599.8 (+2)	599.7
PKA-S2	Ac-Leu-Arg-Arg-Ala-Ser-Leu-Pro-Sox-NH_2	$C_{51}H_{83}N_{17}O_{13}S$	25.9[b]	587.8 (+2)	576.8
PKA-P2	Ac-Leu-Arg-Arg-Ala-pSer-Leu-Pro-Sox-NH_2	$C_{51}H_{84}N_{17}O_{16}PS$	25.1[b]	627.9 (+2)	627.8
PKA-S3	Ac-Leu-Arg-Arg-Ala-Ser-Leu-DPro-Sox-Gly-NH_2	$C_{53}H_{86}N_{18}O_{14}S$	30.0[a]	616.3 (+2)	616.2
PKA-P3	Ac-Leu-Arg-Arg-Ala-pSer-Leu-DPro-Sox-Gly-NH_2	$C_{53}H_{87}N_{18}O_{17}PS$	29.1[a]	656.3 (+2)	656.2
Akt-S1	Ac-Ala-Arg-Lys-Arg-Glu-Arg-Ala-Tyr-Ser-Phe-DPro-Sox-Gly-NH_2	$C_{79}H_{118}N_{26}O_{21}S$	31.0[a]	600.6 (+3)	600.6
Akt-P1	Ac-Ala-Arg-Lys-Arg-Glu-Arg-Ala-Tyr-pSer-Phe-DPro-Sox-Gly-NH_2	$C_{79}H_{119}N_{26}O_{24}PS$	30.0[a]	627.3 (+3)	627.6
Akt-S2	Ac-Ala-Arg-Lys-Arg-Glu-Arg-Ala-Tyr-Thr-Phe-DPro-Sox-Gly-NH_2	$C_{80}H_{120}N_{26}O_{21}S$	29.64[a]	605.4 (+3)	605.3
Akt-P2	Ac-Ala-Arg-Lys-Arg-Glu-Arg-Ala-Tyr-pThr-Phe-DPro-Sox-Gly-NH_2	$C_{80}H_{121}N_{26}O_{24}PS$	28.73[a]	632.0 (+3)	632.0
Akt-P3	Ac-Ala-Arg-Lys-Arg-Glu-Arg-Ala-Tyr-pThr-Phe-Pro-Sox-Gly-NH_2	$C_{80}H_{121}N_{26}O_{24}PS$	27.43[a]	632.0 (+3)	632.0
MK2-S1	Ac-Ala-His-Leu-Gln-Arg-Gln-Leu-Ser-Ile-DPro-Sox-Gly-NH_2	$C_{69}H_{108}N_{22}O_{19}S$	31.4[a]	791.4 (+2)	791.4
MK2-P1	Ac-Ala-His-Leu-Gln-Arg-Gln-Leu-pSer-Ile-DPro-Sox-Gly-NH_2	$C_{69}H_{109}N_{22}O_{22}PS$	30.1[a]	831.4 (+2)	831.4
Pim2-S1	Ac-Ala-Arg-Lys-Arg-Arg-Arg-His-Pro-Ser-Gly-Pro-Sox-Gly-NH_2	$C_{72}H_{117}N_{31}O_{18}S$	24.42[d]	435.0 (+4)	435.0
Pim2-P1	Ac-Ala-Arg-Lys-Arg-Arg-Arg-His-Pro-pSer-Gly-Pro-Sox-Gly-NH_2	$C_{72}H_{118}N_{31}O_{21}PS$	23.84[d]	455.0 (+4)	455.0
Pim2-S2	Ac-Ala-Arg-Lys-Arg-Arg-Arg-His-Pro-Ser-Gly-DPro-Sox-Gly-NH_2	$C_{72}H_{117}N_{31}O_{18}S$	24.2[d]	435.0 (+4)	435.0
Pim2-P2	Ac-Ala-Arg-Lys-Arg-Arg-Arg-His-Pro-pSer-Gly-DPro-Sox-Gly-NH_2	$C_{72}H_{118}N_{31}O_{21}PS$	24.21[d]	455.0 (+4)	455.0
Abl-S1	Ac-Sox-Pro-Gly-Ile-Tyr-Ala-Ala-Pro-Phe-Ala-Lys-Lys-Lys-NH_2	$C_{79}H_{117}N_{19}O_{18}S$	21.1[c]	551.6 (+3)	552.0
Abl-P1	Ac-Sox-Pro-Gly-Ile-pTyr-Ala-Ala-Pro-Phe-Ala-Lys-Lys-Lys-NH_2	$C_{79}H_{118}N_{19}O_{21}PS$	20.1[c]	578.3 (+3)	578.3

[a] 5 min. 10% B followed by linear gradient 10-50% B over 30 min. [b] 5 min. 15% B followed by linear gradient 15-50% B over 30 min. [c] 5 min. 20% B followed by linear gradient 20-70% B over 30 min. [d] 5 min. 10% B followed by linear gradient 10-40% B over 30 min.

Instrumentation

High-Performance Liquid Chromatography (HPLC): Waters 400 and 600 systems (solvent A = water, 0.1% v/v TFA; solvent B = MeCN, 0.1% v/v TFA). Columns used: C_{18} analytical, Beckman Ultrasphere ODS, 5 μm, 150 x 4.6 mm; C_{18} preparatory, YMC-Pack Pro, 5 μm, 250 x 20 mm.

Electrospray Mass Spectrometer: Applied Biosystems Mariner mass spectrometer spattered with a random assortment of dead flies and fly parts thanks to building 18 renovations.

UV-Vis Spectrophotometer: Beckman DU 7500 and Shimadzu UV-2401PC.

Fluorimeter: Fluoromax 3 from Jobin Yvon (λ_{ex} = 360 nm or 400 nm, λ_{em} = 485 nm).

Fluorescence Plate Reader: HTS7000 Bio Assay Reader from PerkinElmer with 360 nm excitation filter (35 nm bandpass), 485 nm emission filter (20 nm bandpass), 40 μs integration, 3 flashes/well, 120 gain.

Materials

Cuvette: Starna Cells (16.100F-Q-10) 100 μl sub-micro cuvette, 1 cm path length, 120 μl reaction volume.

96-well plates : FluoroNunc PolySorp black 96-well plate (475523), 400 μl well volume with 150 μl reaction volume/well.

Quantum Yield Determination

The quantum yield (Φ) was determined for MK2-P1 in 20 mM HEPES (pH 7.4). Quinine sulfate dihydrate (QS, Fluka, puriss. for fluorescence) in 0.1 M H_2SO_4 was used as a standard (Φ = 0.55). A 4 μM solution of MK2-S1 with 50 mM $MgCl_2$ was compared to a 4 μM solution of quinine sulfate to assure that the absorbance (A_{360}) is less than 0.05 at identical excitation wavelengths. The following equation was used to calculate the quantum yield:

$$\Phi = \frac{IA_{QS}\Phi_{QS}}{AI_{QS}}$$

where A = A_{360} and I = integrated fluorescence intensity (λ_{ex} = 360 nm). The calculated Φ assumes that the refractive index of 0.1 M H_2SO_4 is identical to that of 20 mM HEPES (pH 7.4). The error associated with the Φ of quinine sulfate is at least 10%, the error in Φ is no less than 10%.

Stock Solutions:

Stock solutions were prepared by weight and stored in plastic at room temperature unless otherwise noted. Reagents with the highest purity and lowest metal content were used, including ultrapure water (18 MΩ).

1) Concentrations of peptide stock solutions were determined by UV-Vis (based on the determined extinction coefficient of the fluorophore unit, 5-(*N*,*N*-dimethylsulfonamido)-8-hydroxy-2-methylquinoline, ε_{355} = 8247 M^{-1} cm^{-1} in 0.1 M NaOH with 1 mM Na_2EDTA). These solutions were stored at 4°C for two months, or –20°C for longer periods.
2) Stock solutions of magnesium chloride (Puratronic grade, Alfa Aesar, 3 M) and calcium chloride (Puratronic grade, Alfa Aesar, 0.3 M) were prepared in 1 mM HCl (Baseline, Seastar Chemicals). High purity is essential, because most commercially available salts contain Zn^{2+} as significant impurities.[72] The Mg^{2+} and Ca^{2+} concentrations were determined by titration with a standardized solution of EDTA (Aldrich) in the presence of the indicator Eriochrome Black T (Aldrich).[73]
3) 200 mM Hepes (SigmaUltra) was adjusted to pH 7.4 with sodium hydroxide (99.998+%, Aldrich) solution (1 M) and stored at 4°C.
4) 10 mM dithiothreitol (Biotechnology grade, Mallinckrodt) and prepared in degassed ultrapure water and stored at –20° C.
5) 100 mM ATP was prepared with adenosine 5'-triphosphate (Disodium salt, Low Metals Grade, Calbiochem) and stored at –20° C.
6) 10 μg/ml phosphatidylserine and 2 μg/ml diacylglycerol in 20 mM HEPES pH 7.4 were prepared by combination of appropriate volumes of chloroform solutions of 10 mg/ml porcine brain phosphatidylserine (Avanti Polar Lipids, Inc.) and 2 mg/ ml 1,2-dioleoyl-*sn*-glycerol (Avanti Polar Lipids, Inc.). The chloroform was evaporated and 20 mM Hepes (pH 7.4) was added. The solution was sonicated in a bath sonicator for 12 min, stored in aliquots at –20°C, which were each sonicated upon thawing.

7) 2 mg/ml BSA was prepared by dissolving bovine serum albumin (Heat Shock Fraction V, Roche) in ultrapure water and then filtering through a 0.45 micron syringe filter to remove particulates.
8) 10% Brij-35 was prepared from Brij-35P (Biochemika grade, Fluka) and serially-diluted to a working stock of 0.1%.
9) 500 mM EGTA was prepared from ethylene glycol-bis(2-aminoethylether)-*N,N,N',N'*-tetraacetic acid (SigmaUltra) dissolved in 2 M NaOH and stored at 4°C.
10) 5 M NaCl was prepared by dissolving sodium chloride (SigmaUltra) in ultrapure water.

Spectral Comparison of Phosphorylated and Unphosphorylated Peptides:

10 μM each of substrate peptide and product phosphopeptide in 20 mM Hepes (pH 7.4), 10 mM $MgCl_2$, 0.1 mM EGTA were independently measured with an excitation wavelength of 360 nm and 3 nm excitation/emission slit widths.

Mg^{2+} Dissociation Constant Determination:

Single titrations were performed with 1 μM peptide in 20 mM Hepes (pH 7.4), 150 mM NaCl. Aliquots of $MgCl_2$ stock solutions were added and the data were fit with the program Specfit/32[59].

Recombinant Enzyme Assays

Recombinant enzyme was added to begin each reaction unless otherwise noted to varying chemosensor concentrations (0.5–5 × K_M) at 30°C. Reactions to obtain kinetic parameters were performed in the fluorimeter within 10% turnover. Readings were obtained every 10 s for 5 min (λ_{ex} = 360 nm for PKC, PKA, Akt; λ_{ex} = 400 nm for MK2, Abl; λ_{em} = 485 nm; slit widths = 5 nm). For high-throughput inhibitor screening in polystyrene plates, an extra 0.2 mg/ml BSA was used to prevent enzyme activity loss. Assay conditions were optimized for each kinase to assure that the enzyme did not lose activity either the stock solution or the reaction mixture. If no activity loss occurrs in the enzyme stock solution, assays with identical substrate and enzyme concentrations repeated 1 hour apart will exhibit identical slopes. To confirm that the enzyme did not lose activity upon dilution into the reaction mixture, Selwyn's test was used. In this test,

the concentration of substrate is held constant and the concentration of enzyme is varied. If an enzyme does not lose activity upon dilution, the rate of turnover doubles when the amount of enzyme is doubled. Final assay conditions were as follows:

PKC: 20 mM Hepes (pH 7.4), 10 mM $MgCl_2$, 0.3 mM $CaCl_2$, 0.1 mM EGTA, 1 mM ATP, 1 mM DTT, 0.5 μg/ml phosphatidylserine, 0.1 μg/ml diacylglycerol, PKC_α (5.5 ng for serine phosphorylation and 11 ng for threonine phosphorylation, Calbiochem, diluted 1:20 with 20 mM Hepes (pH 7.4), 5 mM DTT). Substrate peptide was added to begin the reaction.

PKA: 20 mM Hepes (pH 7.4), 10 mM $MgCl_2$, 1 mM ATP, 1 mM DTT, 0.1 mM EGTA, 8 ng PKA catalytic subunit (Catalytic Subunit, Calbiochem, diluted 1:80 with 50 mM Tris-HCl pH 7.5, 10 mM $MgCl_2$, 1 mM DTT, 0.15 mg/ml BSA).

Akt1: 20 mM Hepes (pH 7.4), 10 mM $MgCl_2$, 1 mM ATP, 1 mM DTT, 0.1 mM EGTA, 40 ng Akt1 (Upstate, diluted 1:20 with 20 mM Hepes pH 7.4, 1 mM DTT, 0.1% Brij-35, 1 mg/ml BSA).

MK2: 20 mM Hepes (pH 7.4), 10 mM $MgCl_2$, 1 mM ATP, 1 mM DTT, 0.1 mM EGTA, 0.01% Brij-35, 0.1 mg/ml BSA, 20 ng MAPKAP kinase 2 (Upstate, diluted 1:10 with 20 mM Hepes pH 7.4, 1 mM DTT, 0.1% Brij-35, 1 mg/ml BSA).

Abl: 20 mM Hepes (pH 7.4), 10 mM $MgCl_2$, 1 mM ATP, 1 mM DTT, 0.01 % Brij-35, 4 ng Abl (New England Biolabs, diluted 1:5 with 20 mM TRIS pH 7.5, 10 mM $MgCl_2$, 0,1 mM EGTA, 0.01% Brij-35 and 1.0 mg/ml BSA).

Data Workup

Fluorescence slopes were determined by a least-squares fit using KaleidaGraph (3.6.2, Synergy Software). This slope averages out scatter in individual fluorescence readings. This slope was then either converted to a rate (equation (4)) or compared directly to the slopes of other reactions with the same peptide concentration. Values reported are an average ± standard deviation for triplicate experiments.

HPLC and MS Data for Kinase Reactions

All reactions were monitored by fluorescence and quenched with 40 μl of a 0.1 M Na_2EDTA stock solution and then stored on ice prior to HPLC analysis.

Metal Competition Studies

Metal ion solutions were prepared from hydrates of their chloride salts and the concentrations determined based on salt weight, with the exception of $MgCl_2$, $CaCl_2$ and $ZnCl_2$, which were determined by titration with a standardized solution of EDTA (Aldrich) in the presence of the indicator Eriochrome Black T (Aldrich).[73]

Inhibitor Screening

1 mM stock solutions of Bisindolylmaleimides I, IV and V (Calbiochem) in DMSO (spectrophotometric grade, Aldrich) were protected from light. Serial dilutions were prepared in DMSO such that the volume added to each reaction was constant. In addition, an identical volume of DMSO was used as a control in reactions lacking inhibitor. Assays for PKC activity were conducted as for kinetic parameter determination, with inhibitor added with reaction components prior to addition of either enzyme or peptide substrate.

References

(1) Hunter, T. Signaling--2000 and beyond. *Cell* **2000**, *100*, 113-127.

(2) Manning, G.; Whyte, D. B.; Martinez, R.; Hunter, T.; Sudarsanam, S. The protein kinase complement of the human genome. *Science* **2002**, *298*, 1912-1934.

(3) Graves, J. D.; Krebs, E. G. Protein phosphorylation and signal transduction. *Pharmacol. Ther.* **1999**, *82*, 111-121.

(4) Hunter, T. Protein kinases and phosphatases: the yin and yang of protein phosphorylation and signaling. *Cell* **1995**, *80*, 225-36.

(5) Blume-Jensen, P.; Hunter, T. Oncogenic kinase signalling. *Nature* **2001**, *411*, 355-365.

(6) Cohen, P. Protein kinases--the major drug targets of the twenty-first century? *Nat. Rev. Drug Discov.* **2002**, *1*, 309-315.

(7) Sridhar, R.; Hanson-Painton, O.; Cooper, D. R. Protein kinases as therapeutic targets. *Pharm. Res.* **2000**, *17*, 1345-1353.

(8) Braunwalder, A. F.; Yarwood, D. R.; Sills, M. A.; Lipson, K. E. Measurement of the protein tyrosine kinase activity of c-Src using time-resolved fluorometry of europium chelates. *Anal. Biochem.* **1996**, *238*, 159-164.

(9) Sadler, T. M.; Achilleos, M.; Ragunathan, S.; Pitkin, A.; LaRocque, J.; Morin, J.; Annable, R.; Greenberger, L. M.; Frost, P.; Zhang, Y. Development and comparison of two nonradioactive kinase assays for I kappa B kinase. *Anal. Biochem.* **2004**, *326*, 106-113.

(10) Rhyne, P. W.; Scull, J. D.; Stiles, L. M.; Eisinger, D. P. Analysis of apoptotic cells using Beadlyte suspension arrays. *Biotechniques* **2003**, *35*, 624-629.
(11) Forrer, P.; Tamaskovic, R.; Jaussi, R. Enzyme-linked immunosorbent assay for measurement of JNK, ERK and p38 kinase activities. *Biol. Chem.* **1998**, *379*, 1101-1111.
(12) Ross, H.; Armstrong, C. G.; Cohen, P. A non-radioactive method for the assay of many serine/threonine-specific protein kinases. *Biochem. J.* **2002**, *366*, 977-981.
(13) Kolb, A. J.; Kaplita, P. V.; Hayes, D. J.; Park, Y. W.; Pernelle, C.; Major, J. S.; Mathis, G. Tyrosine kinase assays adapted to homogenous time-resolved fluorescence. *Drug Discov. Today* **1998**, *3*, 333-342.
(14) Warner, G.; Illy, C.; Pedro, L.; Roby, P.; Bossé, R. AlphaScreen™ kinase HTS platforms. *Curr. Med. Chem.* **2004**, *11*, 721-730.
(15) Seethala, R.; Menzel, R. A fluorescence polarization competition immunoassay for tyrosine kinases. *Anal. Biochem.* **1998**, *255*, 257-262.
(16) Parker, G. J.; Law, T. L.; Lenoch, F. J.; Bolger, R. E. Development of a high throughput screening assays using fluorescence polarization: nuclear receptor-ligand-binding and kinase/phosphatase assays. *J. Biomol. Screen.* **2000**, *5*, 77-88.
(17) Eglen, R. M. Enzyme fragment complementation: a flexible high throughput screening assay technology. *Assay Drug. Dev. Technol.* **2002**, *1*, 97-104.
(18) Ojida, A.; Mito-oka, Y.; Sada, K.; Hamachi, I. Molecular recognition and fluorescence sensing of monophosphorylated peptides in aqueous solution by bis(zinc(II)-dipicolylamine)-based artificial receptors. *J. Am. Chem. Soc.* **2003**, *126*, 2454-63.
(19) Gast, R.; Glokler, J.; Hoxter, M.; Kiess, M.; Frank, R.; Tegge, W. Method for determining protein kinase substrate specificities by the phosphorylation of peptide libraries on beads, phosphate-specific staining, automated sorting, and sequencing. *Anal. Biochem.* **1999**, *276*, 227-41.
(20) Gaudet, E. A.; Huang, K. S.; Zhang, Y.; Huang, W.; Mark, D.; Sportsman, J. R. A homogeneous fluorescence polarization assay adaptable for a range of protein serine/threonine and tyrosine kinases. *J. Biomol. Screen.* **2003**, *8*, 164-175.
(21) Scott, J. E.; Carpenter, J. W. A homogeneous assay of kinase activity that detects phosphopeptide using fluorescence polarization and zinc. *Anal. Biochem.* **2003**, *316*, 82-91.
(22) Morgan, A. G.; McCauley, T. J.; Stanaitis, M. L.; Mathrubutham, M.; Millis, S. Z. Development and validation of a fluorescence technology for both primary and secondary screening of kinases that facilitates compound selectivity and site-specific inhibitor determination. *Assay Drug. Dev. Technol.* **2004**, *2*, 171-181.
(23) Kupcho, K.; Somberg, R.; Bulleit, B.; Goueli, S. A. A homogeneous, nonradioactive high-throughput fluorogenic protein kinase assay. *Anal. Biochem.* **2003**, *317*, 210-217.
(24) Z'-lyte, Invitrogen, Carlsbad, CA, U.S.A.
(25) PepTag™ Promega Corp., Madison, WI, U.S.A.
(26) Sims, C. E.; Allbritton, N. L. Single-cell kinase assays: opening a window onto cell behavior. *Curr. Opin. Biotechnol.* **2003**, *14*, 23-28.
(27) Li, H.; Sims, C. E.; Kaluzova, M.; Stanbridge, E. J.; Allbritton, N. L. A quantitative single-cell assay for protein kinase B reveals important insights into the biochemical behavior of an intracellular substrate peptide. *Biochemistry* **2004**, *43*, 1599-1608.

(28) Koresawa, M.; Okabe, T. High-throughput screening with quantitation of ATP consumption: a universal non-radioisotope, homogeneous assay for protein kinase. *Assay Drug. Dev. Technol.* **2004**, *2*, 153-160.
(29) Srinivasan, J.; Cload, S. T.; Hamaguchi, N.; Kruz, J.; Keene, S.; Kurz, M.; Boomer, R. M.; Blanchard, J.; Epstein, D.; Wilson, C.; Diener, J. L. ADP-specific sensors enable universal assay of protein kinase activity. *Chem. Biol.* **2004**, *11*, 499-508.
(30) Nagai, Y.; Miyazaki, M.; Aoki, R.; Zama, T.; Inouye, S.; Hirose, K.; Iino, M.; Hagiwara, M. A fluorescent indicator for visualizing cAMP-induced phosphorylation in vivo. *Nat. Biotech.* **2000**, *18*, 313-316.
(31) Kurokawa, K.; Mochizuki, N.; Ohba, Y.; Mizuno, H.; Miyawaki, A.; Matsuda, M. A pair of fluorescent resonance energy transfer-based probes for tyrosine phosphorylation of the CrkII adaptor protein *in vivo*. *J. Biol. Chem.* **2001**, *276*, 31305-31310.
(32) Hofmann, R. M.; Cotton, G. J.; Chang, E. J.; Vidal, E.; Veach, D.; Bornmann, W.; Muir, T. W. Fluorescent monitoring of kinase activity in real time: development of a robust fluorescence-based assay for Abl tyrosine kinase activity. *Bioorg. Med. Chem. Lett.* **2001**, *11*, 3091-3094.
(33) Schleifenbaum, A.; Stier, G.; Gasch, A.; Sattler, M.; Schultz, C. Genetically encoded FRET probe for PKC activity based on pleckstrin. *J. Am. Chem. Soc.* **2004**, *126*, 11786-11787.
(34) Sato, M.; Ozawa, T.; Inukai, K.; Asano, T.; Umezawa, Y. Fluorescent indicators for imaging protein phosphorylation in single living cells. *Nat. Biotech.* **2002**, *20*, 287-294.
(35) Sasaki, K.; Sato, M.; Umezawa, Y. Fluorescent indicators for Akt/Protein Kinase B and dynamics of Akt activity visualized in living cells. *J. Biol. Chem.* **2003**, *278*, 30945-30951.
(36) Sato, M.; Umezawa, Y. Imaging protein phosphorylation by fluorescence in single living cells. *Methods* **2004**, *32*, 451-455.
(37) Zhang, J.; Ma, Y.; Taylor, S. S.; Tsien, R. Y. Genetically encoded reporters of protein kinase A activity reveal impact of substrate tethering. *Proc. Natl. Acad. Sci. USA* **2001**, *98*, 14997-15002.
(38) Ting, A. Y.; Kain, K. H.; Klemke, R. L.; Tsien, R. Y. Genetically encoded fluorescent reporters of protein tyrosine kinase activities in living cells. *Proc. Natl. Acad. Sci. USA* **2001**, *98*, 15003-15008.
(39) Violin, J. D.; Zhang, J.; Tsien, R. Y.; Newton, A. C. A genetically encoded fluorescent reporter reveals oscillatory phosphorylation by protein kinase C. *J. Cell Biol.* **2003**, *161*, 899-909.
(40) Kunkel, M. T.; Ni, Q.; Tsien, R. Y.; Zhang, J.; Newton, A. C. Spatio-temporal dynamics of protein kinase B/Akt signaling revealed by a genetically-encoded fluorescent reporter. *J. Biol. Chem.* **2004**, *280*, 5581-5587.
(41) Kawai, Y.; Sato, M.; Umezawa, Y. Single color fluorescent indicators of protein phosphorylation for multicolor imaging of intracellular signal flow dynamics. *Anal. Chem.* **2004**, *76*, 6144-6149.
(42) Wright, D. E.; Noiman, E. S.; Chock, P. B.; Chau, V. Fluorimetric assay for adenosine 3'-5'-cyclin monophosphate-dependent protein kinase and phosphoprotein phosphatase activities. *Proc. Natl. Acad. Sci. USA* **1981**, *78*, 6048-6050.

(43) McIlroy, B. K.; Walters, J. D.; Johnson, J. D. A continuous fluorescence assay for protein kinase C. *Anal. Biochem.* **1991**, *195*, 148-152.
(44) Higashi, H.; Sato, K.; Ohtake, A.; Omori, A.; Yoshida, S.; Kudo, Y. Imaging of cAMP-dependent protein kinase activity in living neural cells using a novel fluorescent substrate. *FEBS Lett.* **1997**, *414*, 55-60.
(45) Post, P. L.; Trybus, K. M.; Taylor, D. L. A genetically engineered, protein-based optical biosensor of myosin II regulatory light chain phosphorylation. *J. Biol. Chem.* **1994**, *269*, 12880-12887.
(46) Chen, C.-A.; Yeh, R.-H.; Lawrence, D. S. Design and synthesis of a fluorescence reporter of protein kinase activity. *J. Am. Chem. Soc.* **2002**, *124*, 3840-3841.
(47) Yeh, R.-H.; Yan, X.; Cammer, M.; Bresnick, A. R.; Lawrence, D. S. Real time visualization of protein kinase activity in living cells. *J. Biol. Chem.* **2002**, *277*, 11527-11532.
(48) Chen, C.-A.; Yeh, R.-H.; Lawrence, D. S. Biosensors of protein kinase action: from in vitro assays to living cells. *Biochim. Biophys. Acta* **2004**, *1697*, 39-51.
(49) Newton, A. C. Protein kinase C: structural and spatial regulation by phosphorylation, cofactors, and macromolecular interactions. *Chem. Rev.* **2001**, *101*, 2353-2364.
(50) Shabb, J. B. Physiological substrates of cAMP-dependent protein kinase. *Chem. Rev.* **2001**, *101*, 2381-2411.
(51) Taylor, S. S.; Yang, J.; Wu, J.; Haste, N. M.; Radzio-Andzelm, E.; Anand, G. PKA: a portrait of protein kinase dynamics. *Biochim. Biophys. Acta* **2004**, *1697*, 259-269.
(52) Brazil, D. P.; Hemmings, B. A. Ten years of protein kinase B signalling: a hard Akt to follow. *Trends Biochem. Sci.* **2001**, *26*, 657-664.
(53) Downward, J. PI 3-kinase, Akt and cell survival. *Semin. Cell Dev. Biol.* **2004**, *15*, 177-182.
(54) Roux, P. P.; Blenis, J. ERK and p38 MAPK-activated protein kinases: a family of protein kinases with diverse biological functions. *Microbiol. Mol. Biol. Rev.* **2004**, *68*, 320-344.
(55) Kotlyarov, A.; Yannoni, Y.; Fritz, S.; Laab, K., Telliez, Jean-Baptiste; Pitman, D.; Lin, L.-L.; Gaestel, M. Distinct cellular functions of MK2. *Mol. Cell. Biol.* **2002**, *22*, 4827-4835.
(56) White, E. The pims and outs of survival signaling: role for the Pim-2 protein kinase in the suppression of apoptosis by cytokines. *Genes Dev.* **2003**, *17*, 1813-1816.
(57) Pendergast, A. M. The Abl family kinases: mechanisms of regulation and signaling. *Adv. Cancer Res.* **2002**, *85*, 51-100.
(58) Haughland, R. P. *Handbook of Fluorescence Probes and Research Products*; 9th ed.; Molecular Probes: Eugene, OR, 2002.
(59) *SPECFIT/32 for Windows*; 3.0 ed.; Spectrum Software Associates: Marlborough, MA.
(60) Martell, A. E.; Motekaitis, R. J. *Determination and Use of Stability Constants*; 2nd ed.; VCH Publishers: New York, 1992.
(61) Lakowicz, J. R. *Principles of Fluorescence Spectroscopy*; 2nd ed.; Kluwer Academic/Plenum Publishers: New York, 1999.
(62) Cornish-Bowden, A. *Fundamentals of Enzyme Kinetics*; 2nd ed.; Portland Press: London, 1995.
(63) House, C.; Wettenhall, R. E. H.; Kemp, B. E. The influence of basic residues on the substrate specificity of protein kinase C. *J. Biol. Chem.* **1987**, *262*, 772-777.

(64) Cantley, L. C., personal communication.
(65) Songyang, Z.; Carraway III, K. L.; Eck, M. J.; Harrison, S. C.; Feldman, R. A.; Mohammadl, M.; Schlessinger, J.; Hubbard, S. R.; Smith, D. P.; Eng, C.; Lorenzo, M. J.; Ponder, B. A. J.; Mayer, B. J.; Cantley, L. C. Catalytic specificity of protein-tyrosine kinases is critical for selective signalling. *Nature* **1995**, *373*, 536-539.
(66) Kennelly, P. J.; Krebs, E. G. Consensus sequences as substrate specificity determinants for protein kinases and protein phosphatases. *J. Biol. Chem.* **1991**, *266*, 15555-15558.
(67) Kemp, B. E.; Graves, D. J.; Benjamini, E.; Krebs, E. G. Role of multiple basic residues in determining the substrate specificity of cyclic AMP-dependent protein kinase. *J. Biol. Chem.* **1977**, *252*, 4888-4894.
(68) Obata, T.; Yaffe, M. B.; Leparc, G. G.; Piro, E. T.; Maegawa, H.; Kashiwagi, A.; Kikkawa, R.; Cantley, L. C. Peptide and protein library screening defines optimal substrate motifs for Akt/PKB. *J. Biol. Chem.* **2000**, *275*, 36108-36115.
(69) Manke, I. A.; Nguyen, A.; Lim, D.; Stewart, M. Q.; Elia, A. E. H.; Yaffe, M. B. MAPKAP Kinase-2 is a cell cycle checkpoint kinase that regulates the G_2/M transition and S-phase progression in response to UV irradiation. *Mol. Cell* **2005**, *17*, 37-48.
(70) Frausto da Silva, J. J. R.; Williams, R. J. P. *The Biological Chemistry of the Elements: The Inorganic Chemistry of Life*; 2nd ed.; Oxford University Press: Oxford, 2001.
(71) Hendrickson, T. L.; de Crécy-Lagard, V.; Schimmel, P. Incorporation of nonnatural amino acids into proteins. *Annu. Rev. Biochem.* **2004**, *73*, 147-176.
(72) Thompson, R. B.; Whetsell, W. O. J.; Maliwal, B. P.; Fierke, C. A.; Frederickson, C. J. Fluorescence microscopy of stimulated Zn(II) release from organotypic cultures of mammalian hippocampus using a carbonic anhydrase-based biosensor system. *J. Neurosci. Methods* **2000**, *96*, 35-45.
(73) Basset, J.; Denney, R. C.; Jeffery, G. H.; Mendham, J. *Vogel's Textbook of Quantitative Inorganic Analysis*; William Clowers: London, 1978.

Chapter 5:
A Multiplexed Homogeneous Fluorescence-Based Assay for Protein Kinase Activity in Cell Lysates

My collaborator, Kevin Janes, made significant intellectual contributions to this work, prepared all cell lysates and performed all immunodepletions and western blot analyses.

Nearly all of the work described in this chapter has been published in:
Shults, M. D.; Janes, K. A.; Lauffenburger, D. A.; Imperiali, B. A multiplexed homogenous fluorescence-based assay for protein kinase activity in cell lysates. *Nat. Methods.* **2005**, *2*, 277-284.

A portion of the introduction has been submitted for publication:
Rothman, D. R.; Shults, M. D.; Imperiali, B. Chemical approaches for investigating phosphorylation in signal transduction networks, submitted.

Introduction

New methods to quantify protein kinase activities directly from complex cellular mixtures are critical for understanding biological regulatory pathways. Since the catalytic activities of these enzymes are the clearest measure of signaling information "flow",[1] there is tremendous interest in quantifying the dynamics of kinase activities in complex cellular media.

As discussed in Chapter 4, the most common methods for measuring cellular kinase activities involve isolation of the target kinase from cell lysates.[2,3] Then, *in vitro* kinase assays are performed, such as with [γ-^{32}P]ATP or one of the discontinuous methods discussed in Chapter 4. The processing steps needed to isolate the kinase and measure activity are time-consuming and inherently low-throughput. To more directly and rapidly analyze crude cell lysates, a continuous, fluorescence-based, homogeneous kinase activity assay is very desirable. Despite numerous reports of kinase chemosensors in the literature, only a fraction are compatible with unfractionated cell lysates or within cells.[4-16] These continuous sensing strategies were all introduced in Chapter 4; their application to assessing cellular kinase activities will be discussed in further detail here.

Assessing Cellular Kinase Activities with Genetically-Encoded Sensors

The genetically encoded probes containing AFP variants have begun to provide valuable spatio-temporal information about cellular signaling in living cells. One example is an AFP-based FRET sensor for Abl, which provided the first real-time evidence that an increase in Abl activity is localized to membrane ruffles following PDGF stimulation.[11] In a different example, a single-color AFP-based probe cyan sinphos imaged the timing of insulin receptor activity relative to the subsequent translocation of GFP-labeled mitogen-activated protein kinase from the cytoplasm to the nucleus.[5]

Since these probes are expressible, straightforward genetic modifications allow the probe to be directed to a specific location or signaling complex within a cell. In general, targeting improves spatial signal resolution, because probes distributed in the cytosol diffuse too rapidly for resolution. Kurokawa *et. al.* showed that a membrane-targeted version of their CrkII-based reporter responded more quickly to EGF stimulation than an analogous cytosolic probe; the use of the two probes simultaneously illustrate the progression of the signal from the membrane into

the cytosol.[13] Zhang *et al.* tethered their PKA probe (AKAR) to proteins and peptides that bind the PKA catalytic subunit; these constructs were phosphorylated faster than nontargeted constructs. In particular, AKAR tethered to the PKA regulatory subunit provided the most rapid response.[12]

In addition, probe targeting allows the probes to mimic endogenous substrates. Sasaki *et. al.* found that localization of their Akt sensor (Aktus) to either the mitochondria or the golgi apparatus influenced the type of stimuli to which it responded.[7] Finally, the most elegant experiments involving targeting by Violin *et. al.* show that membrane-targeted PKC sensor (CKAR) responds to histamine with an oscillatory pattern of phosphorylation.[8] The careful design and characterization of CKAR enabled a report on these periods of PKC activity and inactivity (lack of active PKC allows the probe to be dephosphorylated by phosphatases). Concomitant use of a longer-wavelength Ca^{2+} indicator showed this pattern to be coupled with Ca^{2+} oscillations.

The small signal changes of all of these probes may limit use in living cells with less abundant kinases. In fact, kinase overexpression is necessary in some instances, such as Aktus[7]. This illustrates the importance of a larger fluorescence change and good reactivity. For these reasons, the Akt sensor reported by Kunkel *et. al.* is sufficiently sensitive to detect endogenous Akt.[9]

Despite their small fluorescence changes, these probes have been useful because their genetic templates are easily and noninvasively incorporated into cells by transfection. In addition, the reversible nature of many of these probes reports the dynamic interplay between kinase and phosphatase activities within a cell. New strategies for both site-specific labeling of proteins and native chemical ligation approaches to attach small-molecule fluorophores to proteins *in vivo* may ultimately prove valuable for overcoming some of the limitations presented by the AFP-based probes.

Assessing Cellular Kinase Activities with Peptide-based Chemosensors

Abiotic peptide-based probes have been used to detect kinase activities from cells and cell lysates, though these probes are still in early stages of development compared to their expressible counterparts. Capillary electrophoresis analysis on lysates from single cells has been

used to monitor phosphorylation of fluorescently-labeled peptide substrates for protein kinases. These assays are quantitative and show extremely high resolution. Their use has demonstrated that insulin-stimulated cell populations exhibit significant cell-to-cell variation in Akt activities.[4] However, they require technically challenging microfluidic setups and are limited in throughput. Peptides exhibiting a fluorescence change have the advantage that they do not require separation for analysis. The Lawrence laboratory has demonstrated selectivity of their NBD-based PKC chemosensor with preliminary, qualitative studies in cell lysates and in living cells.[16]

The substantial fluorescence changes attainable with peptide-based probes will be important for sensing the activity of less abundant endogenous kinases. The ability to chemically synthesize the corresponding phosphopeptide product provides knowledge of the maximal response that is critical for quantifying turnover. In addition, functionalities such as cell permeable peptide sequences, targeting peptide sequences, or additional fluorophores as internal standards can be readily incorporated.

Adaptation of Sox-based Probes to Assessing Kinase Activities in Cell Lysates

The fluorescence-based chemosensor strategy introduced in Chapter 4 should provide a sensitive measure of endogenous kinase activities. The chemosensor comprises a small sensing module appended to an optimized peptide substrate for the target kinase. The fluorescence signal is generated when the nonnatural Sox amino acid undergoes chelation-enhanced fluorescence in the presence of divalent magnesium. The Mg^{2+}-binding affinity of the product phosphopeptide is much greater than the substrate peptide, which results in a large fluorescence increase upon phosphorylation. These chemosensors are excellent reporters of recombinant kinase activity *in vitro* and the versatility of their design allows the generation of a chemosensor for any target kinase.

Herein we report that the sensitivity and selectivity of Sox-based chemosensors are sufficient to measure kinase activities directly from unfractionated cell lysates. We established optimized assay conditions for preferential, quantitative detection of cellular Akt, MK2, and PKA activation. The homogeneous assay format is high-throughput, remarkably straightforward, and reproducible; notably, it is also compatible with physiological concentrations of ATP (1 mM). The general protocol was developed for the kinase Akt and then easily extended to

measure protein kinase A (PKA) and mitogen-activated protein kinase-associated protein kinase 2 (MK2) activities. This strategy was also successful due to a combination of the selectivity and reactivity of the optimized peptide substrate upon which these chemosensors were based, as well as the knowledge and use of appropriate inhibitors for off-target kinase. This work establishes an important tool for studying the roles of protein kinases in cellular regulation.

Results:

Chemosensor Properties

The optimized chemosensors for Akt, MK2 and PKA described in Chapter 4 were used. Due to the significantly different assay buffer composition and instrumentation used for these experiments, the fluorescence response of these peptides were re-evaluated (Table 5-1).

Table 5-1. Fluorescence response of chemosensors under lysates assay conditions[a]

Sensor	Sequence	Fold fluorescence increase
Akt-S1	AcARKRERAYSF-DPro-Sox-Gly-NH_2	9.3
MK2-S1	AcAHLQRQLSI-DPro-Sox-Gly-NH_2	8.5
PKA-S3	AcLRRASL-DPro-Sox-Gly-NH_2	5.6

[a] 20 mM Tris-HCl (pH 7.5), 150 mM NaCl, 15 mM $MgCl_2$, 5 mM β-glycerophosphate, 1 mM EGTA, 0.2 mM Na_3VO_4, 0.2 mM DTT, 1 mM ATP, 10 μM peptide, off-target kinase inhibitors (see Experimental).

Development of an Akt-S1 Kinase Activity Assay

The sensitivity and efficacy of these kinase chemosensors prompted an investigation of how each would perform in more complex environments. Whereas direct *in vivo* applications are a common next step for most kinase activity chemosensors,[4-15] there are several advantages to testing chemosensor properties in cell extracts. For instance: a) sensitivity and specificity can be improved by adding inhibitors of phosphatases and off-target kinases, b) quantification of fluorescence changes is more straightforward, and c) many distinct lysate-based assays can be performed using different aliquots of the same sample.

An Akt-S1 activity assay was first developed, because this chemosensor had the largest fluorescence increase after phosphorylation. An initial concern for a homogeneous assay was compatibility between the lysis buffer (containing crude cellular proteins, nonionic detergents,

and various inhibitors) and a typical kinase assay buffer[1] (containing kinase and phosphatase inhibitors, ATP, and substrate).

Initial attempts to analyze lysates led to precipitation and increased fluorescence emission due to light scattering. When precipitation was observed visually, centrifugation of the sample decreased emission at 400 nm back to the same level as a lysis buffer control and removed the contribution of light scattering from the fluorescence emission at 485 nm. Inclusion of 150 mM NaCl in the final assay mixture remedied the precipitation problem, as verified by a stable emission at 400 nm. Under these conditions, up to 150 μg of lysate protein in 7.5 vol% of the total reaction could be assayed without precipitation.

Typically, 40-100 μg of cell lysate in 7.5 vol% of the total reaction was used in the Akt-S1 assay. Radioactive Akt assays[1,17] typically use 500 μg lysate and micromolar concentrations of ATP. Here, less lysate is needed because the Akt-S1 assay is compatible with 1 mM ATP. Assay sensitivity improves by an order of magnitude when the ATP concentration was increased from 10 μM to 1 mM (Figure 5-1).

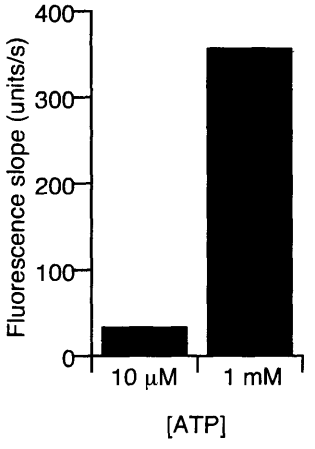

Figure 5-1. Akt-S1 kinase assay sensitivity improves by an order of magnitude when the ATP concentration is increased from 10 μM to 1 mM. Insulin-treated HT-29 lysates were assayed as described in Methods, but in a fluorescence microcuvette.

Another challenge for a crude lysate assay was the presence of competing cellular processes, such as off-target kinases and phosphatases. To improve specificity for Akt, a cocktail of phosphatase and kinase inhibitors was included in the assay buffer. This cocktail included the

phosphatase inhibitors β-glycerophosphate and sodium orthovanadate, as well as inhibitors for PKA (PKItide[18]), PKC isoforms (PKC peptide inhibitor and GF109203X) and CaMK (calmidazolium chloride). These kinase inhibitors did not affect recombinant Akt1 activity, but they completely inhibited their target enzymes (Figure 5-2). For the Akt-S1 assay, it was critical to add the small-molecule bisindolylmaleimide PKC inhibitor, GF109203X, which targets all PKC isozymes as well as p70S6 kinase and MAPKAP-K1.[19] Inclusion of 5 μM GF109203X in the assay buffer reduced non-specific Akt-S1 kinase activity by 75%.

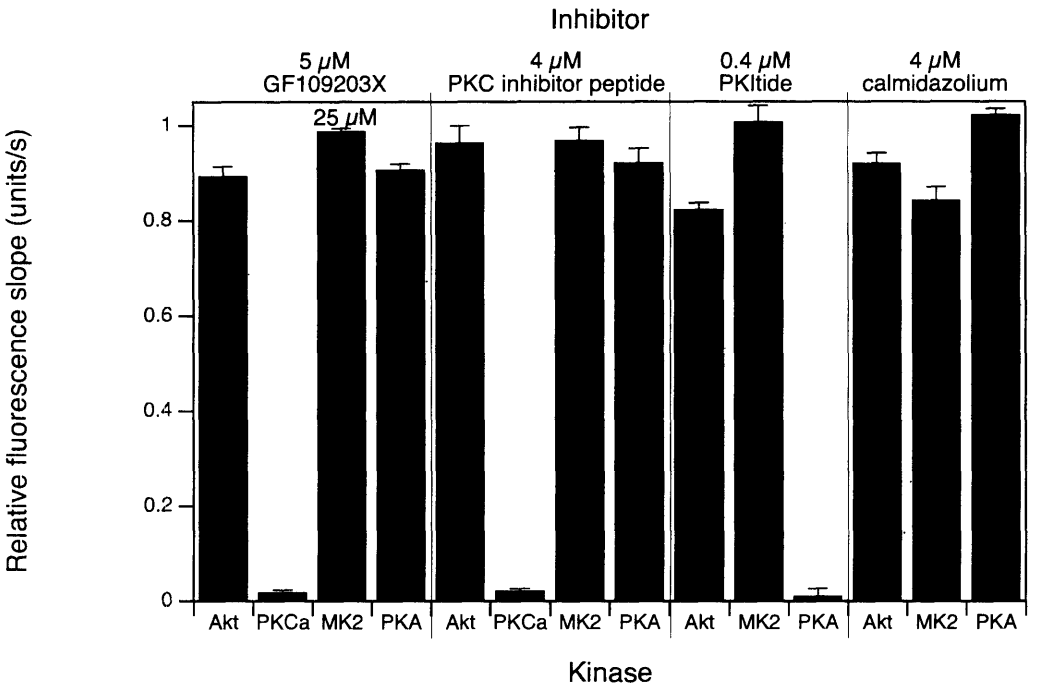

Figure 5-2. Kinase inhibitors used in the assay mixture do not affect recombinant Akt, MK2 and PKA activity, but each inhibitor does completely inhibit its target enzyme. Recombinant Akt1, MK2, PKA and PKC_{α} were assayed with the indicated concentrations of GF109203X, PKC inhibitor, PKItide and calmidazolium. Fluorescence slopes are normalized a kinase reaction lacking inhibitor. Recombinant Akt1, MK2, PKA and PKC_{α} assay conditions are described in the Experimental section. Plotted values indicate mean ± s.e.m for triplicate measurements.

Additional inhibition studies verified that atypical PKC isoforms, p70S6 kinase, and MAPKAP-K1 did not affect Akt-S1 fluorescence under the final assay conditions. To verify inhibition of atypical PKC isozymes, 5 μM Gö 6983 was included in the assay buffer with insulin-treated lysates. To verify inhibition of p70S6 kinase and MAPKAP-K1, *in vivo* inhibition

of the upstream kinases, mTor and MEK, was performed, respectively. HT-29 cells were pretreated prior to insulin stimulation with either rapamycin or PD 98059, respectively. No influence on measured Akt-S1 activity was observed in any of these assays when compared to the standard insulin-treated lysates.

The Akt-S1 kinase activity assay was optimized in a fluorescence microcuvette and then adapted to a 96-well glass-plate format. In polystyrene plates, significant absorption of assay components occurred, especially peptide (observed as a 10% fluorescence decrease over 20 min). A variety of traditional enzyme-linked immunosorbent assay (ELISA) blocking conditions were tried unsuccessfully. In glass plates, peptide adsorption is minimal and the assay is highly reproducible. In a plate format, longer path lengths improve the signal but require larger volumes per well. For efficient use of reagents, a compromise of 250 μl/well (for 500 μl/well volume plates) or 150 μl/well (for 300 μl/well volume plates) was reached, corresponding to a path length of 4 mm.

To obtain Akt activity measurements, cell lysates were added to the complete assay mixture, and fluorescence readings were taken each minute for 60 min. The change in fluorescence is linear during this time (Figure 5-3a), and the slope was used as the measure of activity because it is the best aggregate metric for the increase in fluorescence. All subsequent data were collected in this high-throughput format.

Validation of the Akt-S1 Kinase Assay

After generically characterizing lysate activity, the assay format was applied to quantitatively detect changes in activity from cell samples stimulated with known Akt activators. HT-29 cells were treated with insulin for 5 min and lysed by standard techniques (see Experimental section). Then, Akt-S1 fluorescence changes were monitored in triplicate with insulin-stimulated or untreated control lysates (Figure 5-3a). The assay revealed a threefold increase in Akt-S1 kinase activity (Figure 5-3b). Using recombinant active Akt1, the untreated and insulin-treated lysates were found to correspond to about 8 ng and 23 ng active Akt1 equivalents per 93 μg lysate, respectively. The amount of turnover in the insulin-treated samples after 60 min was 7%.

The Akt-S1 fluorescence slope varied linearly with dilutions of both insulin-treated and untreated lysates over at least a fivefold concentration range of cellular protein (Figure 5-3b Figure 5-3c). In addition, the fold difference between insulin-stimulated and unstimulated activities correlates with the activation measured by a quantitative radioactive assay[1] (Figure 5-3d). These results indicate that the fluorescence-based readings quantitatively report Akt-S1 kinase activity in cell lysates.

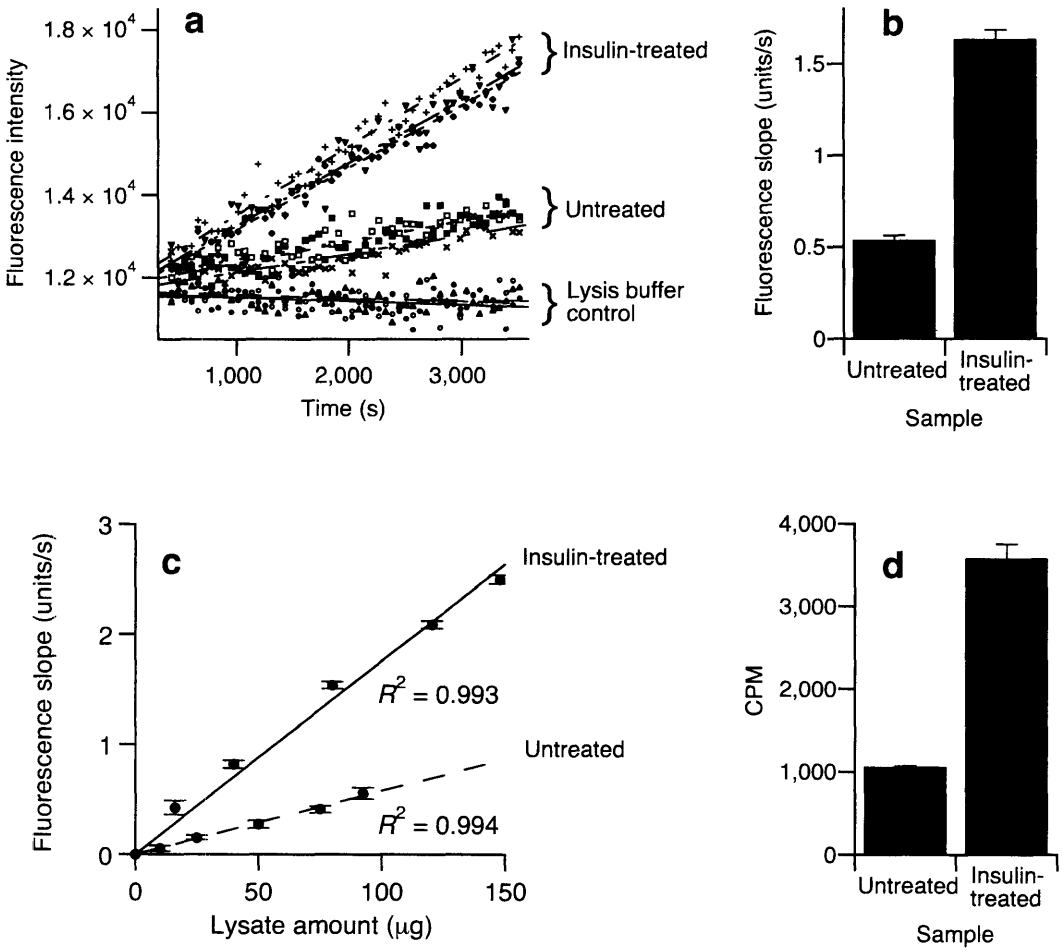

Figure 5-3. Akt-S1 kinase activity is quantitatively linear and correlates with an established radioactivity assay. (**a**) Triplicate fluorescence measurements of lysis buffer (●,○,▲), untreated HT-29 lysates (■,□,×) and insulin-stimulated HT-29 lysates (+,▼,◆) over 60 min. R^2 values range from 0.72 to 0.97 (**b**) Summary of fluorescence slopes from data in **a**. (**c**) Summary of fluorescence slopes for the insulin-treated (—) and untreated (- -) samples that were diluted in lysis buffer to vary the total protein content; the volume of lysis buffer was kept constant for all data points. (**d**) Results of a radioactive assay[1] using the same lysates as in **a**. Plotted values indicate mean ± s.e.m for triplicate measurements.

Akt-S1 also could report Akt activity in a quenched-point fluorescence assay with immunopurified Akt (Figure 5-4a). Quantitatively, the extent of Akt activation by insulin was smaller and less reproducible than the Akt-S1 kinase assay (Figure 5-3b), single time-point readings from the Akt-S1 kinase assay (Figure 5-4b), and the radioactive Akt assay (Figure 5-3d). In fact, the magnitude of the fluorescence increase after 30 min for both the quenched-point immunopurification assay (1250 μg lysate) and single time-point readings from the Akt-S1 kinase assay (90 μg lysate) are identical, though the lysate amount is an order of magnitude less for the crude cell lysates assay. This suggests that kinase activity loss and diffusional reaction limitations for plate-bound kinase are problematic with immunopurification strategies. It is likely that kinase activity is compromised with several hours of manipulations and/or upon binding to the antibody. Also, comparison of fluorescence slopes (Figure 5-3b) leads to the same fold-difference in activity as single time-points (Figure 5-4b) but with less error. Thus, verification of reaction specificity by other means than immunopurifying the target kinase is desirable.

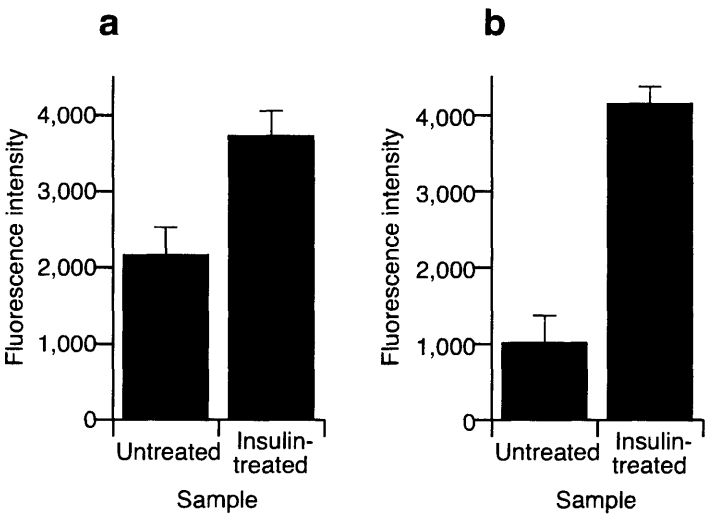

Figure 5-4. Quenched-point fluorescence assays with immunopurified Akt report insulin-stimulated phosphorylation of Akt-S1. (**a**) Fluorescence intensities after 30 min with Akt immunopurified from 1250 μg HT-29 cell lysates. (**b**) Fluorescence intensities of Akt-S1 kinase assays after 30 min with 90 μg crude cell lysate. Plotted values indicate mean ± s.e.m for triplicate measurements.

Next, we tested whether the Akt-S1 kinase assay was specific for measuring Akt activity in crude biological samples by using two small-molecule inhibitors (wortmannin and LY294002) of phosphatidylinositol 3-kinase (PI3K). PI3K initiates recruitment of Akt to the plasma membrane; this recruitment is required and sufficient for Akt activation.[20] Cells were preincubated with the indicated concentration of each PI3K inhibitor for one hour, then stimulated with insulin for 5 min. Dose-dependent inhibition of Akt-S1 kinase activity was observed for both wortmannin (Figure 5-5a, IC_{50} = 3.6 nM) and LY294002 (Figure 5-5b, IC_{50} = 8.2 μM). These values agreed with reported IC_{50} values for the upstream PI3K inhibition by wortmannin (5 nM) and LY294002 (1.4 μM), considering differences in ATP concentrations.[21] because wortmannin and LY294002 inhibit PI3K by different mechanisms,[21] sensitivity to both strongly implicates a PI3K pathway in Akt-S1 phosphorylation.

Since other PI3K-dependent kinases might nonspecifically phosphorylate Akt-S1, Akt was removed *in vitro* by immunodepletion. Insulin-stimulated lysates were depleted with an Akt-specific antibody, and Akt-S1 kinase activity was compared to both the input lysate and a sample that had been deplted with naïve mouse IgG. Akt-immunodepleted lysates showed threefold less activity than naïve IgG-immunodepleted lysates (Figure 5-5c), strongly suggesting that the Akt-S1 signal predominantly is due to Akt-mediated phosphorylation. Immunodepletion was confirmed by western blot analysis with the immunodepleting antibody (Figure 5-5c, inset), as well as with an independent anti-Akt antibody. Slightly reduced activity in the naïve immunodepletion sample was due to nonspecific loss of Akt (~23% loss, estimated by densitometry). Also, there was a small but detectable amount of residual Akt in the Akt-depleted lysates (~5% of input). Therefore, the measurements in the immunodepleted samples are a conservative estimate for the selectivity of the assay.

To test the general applicability of the Akt-S1 kinase assay to other mammalian cell types, Akt-S1 activity in Chinese hamster ovary (CHO) cells was measured. Here, epidermal growth factor (EGF) was used as the Akt agonist. Similarly to the insulin-stimulated Akt activity in HT-29 cells (Figure 5-3b,d), EGF-induced Akt activation in CHO cells quantitatively correlated with the activation observed in a radioactive Akt assay[1] (Figure 5-6). Together, these results indicate that the Akt-S1 assay is a quantitative, selective and generalizable format for studying Akt signaling.

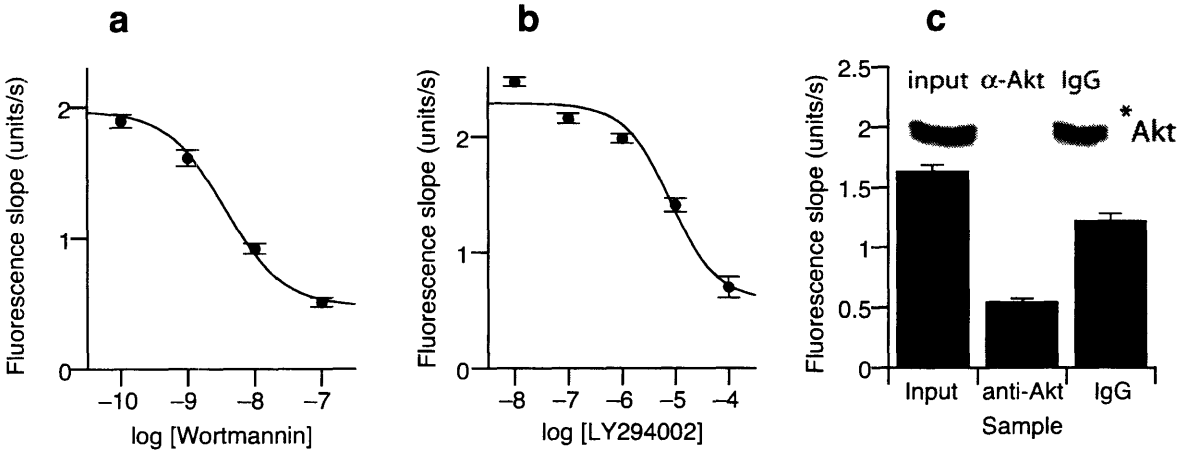

Figure 5-5. The Akt-S1 kinase activity assay is preferential for Akt. (**a,b**) HT-29 lysates were pretreated with various concentrations of the PI3K inhibitors (**a**) wortmannin and (**b**) LY294002 for one hour prior to stimulation with 500 ng/ml insulin. The carrier (DMSO) was kept constant at 0.1% for all stimulation conditions. (**c**) Kinase activity was measured from an insulin-treated HT-29 lysate (input), and after immunodepletion of this lysate with anti-Akt1/2 or naïve mouse IgG. Inset: western blot for Akt in the measured samples (asterisk indicates a nonspecific band). Plotted values indicate mean ± s.e.m for triplicate measurements.

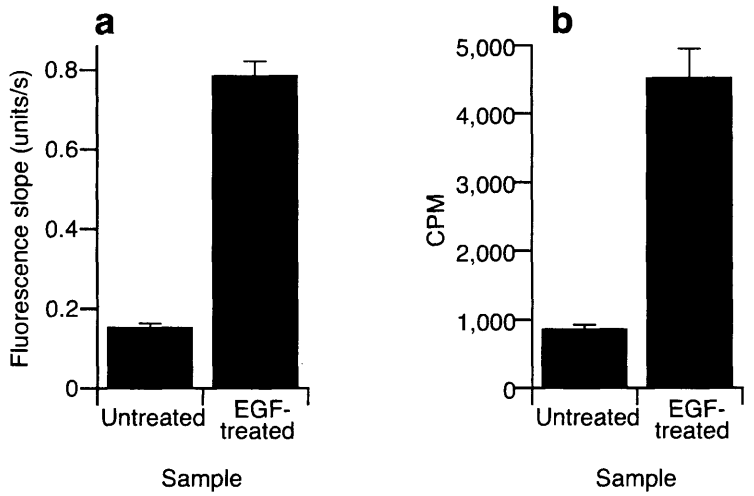

Figure 5-6. Measured Akt-S1 kinase activity in CHO cell lysates is quantitatively comparable to a radioactive assay. (**a**) Akt-S1 fluorescence slopes were monitored over 60 min in triplicate with EGF-stimulated or untreated-control CHO cell lysates. (**b**) Results of a radioactive assay using the same lysates as in **a**. Plotted values indicate mean ± s.e.m for triplicate measurements.

Development of MK2-S1 and PKA-S3 Kinase Activity Assays

After successfully developing an Akt-S1 kinase activity assay, we investigated whether the protocol could be applied more broadly to the other target kinases. To design activity assays for PKA and MK2 in HT-29 cell lysates, the assay mixture from the Akt assay was used as a starting point and then refined for each kinase. The panel of inhibitors for each assay mixture was confirmed not to affect recombinant MK2 and PKA activities (Figure 5-2). The MK2-S1 and PKA-S3 activity assays were evaluated in HT-29 lysates similarly to the Akt-S1 activity assay.

Validation of the MK2-S1 Kinase Activity Assay

The MK2-S1 activity assay was linear for 15 min (Figure 5-7a) and over a fivefold range of lysate concentrations (Figure 5-7c). MK2 activation by NaCl treatment resulted in a 4.6-fold increase in MK2-S1 phosphorylation (Figure 5-7b). 53 μg of the stimulated lysate contains the equivalent of 51 ng recombinant MK2 with 18% turnover in 15 min. There was a somewhat weaker correlation between the MK2-S1 assay (Figure 5-7b) and a radioactive MK2 assay (Figure 5-7d), so the chemosensor selectivity was examined in detail.

MK2-S1 phosphorylation was abrogated in NaCl-treated lysates when cells were pretreated with SB202190, a small molecule inhibitor of the MK2 kinase p38 (Figure 5-8a). The apparent IC_{50} value (430 nM) correlates reasonably well with that reported for upstream p38 inhibition (50-100 nM), considering differences in ATP concentrations.[19] When MK2 was removed *in vitro*, the immunodepleted lysate lost 50% of its activity as compared to that of the input lysate (Figure 5-8b). In addition, western blot analysis showed that the immunodepleted sample had retained 25% of input MK2, and the naïve immunodepleted sample had nonspecifically lost ~15% of input MK2 (Figure 5-8b, inset). Together, these data suggest that 75% of MK2-S1 activity is due to MK2. The residual 25% of nonspecific activity likely explains the higher untreated background activity observed with the MK2-S1 assay relative to the radioactive MK2 assay[1] (Figure 5-7d).

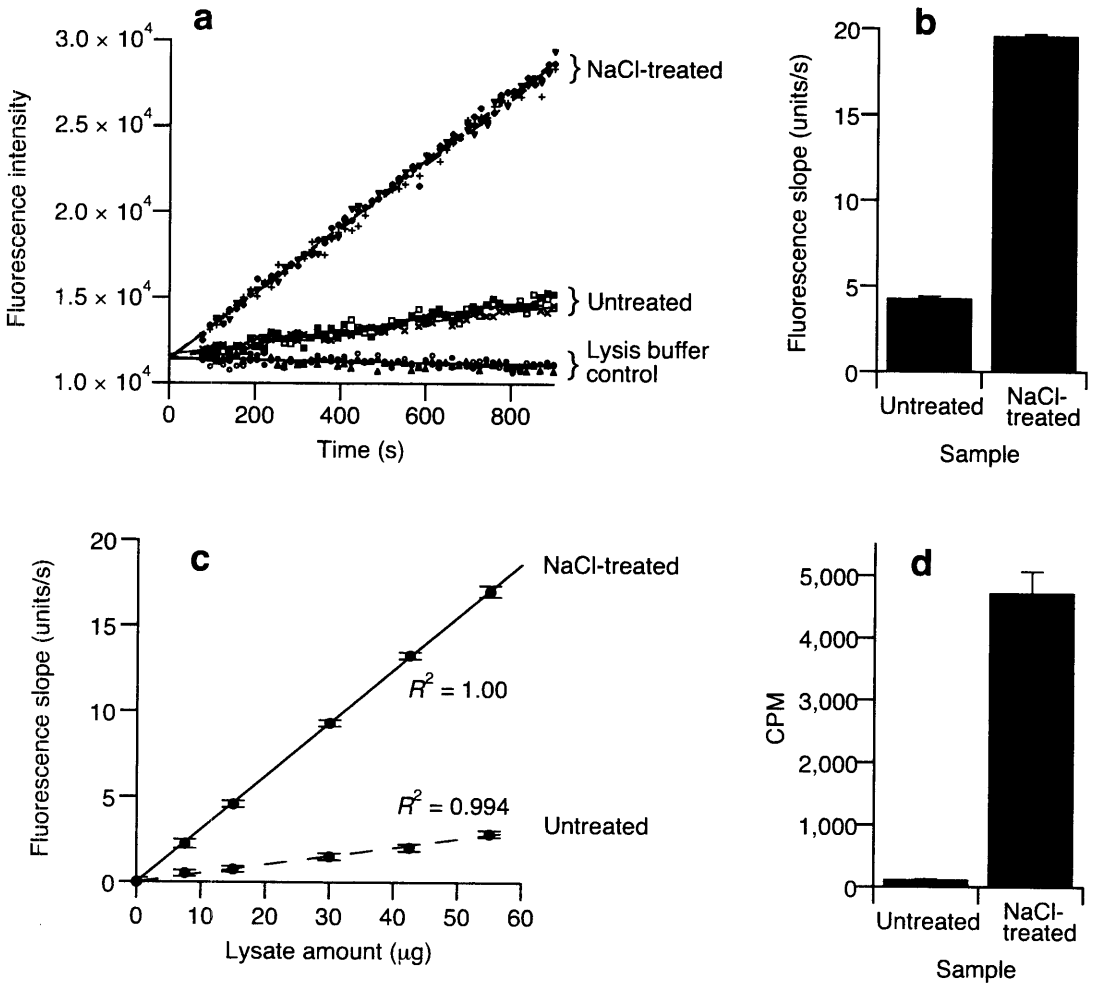

Figure 5-7. MK2-S1 kinase activity is quantitatively linear and correlates with an established radioactivity assay. (**a**) Triplicate fluorescence measurements of lysis buffer (●,○,▲), untreated HT-29 lysates (■,□,×) and NaCl-stimulated HT-29 lysates (+,▼,◆) over 15 min. R^2 values range from 0.93 to 1.0 (**b**) Summary of fluorescence slopes from data in **a**. (**c**) Summary of fluorescence slopes for the NaCl-treated (—) and untreated (- -) samples that were diluted in lysis buffer to vary the total protein content; the volume of lysis buffer was kept constant for all data points. (**d**) Results of a radioactive assay[1] using the same lysates as in **a**. Plotted values indicate the mean ± s.e.m. for triplicate measurements.

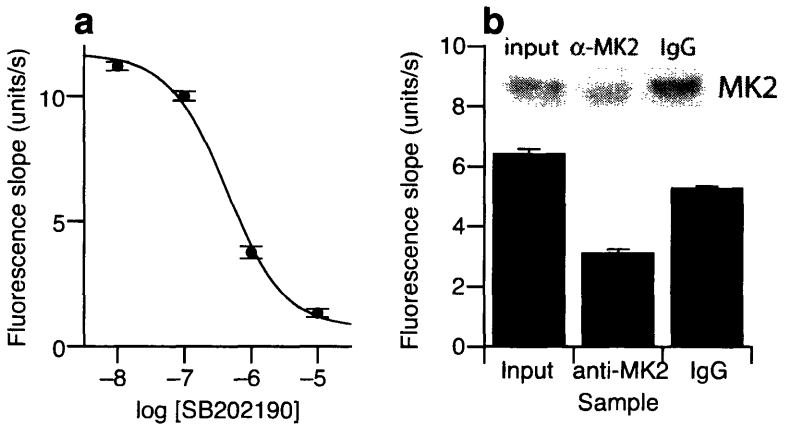

Figure 5-8. The MK2-S1 kinase activity assay is preferential for MK2. (**a**) HT-29 lysates were pretreated with various concentrations of the p38 inhibitor SB202190 for one hour prior to stimulation with 250 mM NaCl. The carrier (DMSO) was kept constant at 0.1% for all stimulation conditions. (**b**) Kinase activity was measured from an NaCl-treated HT-29 lysate (input), and following immunodepletion of this lysate with anti-MK2 or naïve sheep IgG. Inset: western blot for MK2 in the measured samples. Plotted values indicate mean ± s.e.m for triplicate measurements.

MK2-S1 also reported MK2 activity in a quenched-point fluorescence assay with immunopurified MK2 (Figure 5-9a). The extent of MK2 activation by NaCl was smaller and less reproducible than single time-point readings from the MK2-S1 kinase assay (Figure 5-9b) and the radioactive MK2 assay (Figure 5-7d). These results again illustrate some of the limitations of immunopurification strategies.

Finally, using the MK2-S1 activity assay, we also detected MK2 activation in CHO cell lysates treated with tumor necrosis factor (TNF) (Figure 5-10a). This activation correlated with a radioactive MK2 assay[1] (Figure 5-10b) and demonstrated that the assay could be used with diverse stimuli and cell types.

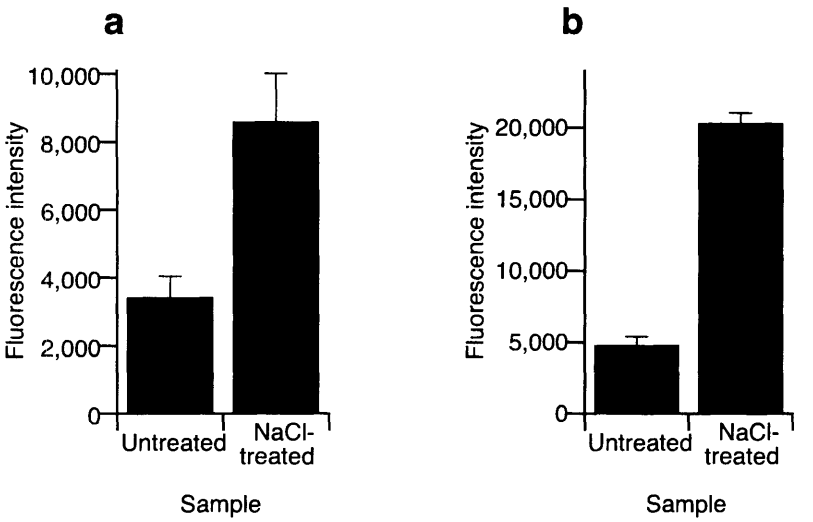

Figure 5-9. Quenched-point fluorescence assays with immunopurified MK2 report osmolarity-stimulated phosphorylation of MK2-S1. (**a**) Fluorescence intensities after 15 min with MK2 immunopurified from 750 μg HT-29 cell lysates. (**b**) Fluorescence intensities of MK2-S1 kinase assays after 15 min with 90 μg crude cell lysate. Plotted values indicate mean ± s.e.m for triplicate measurements.

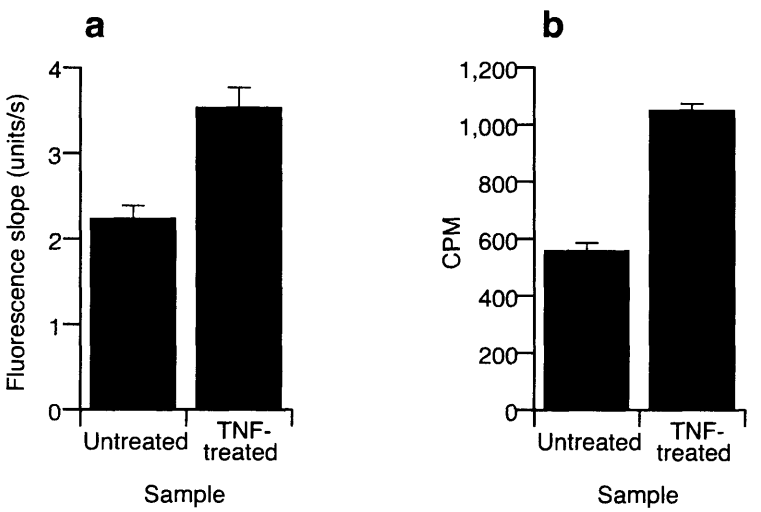

Figure 5-10. Measured MK2-S1 kinase activity in CHO cell lysates is quantitatively comparable to a radioactive assay. (**a**) MK2-S1 fluorescence slopes were monitored over 15 min in triplicate with TNF-stimulated or untreated-control CHO cell lysates. (**b**) Results of a radioactive assay using the same lysates as in **a**. Plotted values indicate mean ± s.e.m for triplicate measurements.

Validation of the PKA-S3 Kinase Activity Assay

The PKA-S3 activity assay was linear for 15 min (Figure 5-11a) and over a fivefold range of lysate concentrations (Figure 5-11c). PKA activation by forskolin treatment resulted in a 3.5-fold increase in PKA-S3 phosphorylation (Figure 5-11b), which corresponds to 12 ng recombinant PKA in 18 μg of HT-29 cell lysate with 9.1% turnover in 15 min. An adequate anti-PKA antibody was not commercially available to perform a radioactive PKA assay.

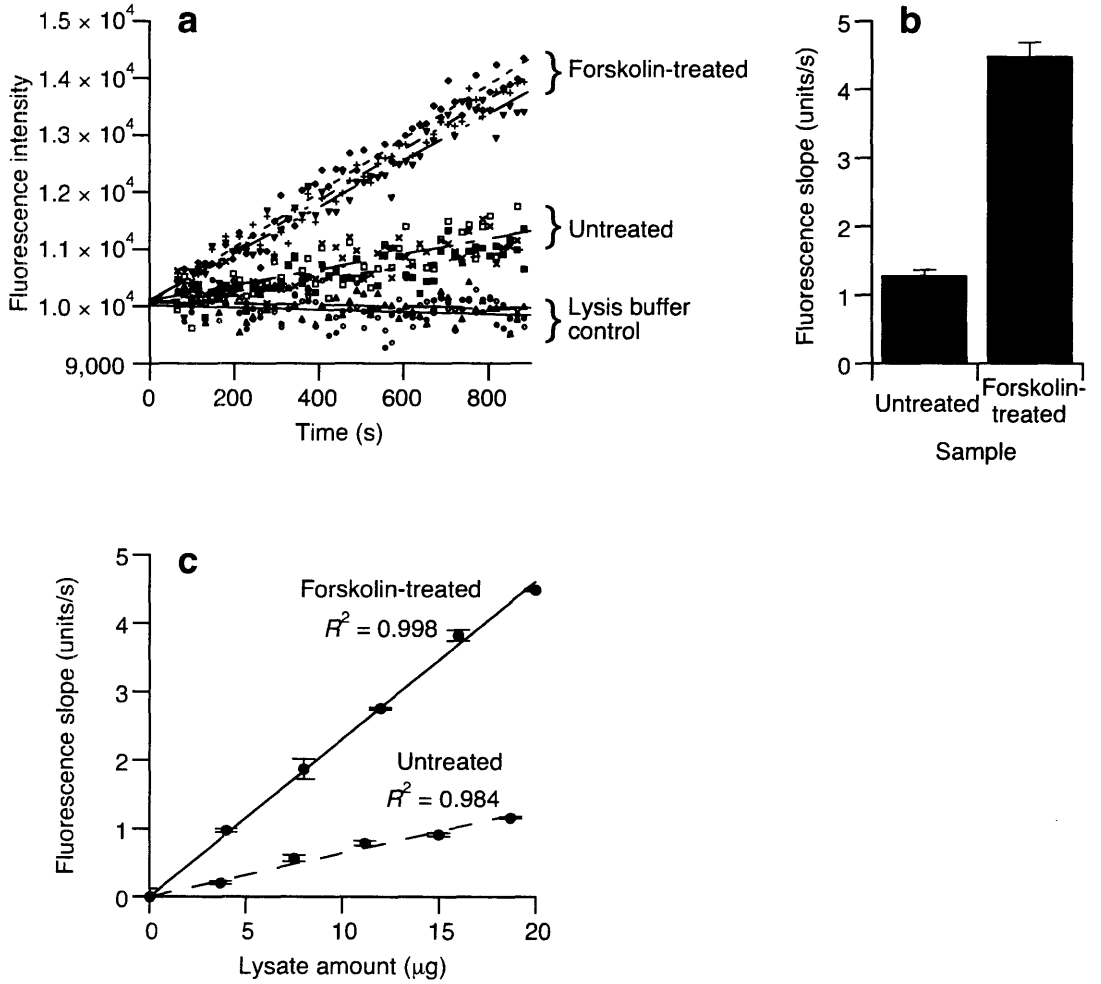

Figure 5-11. PKA-S3 kinase activity is quantitatively linear. (**a**) Triplicate fluorescence measurements of lysis buffer (●,○,▲), untreated HT-29 lysates (■,□,×) and forskolin-stimulated HT-29 lysates (+,▼,◆) over 15 min. R^2 values range from 0.60 to 0.97 (**b**) Summary of fluorescence slopes from data in **a**. (**c**) Summary of fluorescence slopes for the forskolin-treated (—) and untreated (- -) samples that were diluted in lysis buffer to vary the total protein content; the volume of lysis buffer was kept constant for all data points. Plotted values indicate mean ± s.e.m for triplicate measurements.

Two mechanistically distinct PKA inhibitors were used to interrogate the selectivity of the PKA-S3 kinase assay: H89, a small molecule ATP-competitive inhibitor, and PKItide, the active fragment of a PKA-specific inhibitor protein.[18] PKA-S3 activity was abolished in a dose-dependent manner with both inhibitors (Figure 5-12a,b). The calculated IC_{50} values (3.6 μM for H89 and 0.91 nM for PKItide) match those for the inhibition of recombinant PKA activity measured under identical conditions (Figure 5-12c,d). This inhibition data provides strong evidence that the PKA-S3 assay is highly preferential, because an adequate antibody is not available to rigorously quantify specificity.

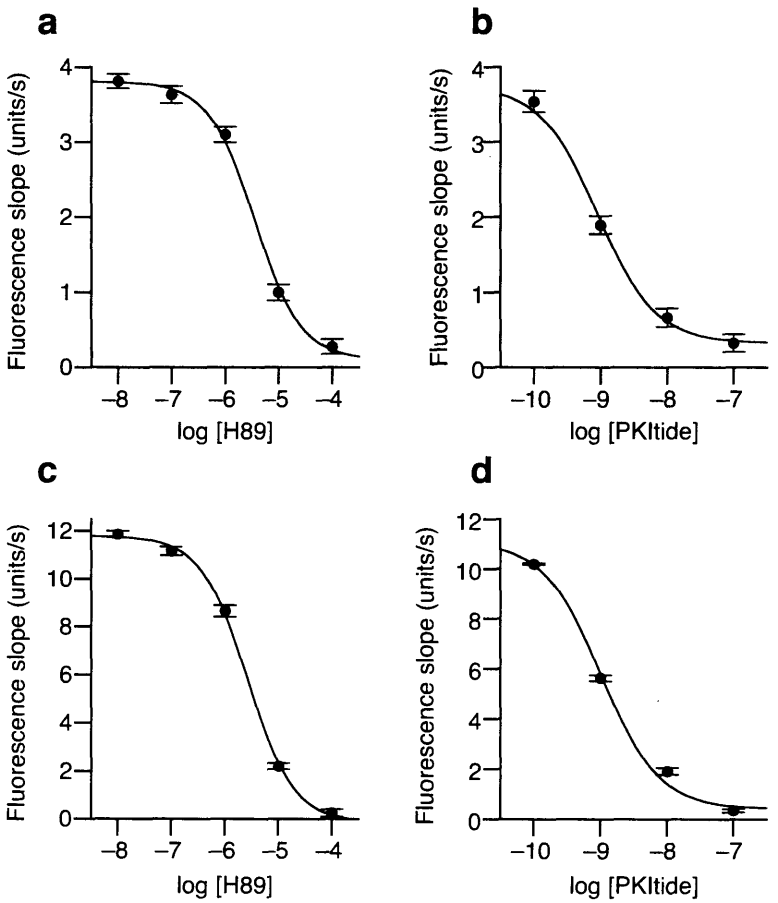

Figure 5-12. Dose-dependent inhibition of (**a,b**) endogenous PKA in forskolin-treated lysates by H89 and PKItide parallels that for (**c,d**) recombinant PKA; this data suggests that the PKA-S3 activity assay is highly preferential. (**a,b**) Forskolin-treated HT-29 lysates were assayed in the presence of various concentrations of (**a**) H89 and (**b**) PKItide. (**c,d**) Recombinant PKA was assayed in the presence of various concentrations of (**c**) H89 (IC_{50} = 2.6 μM) and (**d**) PKItide (IC_{50} = 1.0 μM). Plotted values indicate mean ± s.e.m for triplicate measurements.

The multiplex Akt-MK2-PKA kinase assay

To illustrate how these chemosensors can be used in a multiplex assay format, the signaling responses of Akt, MK2, and PKA to two growth factors, insulin and EGF, were examined. HT-29 cells were treated with saturating concentrations of insulin or EGF and lysed in triplicate at various times between zero and two hours. These lysates were then analyzed for Akt, MK2 and PKA activity with their respective kinase assays, and activation levels were calculated by normalizing to the zero minute samples. For each growth factor, 63 independent activity assays were performed in parallel with less than 170 μg cell lysate. By comparison, a similar quantitative radioactive assay[1] for Akt and MK2 would require at least 700 μg cell lysate and would not be possible for PKA.

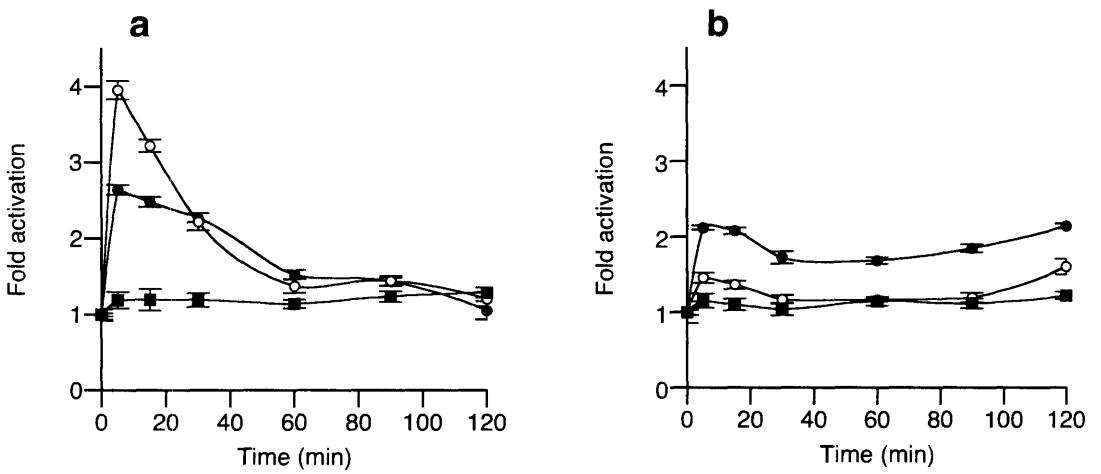

Figure 5-13. The multiplex kinase assay reveals differential responses of Akt, MK2 and PKA to stimulation by EGF and insulin. Akt-S1 (●), MK2-S1 (O) or PKA-S3 (■) kinase activities were measured in HT-29 lysates after stimulation by (**a**) EGF or (**b**) insulin for various times as described in the Experimental section. Plotted values indicate mean ± s.e.m for triplicate measurements. Changes in kinase activity were normalized to the baseline (0 min) fluorescence slope.

The multiplexed three-kinase assay revealed qualitatively and quantitatively different responses to EGF (Figure 5-13a) and insulin (Figure 5-13b). EGF activated MK2 more potently and transiently. Akt was also activated transiently in response to EGF, but to a lesser extent, and

PKA was not activated at all. In contrast, insulin activated Akt potently, and the response was sustained over the time course. MK2 was slightly activated in response to insulin, and again, PKA was not activated at all. The features of these time courses correlate with those reported for Akt[22,23] and MK2[24] (or upstream p38[25]) activity dynamics in other mammalian cell lines. To the best of our knowledge, there is no evidence that either EGF or insulin activate PKA.

Discussion

For biological applications, the specificity of any peptide substrate must be validated amidst total cellular proteins. Here, this issue was addressed in several ways. First, the design of each substrate peptide was based on the optimal peptide sequences, implying that it is least likely to be out-competed as a substrate for off-target kinases. Second, the Sox-based fluorescence readout is specifically attributable to Akt-S1, MK2-S1 or PKA-S3 phosphorylation, in contrast to other assays that measure bulk phosphotyrosine- or ^{32}P-labeled proteins. Third, assay selectivity was explicitly verified *in vivo* by small-molecule inhibitors and *in vitro* by immunodepletion. When inhibitor selectivity was questionable, another inhibitor that operates by a different mechanism was also used. These overlapping selectivity controls showed that the Akt-S1, MK2-S1, and PKA-S3 kinase activity assays are preferential, solution-phase assays for endogenous Akt, MK2, and PKA activities in cell lysates.

The homogeneous, fluorescence-based kinase activity assays reported here have several advantages over existing assays. The Sox-based chemosensors are uniquely quantitative in their ability to estimate enzymatic activity and phosphorylated product generated from cell samples. The amount of lysate activity can easily be related to recombinant protein standards or normalized to untreated control lysates (Figure 5-13). In addition, the assay is compatible with physiological concentrations of ATP. Together with the solution-phase format, this dramatically increases the sensitivity of the assay.

Whereas most immune complex kinase activity assays require 200-500 μg total cell protein,[17] the kinase assays presented here can make equivalent measurements at less than 100 μg (Figures 6-3b,d and 6-7b,d). This sensitivity is critical for applications where cell samples are limited, such as high-throughput cell-based screening and clinical diagnostics. Immunopurification approaches are typically used both to ensure signal specificity and also to

remove cellular components that interfere with the *in vitro* assay. While this approach could be adapted for an immune complex assay with improved immunopurification protocols, crude cell lysate assays eliminate several hours of manipulations, such as incubation and washing steps, before and after the *in vitro* reaction. During the kinase reaction, the 60 time points collected provide additional activity information and reduce error without extra experimental effort. In addition, the crude cell lysates assay avoids a significant loss in kinase activity upon immunopurification.

An important feature of these lysate-based assays is that selectivity can be improved by pharmacologically inhibiting kinases with overlapping substrate specificity. Because the relevant off-target enzymes will depend upon the peptide chemosensor, kinase-by-kinase optimization will be needed to ensure maximum possible specificity. Although some residual off-target activity is inevitable (here, < 30% for Akt and 25% for MK2, Figures 6-5c and 6-8b), this singular limitation is outweighed by the many benefits of these fluorescent kinase activity assays, in that they are straightforward, rapid, continuous, non-radioactive, quantitative, and sensitive. The format is conceptually similar to many fluorogenic protease assays[26] that, because of these same benefits, have found widespread use in a number of applications[27]. Finally, this work provides a general protocol for developing lysates assays using other Sox-based chemosensors. because it is straightforward to multiplex chemosensors to measure several cellular kinase activities in parallel (Figure 5-13), this assay platform is of immediate and expanding utility in drug discovery and molecular biology.

Conclusion

A homogeneous kinase assay was developed for Akt, MK2 and PKA from unfractionated cell lysates that is reproducible, linear, and highly preferential for monitoring changes in cellular activity of the target kinase. The general protocol was developed for the kinase Akt and then easily extended to measure PKA and MK2 activities. This assay platform is immediately useful for studying protein kinase signaling in crude cellular extracts.

Future Directions

These probes can now be used to assay lysates to map normal and disease-state signaling networks. Due to the successful development of the lysate assay and the understanding of probe specificity, these chemosensors can be used to monitor signaling inside living cells. For this purpose, the creation of more specific probes is underway, because the use of off-target kinase inhibitors is undesirable for studies in living cells. Additionally, lysate assays will be enhanced by the use of more specific probes. Preliminary experiments toward a PKC-S1 lysate assay showed little increase in PKC activity relative to untreated control HT-29 lysates, despite the use of an extremely potent activator of PKC, phorbol myristate acetate (PMA) (Figure 5-14). Inclusion of the PKC-specific inhibitor Gö 6983 in the assay mixture for PMA-treated lysates reduced the activity to the untreated control levels. Together, these results indicate that there is a significant amount of phosphorylation of PKC-S1 by kinases other than PKC. Thus, the lack of selectivity of the PKC-S1 peptide is problematic without knowing which off-target kinase inhibitors to include in the assay mixture.

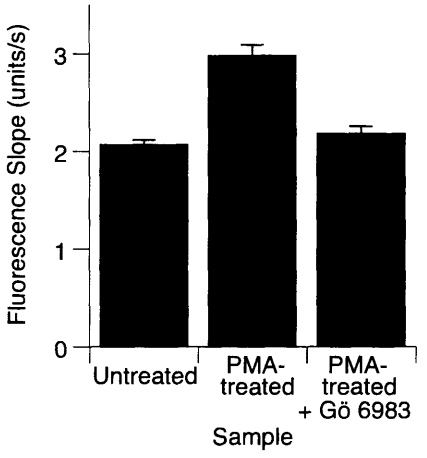

Figure 5-14. PKC-S1 kinase activity is not yet sufficiently specific. (**a**) Summary of fluorescence slopes for data from untreated HT-29 lysates, PMA-treated HT-29 lysates and PMA-treated HT029 lysates where 5 mM Gö 6983 has been included in the assay buffer. Plotted values indicate the mean ± standard deviation for triplicate measurements.

Acknowledgments:

For the work presented in this chapter, I have had the pleasure of collaborating with Kevin Janes and Professor Douglas Lauffenburger in the Biological Engineering Division at MIT. Kevin provided all of the lysates and performed all of the radioactive assays, immunodepletions and Western blot analyses. I would like to thank him for stimulating discussions, for sharing with me a biologist's perspective on my work, and for the opportunity to learn from his work and his knowledge. True to the spirit of collaboration, this work could never have been accomplished by either one of us on our own and we both learned a great deal from each other in the process. I would like to thank Professor Doug Lauffenburger for his enthusiasm for the project, resources and his very positive attitude. I would like to thank Isaac A. Manke and Professor Michael B. Yaffe for providing the MK2tide sequence for this work ahead of publication. This research was supported by the National Institutes of Health (GM64346 Cell Migration Consortium, P50-068762 Cell Decision Processes Center), the National Science Foundation (CHE-9996335), the Whitaker Foundation, and the Department of Defense Institute for Collaborative Biotechnologies.

Experimental

Materials: All small-molecule kinase inhibitors were obtained from Calbiochem unless otherwise noted.

Peptide Synthesis: Peptide chemosensors used in this chapter were reported in Chapter 4. Additional peptide inhibitors for PKA and PKC were synthesized here by the same methods. Concentrations of peptide inhibitor stock solutions were determined by quantitative amino acid analysis.

Peptide Characterization Data

Peptide	Sequence	Mol. formula	HPLC ret. time (min)[a]	*m/z* (*z*+) calcd	*m/z* found[b]
PKItide	H_2N-Thr-Tyr-Ala-Asp-Phe-Ile-Ala-Ser-Gly-Arg-Thr-Gly-Arg-Arg-Asn-Ala-Ile-NH_2	$C_{80}H_{130}N_{28}O_{24}$	20.6[c]	623.3 (+3)	623.1
PKC inhibitor	H_2N-Arg-Phe-Ala-Arg-Lys-Gly-Ala-Leu-Arg-Gln-Lys-Asn-Val-NH_2	$C_{67}H_{119}N_{27}O_{15}$	24.0[c]	386.5 (+4)	386.4

[a] C_{18}, Beckman Ultrasphere ODS, 5 μm, 150 x 4.6 mm; solvent A = water, 0.1% v/v TFA; solvent B = MeCN, 0.1% v/v TFA, 5 min 7% B followed by linear gradient 7-70% B over 30 min. [b] ESI-MS data were collected on a Applied Biosystems Mariner mass spectrometer.

Fluorescence Instrumentation:

Fluorimeter: Fluoromax 3 from Jobin Yvon (λ_{ex} = 360 nm, λ_{em} = 485 nm, slit widths = 5 nm, integration = 1 s). Cuvette: Starna Cells (16.100F-Q-10) 100 μl sub-micro cuvette, 1 cm path length.

Plate Reader: HTS7000 Bio Assay Reader from PerkinElmer with 360 nm excitation filter (35 nm bandpass), 485 nm emission filter (20 nm bandpass), 40 μs integration, 3 flashes/well, 120 gain. 96-well glass plate: Zinsser #3600500 with 500 μl well volume or Zinsser #3600501 with 300 μl well volume.

Buffer Recipes

Buffer A: 20 mM Hepes pH 7.4, 10 mM $MgCl_2$, 1 mM ATP, 1 mM DTT, 0.1 mM EGTA.

Buffer B: 20 mM Hepes pH 7.4, 1 mM DTT, 0.1% Brij-35, 1 mg/ml BSA.

Buffer C: 1% Triton X-100, 50 mM Tris-HCl (pH 7.5), 150 mM NaCl, 50 mM β-glycerophosphate, 10 mM sodium pyrophosphate, 30 mM NaF, 1 mM benzamidine, 2 mM EGTA, 100 μM Na_3VO_4, 1 mM DTT, 1 mM PMSF, 10 μg/ml aprotinin, 10 μg/ml leupeptin, 1 μg/ml pepstatin, 1 μg/ml microcystin-LR.

Buffer D: 20 mM Tris-HCl pH 7.5, 150 mM NaCl, 15 mM $MgCl_2$, 5 mM β-glycerophosphate, 1 mM EGTA, 0.2 mM Na_3VO_4, 0.2 mM DTT.

Assays with Recombinant Enzymes

Recombinant enzyme was added to 10 μM of each chemosensor. Assay conditions were as follows: *Akt1:* Buffer A with 40 ng Akt1 (Upstate, diluted 1:20 with Buffer B). *MK2:* Buffer A with 0.01% Brij-35, 0.1 mg/ml BSA, 20 ng MAPKAP kinase 2 (Upstate, diluted 1:10 with

Buffer B). *PKA:* Buffer A with 8 ng PKA catalytic subunit (Calbiochem, diluted 1:80 with 20 mM Tris-HCl (pH 7.5), 1 mM DTT, 0.15 mg/ml BSA). *PKC_α*: Buffer A with 0.3 mM $CaCl_2$, 10 μg/ml phosphatidylserine (porcine brain, Avanti Polar Lipids) 0.2 μg/ml diacylglycerol (dioleoyl, Avanti Polar Lipids), 11 ng PKC_α (Calbiochem, diluted 1:20 with 20 mM Hepes (pH 7.4), 5 mM DTT).

Cell Stimulation and Lysis

HT-29 cells for assay development and validation: HT-29 human colon epithelial cells (ATCC) were grown according to the manufacturer's recommendations. Confluent ten-cm plates (~15 million cells) of HT-29 cells were left untreated or stimulated with 500 ng/ml insulin for 5 min, 250 mM NaCl for 30 min, 25 μM forskolin for 30 min, or 1 μM PMA for 1 h, and lysed in 300 μl Buffer C. Whole cell lysates were incubated on ice for 15 min, then clarified by centrifugation at 16,000 × g for 15 min at 4°C. Protein concentrations of clarified extracts were determined with a bicinchoninic acid assay (Pierce). For inhibitor studies, cells were pretreated with various concentrations of wortmannin, LY294002, SB202190, rapamycin (300 nM), or PD 98059 (50 μM) for one hour before stimulation. The carrier concentration (0.1% DMSO) was maintained constant for all pretreatments.

Chinese Hamster Ovary (CHO) Cells

CHO cells stably overexpressing the EGF receptor[28] were grown in DMEM supplemented with 2 mM L-glutamine, 1 mM sodium pyruvate, 1 mM nonessential amino acids, 100 U/ml penicillin, 100 μg/ml streptomycin and 500 μg/ml G418. Cells were stimulated with 100 ng/ml EGF for 5 min or 100 ng/ml TNF (Peprotech) for 15 min and lysed as described for HT-29 cells. 250 μg CHO cell lysate was used for the Akt assay, and 200 μg CHO cell lysate was used for the MK2 assay.

Insulin and EGF Time Courses: Time courses were performed as described previously[1]. Briefly, HT-29 cells were plated at 50,000 cells/cm^2 for 24 hours. The cells were sensitized with 200 U/ml interferon-γ (Roche) for 24 hours and then treated with 500 ng/ml insulin (Sigma) or 100

ng/ml EGF (Peprotech), each dissolved in 50% DMSO/50% H_2O. At various time points after stimulation, clarified lysates were collected as described above.

Fluorescent Kinase Activity Assays

Activity assays were performed in a glass 96-well plate (Zinsser #3600500 with 250 µl or Zinsser #3600501 with 150 µl per well) at 30°C in a fluorescence plate reader in Buffer D with 4 µM PKC inhibitor, 4 µM calmidazolium (Sigma), 10 µM substrate peptide, 1 mM ATP (Calbiochem, Low Metals Grade) and for Akt, 0.4 µM PKItide, 5 µM GF 109203X; for MK2, of 0.4 µM PKItide, 25 µM GF 109203X; for PKA, 5 µM GF 109203X. For preliminary experiments with PKC, the assay buffer was composed of Buffer D without EGTA and with 10 µM PKC-S1, 1 mM ATP, 0.4 µM PKItide, 0.3 mM $CaCl_2$, 10 µg/ml phosphatidylserine, 0.2 µg/ml diacylglycerol. This assay buffer was prepared in bulk at 30°C and aliquoted to each well to ensure equal concentrations of the chemosensor. To begin each reaction, 7.5 vol% lysis buffer (Buffer C) or lysate (18.5 µl in 250 µl for Akt, and 11 µl in 150 µl for MK2 and PKA) was added and the contents of each well mixed gently. 60 data points were collected over each reaction. Akt-S1 activity was monitored over 60 min typically with 93 µg lysate. MK2-S1 and PKA-S3 activities were monitored for 15 min typically with 50 µg and 20 µg lysate, respectively. To quantify product formation, different turnover amounts (5%, 10%, 15%) were simulated in triplicate and lysis buffer was added as for a blank sample. For recombinant enzyme comparison, different amounts ($\geq$ 3) of recombinant enzyme were added with lysis buffer to begin the reaction. For PKA inhibition studies, the indicated concentration of H89 or PKItide was included in the assay buffer. Chemosensor sensitivities were determined by comparing the absolute fluorescence of 10 µM substrate and 10 µM corresponding product phosphopeptides in triplicate under the optimized assay conditions.

Data Workup

Fluorescence slopes were determined by a least-squares fit using KaleidaGraph (3.6.2, Synergy Software). This slope averages out scatter in individual fluorescence readings, because it is determined from 60 readings over the reaction time-course. To average out well-to-well variations in path length due to sample loading, each set of data points are normalized based on

their starting values. Plotted values are an average ± standard error for triplicate experiments. For all samples except Figure 5-13, these triplicate measurements are separate reactions from the same cell population. For Figure 5-13, the results from 3 different populations were averaged for each data point. Average slopes of wells containing lysis buffer only were subtracted from average slopes of samples and the error propagated accordingly. Slight day-to-day variation in plate reader lamp intensity and in solution preparation were observed and thus comparisons were only made between samples run at the same time. Thus, the fluorescence slope in figures is not comparable between graphs. For comparisons of absolute fluorescence readings, wells were loaded carefully to obtain equivalent path lengths and measurements were performed in triplicate with multiple readings averaged for each well. Percent turnover was determined based on the fluorescence endpoint reading of each assay and a linear fit of absolute fluorescence vs. simulated turnover (see also Kinase Activity Assays Section). Recombinant enzyme equivalents were determined by comparison of the fluorescence slope with a linear fit of the fluorescence slope vs. amount of recombinant enzyme (see also Kinase Activity Assays Section). IC_{50} values were calculated by fitting the data to the following equation:

$$I = I_{\min} + \left(\frac{I_{\max} - I_{\min}}{1 + 10^{x - \log IC_{50}}} \right)$$

where I = fluorescence intensity.

Radioactive Akt and MK2 Activity Assays

A microtiter-based kinase activity assay was performed as previously described.[1]

Very briefly, Protein A or G microtiter strips were coated overnight with 10 μg/ml anti-Akt PH domain (Upstate) or anti-MK2 (Upstate) and washed three times with blocking buffer (1% BSA, 50 mM Tris-HCl pH 7.5, 150 mM NaCl, 0.05% Trition X-100). Either 500 μg lysate for Akt and 200 μg lysate for MK2 was added for 3 h, and washed twice with Buffer D. Assays were conducted at 37°C in 60 μl Buffer D with 0.4 μM PKItide, 4 μM PKC inhibitor, 4 μM calmidazolium, ATP (10 μM for Akt and 25 μM for MK2), [γ-^{32}P]ATP (5 μCi for Akt and 2 μCi for MK2) and 10 μM Atkide or 10 μM MK2tide. The Akt assay was quenched after 30 min with

60 µl 75 mM H_3PO_4 and the MK2 assay was quenched after 15 min with 60 µl 20 mM EDTA. The reactions were prepared for scintillation counting as described.[1]

Quenched-point Fluorescence Assay

Akt and MK2 were immunopurified from HT-29 lysates in multiples of nine as described for the radioactive activity assays. Assays were then conducted at 37°C in 60 µl Buffer D with 0.4 µM PKItide, 4 µM PKC inhibitor, 4 µM calmidazolium, 1 mM ATP and 10 µM Akt-S1 or 10 µM MK2-S1. 50 µl from three identical wells was transferred into a single well of the 96-well glass plate after 15 min for MK2 and 30 min for Akt at 25°C. Multiple fluorescence readings were averaged for each well. This resulted in triplicate measurements of 1250 µg lysate for Akt and 750 µg lysate for MK2 with a 4 mm fluorescence path length. A control reading of assay mixture that was not exposed to immunopurified kinase was subtracted from average sample readings.

Immunodepletions

For Akt immunodepletions, 500 µg of insulin-stimulated HT-29 lysate was incubated with 4 µg anti-Akt PH domain (Upstate) or naïve mouse IgG (Santa Cruz) for two hours at 4°C on a rotating shaker. The immune complexes were precipitated with 40 µl Protein G sepharose beads (Amersham) for one hour with mixing at 4°C. For MK2 immunodepletions, 40 µl Protein G sepharose beads were incubated with 8 µg anti-MAPKAP kinase 2 (Upstate) or naïve sheep IgG (Santa Cruz) for one hour at 4°C on a rotating shaker. The beads were washed two times with 1 ml of blocking buffer (1% BSA in 50 mM Tris-HCl (pH 7.5), 150 mM NaCl, 0.05% Triton X-100) and then incubated with 200 µg NaCl-stimulated HT-29 lysate for three hours with mixing at 4°C.

Western blot analysis

To confirm immunodepletion, 100 µg of the starting lysate, kinase-immunodepleted lysate, and naïve-immunodepleted lysate were run on a 10% SDS-PAGE gel and transferred to PVDF (Millipore). The membrane was blocked with 5% nonfat skim milk in 20 mM Tris-HCl (pH 7.5), 137 mM NaCl, 0.1% Tween-20 and probed overnight with anti-Akt PH domain (Upstate), anti-Akt (Cell Signaling), or anti-MAPKAP K2 (Stressgen) at 1:1,000 dilution. The membranes were

then probed with horseradish peroxidase conjugated anti-mouse or anti-rabbit secondary antibody (Amersham) at 1:10,000 dilution and visualized by enhanced chemiluminescence (Amersham) on a Kodak Image Station (Perkin Elmer). Bands were selected and quantified according to manufacturer recommendations. Additional rounds of immunodepletion substantially depleted Akt and MK2 from the naïve lysate.

References

(1) Janes, K. A.; Albeck, J. G.; Peng, L. X.; Sorger, P. K.; Lauffenburger, D. A.; Yaffe, M. B. A high-throughput quantitative multiplex kinase assay for monitoring information flow in signaling networks. *Mol. Cell. Proteomics* **2003**, *2*, 463-473.

(2) Hall, J. P.; Davis, R. J. Analysis of c-Jun N-terminal kinase regulation and function. *Methods Enzymol.* **2002**, *345*, 413-425.

(3) Whitmarsh, A. J.; Davis, R. J. Analyzing JNK and p38 mitogen-activated protein kinase activity. *Methods Enzymol.* **2001**, *332*, 319-336.

(4) Li, H.; Sims, C. E.; Kaluzova, M.; Stanbridge, E. J.; Allbritton, N. L. A quantitative single-cell assay for protein kinase B reveals important insights into the biochemical behavior of an intracellular substrate peptide. *Biochemistry* **2004**, *43*, 1599-1608.

(5) Kawai, Y.; Sato, M.; Umezawa, Y. Single color fluorescent indicators of protein phosphorylation for multicolor imaging of intracellular signal flow dynamics. *Anal. Chem.* **2004**, *76*, 6144-6149.

(6) Schleifenbaum, A.; Stier, G.; Gasch, A.; Sattler, M.; Schultz, C. Genetically encoded FRET probe for PKC activity based on pleckstrin. *J. Am. Chem. Soc.* **2004**, *126*, 11786-11787.

(7) Sasaki, K.; Sato, M.; Umezawa, Y. Fluorescence indicators for Akt/protein kinase B and dynamics of Akt activity visualized in living cells. *J. Biol. Chem.* **2003**, *278*, 30945-30951.

(8) Violin, J. D.; Zhang, J.; Tsien, R. Y.; Newton, A. C. A genetically encoded fluorescent reporter reveals oscillatory phosphorylation by protein kinase C. *J. Cell Biol.* **2003**, *161*, 899-909.

(9) Kunkel, M. T.; Ni, Q.; Tsien, R. Y.; Zhang, J.; Newton, A. C. Spatio-temporal dynamics of protein kinase B/Akt signaling revealed by a genetically-encoded fluorescent reporter. *J. Biol. Chem.* **2004**, *280*, 5581-5587.

(10) Sato, M.; Ozawa, T.; Inukai, K.; Asano, T.; Umezawa, Y. Fluorescent indicators for imaging protein phosphorylation in single living cells. *Nat. Biotechnol.* **2002**, *20*, 287-294.

(11) Ting, A. Y.; Kain, K. H.; Klemke, R. L.; Tsien, R. Y. Genetically encoded fluorescent reporters of protein tyrosine kinase activities in living cells. *Proc. Natl. Acad. Sci. U.S.A.* **2001**, *98*, 15003-15008.

(12) Zhang, J.; Ma, Y.; Taylor, S. S.; Tsien, R. Y. Genetically encoded reporters of protein kinase A activity reveal impact of substrate tethering. *Proc. Natl. Acad. Sci. U.S.A.* **2001**, *98*, 14997-15002.

(13) Kurokawa, K.; Mochizuki, N.; Ohba, Y.; Mizuno, H.; Miyawaki, A.; Matsuda, M. A pair of fluorescent resonance energy transfer-based probes for tyrosine phosphorylation of the CrkII adaptor protein *in vivo*. *J. Biol. Chem.* **2001**, *276*, 31305-31310.

(14) Nagai, Y.; Miyazaki, M.; Aoki, R.; Zama, T.; Inouye, S.; Hirose, K.; Iino, M.; Hagiwara, M. A fluorescent indicator for visualizing cAMP-induced phosphorylation *in vivo*. *Nat. Biotechnol.* **2000**, *18*, 313-316.

(15) Higashi, H.; Sato, K.; Ohtake, A.; Omori, A.; Yoshida, S.; Kudo, Y. Imagining of cAMP-dependent protein kinase activity in living neural cells using a novel fluorescent substrate. *FEBS Lett.* **1997**, *414*, 55-60.

(16) Yeh, R.-H.; Yan, X.; Cammer, M.; Bresnick, A. R.; Lawrence, D. S. Real time visualization of protein kinase activity in living cells. *J. Biol. Chem.* **2002**, *277*, 11527-11532.

(17) Hill, M. M.; Hemmings, B. A. Analysis of protein kinase B/Akt. *Methods Enzymol.* **2002**, *345*, 448-463.

(18) Glass, D. B.; Cheng, H.-C.; Mende-Mueller, L.; Reed, J.; Walsh, D. A. Primary structural determinants essential for potent inhibition of cAMP-dependent protein kinase by inhibitory peptides corresponding to the active portion of the heat-stable inhibitor protein. *J. Biol. Chem.* **1989**, *264*, 8802-8810.

(19) Davies, S. P.; Reddy, H.; Caivano, M.; Cohen, P. Specificity and mechanism of action of some commonly used protein kinase inhibitors. *Biochem. J.* **2000**, *351*, 95-105.

(20) Andjelkovic, M.; Alessi, D. R.; Meier, R.; Fernandez, A.; Lamb, N. J.; Frech, M.; Cron, P.; Cohen, P.; Lucocq, J. M.; Hemmings, B. A. Role of translocation in the activation and function of protein kinase B. *J. Biol. Chem.* **1997**, *272*, 31515-31524.

(21) Coffer, P. J. Phosphatidylinositol 3-kinase signalling: a tale of two kinase activities. In *Protein Kinase Functions*; 2nd ed.; Woodgett, J. R., Ed.; Oxford University Press: Oxford, 2000; Vol. 29, p 1-39.

(22) Cross, D. A. E.; Alessi, D. R.; Cohen, P.; Andjelkovic, M.; Hemmings, B. A. Inhibition of glycogen synthase kinase-3 by insulin mediated by protein kinase B. *Nature* **1995**, *378*, 785-789.

(23) Cross, D. A. E.; Watt, P. W.; Shaw, M.; van der Kaay, J.; Downes, C. P.; Holder, J. C.; Cohen, P. Insulin activates protein kinase B, inhibits glycogen synthase kinase-3 and activates glycogen synthase by rapamycin-insensitive pathways in skeletal muscle and adipose tissue. *FEBS Lett.* **1997**, *406*, 211-215.

(24) Hazzalin, C. A.; Cuenda, A.; Cano, E.; Cohen, P.; Mahadevan, L. C. Effects of the inhibition of p38/RK MAP kinase on induction of five *fos* and *jun* genes by diverse stimuli. *Oncogene* **1997**, *15*.

(25) Neve, R. M.; Holbro, T.; Hynes, N. E. Distinct roles for phosphoinositide 3-dinase, mitogen-activated protein kinase and p38 MAPK in mediating cell cycle progression of breast cancer cells. *Oncogene* **2002**, *21*, 4567-4576.

(26) Smith, R. E.; Bissell, E. R.; Mitchell, A. R.; Pearson, K. W. Direct photometric or fluorometric assay of proteinases using substrates containing 7-amino-4-trifluoromethylcoumarin. *Thromb. Res.* **1980**, *17*, 393-402.

(27) Gurtu, V.; Kain, S. R.; Zhang, G. Fluorometric and colorimetric detection of caspase activity associated with apoptosis. *Anal. Biochem.* **1997**, *251*, 98-102.

(28) Harms, B. D.; Bassi, G. M.; Horwitz, A. R.; Lauffenburger, D. A. Directional persistence of EGF-induced cell migration is associated with stabilization of lamellipodial protrusions. *Biophys. J.* **2005**, *88*, 1479-1488.

Appendix

^{1}H NMR Spectra

8-tert-butyldiphenylsilyloxy-5-(N,N-dimethyl)sulfonamido-2-methylquinoline (**2**)

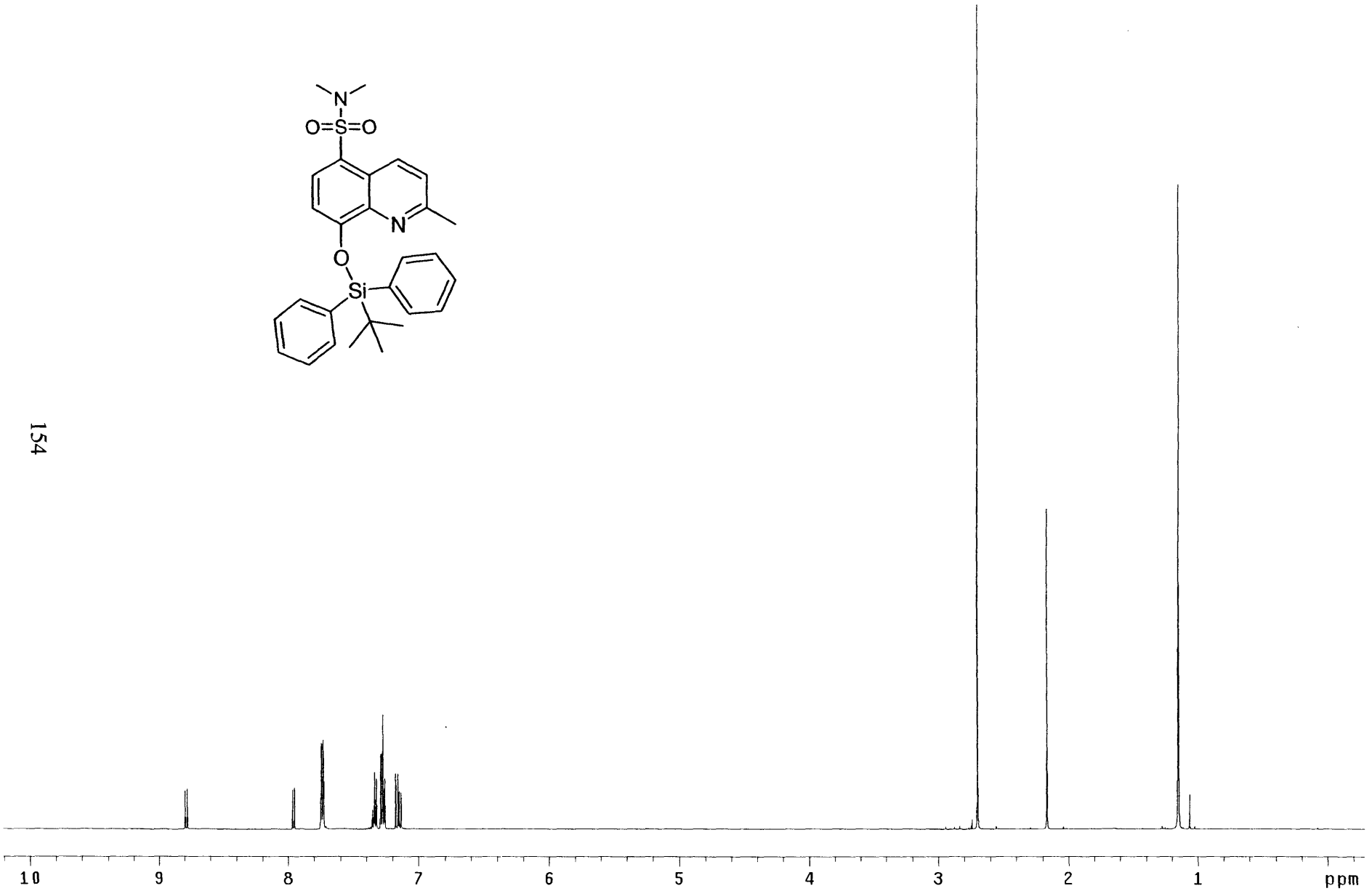

8-tert-butyldiphenylsilyloxy-5-(N,N-dimethyl)sulfonamido-2-formylquinoline (**3**)

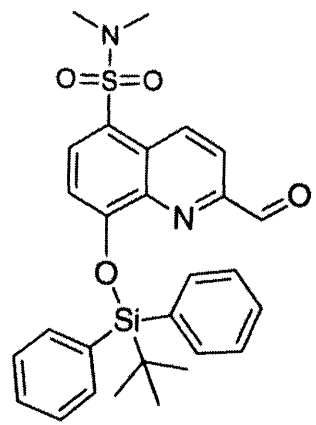

8-tert-butyldiphenylsilyloxy-5-(N,N-dimethyl)sulfonamido-2-(hydroxymethyl)quinoline (**4**)

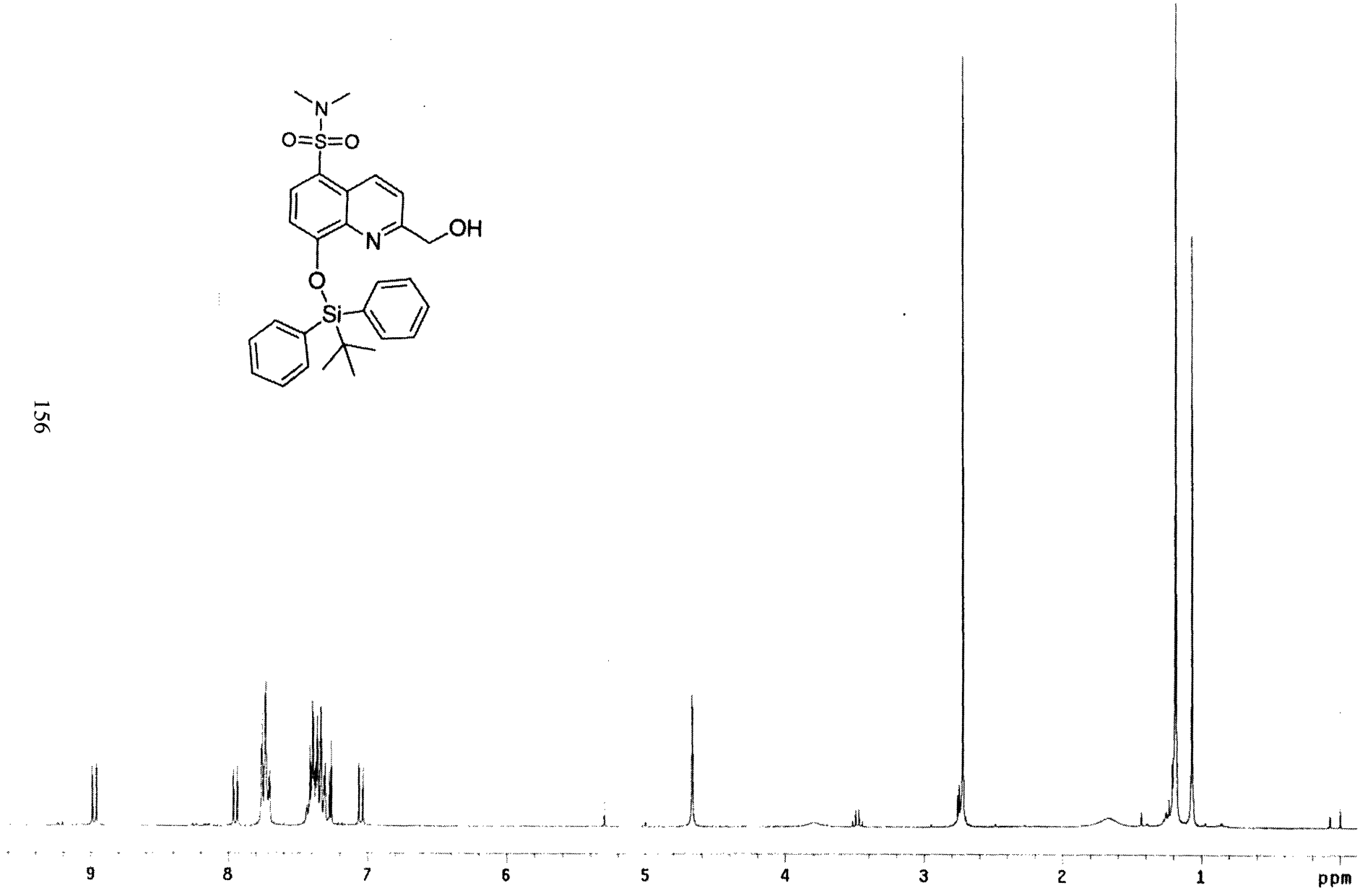

2-bromomethyl-8-tert-butyldiphenylsilyloxy-5-(N,N-dimethyl)sulfonamidoquinoline (**5**)

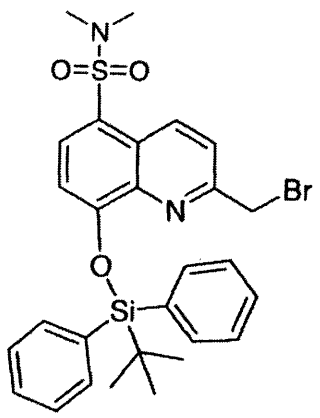

(S)-2-Amino-3-(8-hydroxy-5-(N,N-dimethyl)sulfonamidoquinoline-2-yl)propionic Acid Hydrochloride Salt (**Sox**)

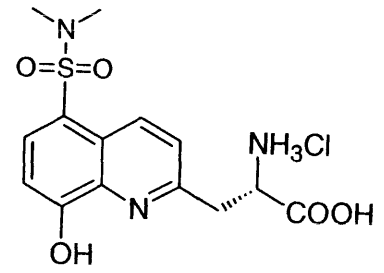

(S)-2-Amino-N$^{\alpha}$-(9-fluorenylmethyloxycarbonyl)-
3-(8-hydroxy-5-(*N*,*N*-dimethyl)quinoline-2-yl) Propionic Acid (**Fmoc-Sox-OH**)

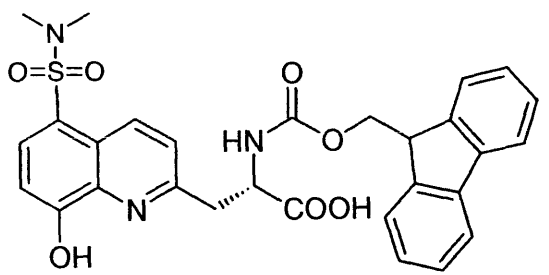

159

Fmoc-Glu(cs124) tert-butyl ester

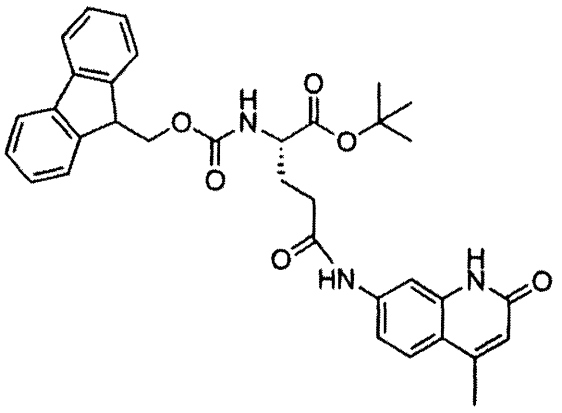

Fmoc-Glu(cs124)-OH

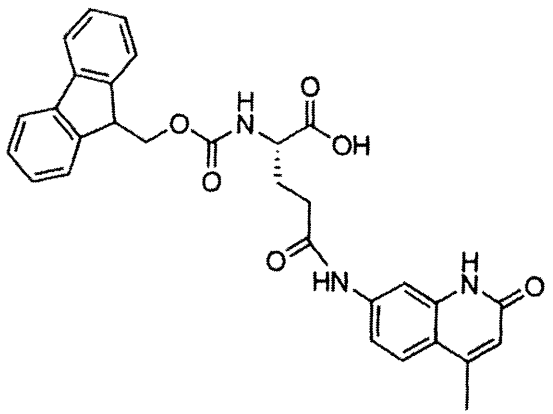

MELISSA DAWN SHULTS

EDUCATION

Massachusetts Institute of Technology (MIT), Cambridge, MA
Ph.D. Organic Chemistry, 2005

University of California San Diego (UCSD), La Jolla, CA
B.S. Chemistry with Honors, 2000

EXPERIENCE

RESEARCH

MIT Department of Chemistry
Graduate Research Assistant, Advisor: Professor Barbara Imperiali, 2000-2005
Chemosensing Strategies Utilizing the Nonnatural Sulfonamidohydroxylquinoline Amino Acid Sox

UCSD Department of Chemistry and Biochemistry
Undergraduate Research Assistant, Advisor: Professor Jay Siegel, 1997-2000
Synthesis of Ligand Precursors for Topologically Interesting Molecules

TEACHING

MIT Department of Chemistry
Teaching Assistant, Bioorganic Chemistry 5.55 (Spring 2003 and Spring 2004)
Teaching Assistant, Organic Chemistry 5.12 (Fall 2000)

UCSD Department of Chemistry and Biochemistry
Teaching Assistant, Organic Chemistry 140A (Fall 1998 and Fall 1999)
Teaching Assistant, Organic Chemistry 140B (Winter 2000)

AWARDS

National Science Foundation Graduate Research Fellowship (2000-2003)
Barry M. Goldwater and Excellence in Education Foundation Scholarship (1998-2000)
Pfizer Summer Undergraduate Research Fellowship (1999)

PUBLICATIONS

Shults, M. D.; Janes, K. A.; Lauffenburger, D. A.; Imperiali, B. "A multiplexed homogenous fluorescence-based assay for protein kinase activity in cell lysates," *Nat. Methods*, **2005**, *2*, 277-283.

Shults, M. D.; Imperiali B. "Versatile fluorescence probes of protein kinase activity," *J. Am. Chem. Soc.* **2003**, *125*, 14248-14249.

Shults, M. D.; Pearce, D. A.; Imperiali, B. "Modular and tunable chemosensor scaffold for divalent zinc," *J. Am. Chem. Soc.* **2003**, *125*, 10591-10597.

MELISSA DAWN SHULTS

PATENTS

Imperiali, B.; Shults, M. D. "Versatile and continuous fluorescence assay for kinase activity utilizing the fluorescent amino acid Sox," U.S. Patent Application Filed October 8, 2003.

PRESENTATIONS

Shults, M. D.; Imperiali, B. "Versatile fluorescence probes of protein kinase activity," Poster, Gordon Research Conference in Bioorganic Chemistry, Andover, NH, June 2004.

Shults, M. D.; Imperiali, B. "Readily tunable fluorescent peptidyl sensors for zinc(II)," Poster, 224th ACS National Meeting, Boston, MA, August 2002.

AFFILIATIONS

American Chemical Society (1997-present)
Phi Beta Kappa (1999-present)
American Peptide Society (2005-present)

FUTURE PLANS

Scientist I/Post-doc at Illumina, Inc. in San Diego, CA